Dynamical Pairing States in Cold Gases

by

Roman A. Barankov

Diploma, Moscow Engineering Physics Institute, 1998

Submitted to the Department of Physics
in partial fulfillment of the requirements for the degree of

Doctor of Philosophy

at the

MASSACHUSETTS INSTITUTE OF TECHNOLOGY

February 2006

Author .....
Department of Physics
September 16th, 2005

Certified by .....
Leonid S. Levitov
Professor
Thesis Supervisor

Accepted by .....
Thomas J. Greytak
Professor, Associate Department Head for Education

Dynamical Pairing States in Cold Gases

by

Roman A. Barankov

Submitted to the Department of Physics
on September 16th, 2005, in partial fulfillment of the
requirements for the degree of
Doctor of Philosophy

Abstract

In this thesis, we study dynamical pairing of fermions caused by the time-dependent interaction. Fermionic pairing develops on time scales short compared to the quasiparticle relaxation time where existing approaches to the problem including the Boltzmann kinetic equation and time-dependent Ginzburg-Landau theory are not applicable. The nonequilibrium dynamics can be explored in cold Fermi gas at a Feshbach resonance, a system with magnetically tunable interaction. Motivated by recent experiments, in Chapters 2 and 3 we study the pairing of fermions when a sudden switch of interaction induces the Bardeen-Cooper-Schrieffer (BCS) instability of the system. In this case, the pairing amplitude is found to be an oscillatory function of time with predictable characteristics. Another dynamical regime corresponding to a linear magnetic field sweep from atomic to molecular side at a Feshbach resonance is explored in Chapter 4. We find that pairing correlations of fermions in the initial state are encoded in the momentum distribution of molecules after the sweep. Finally, in Chapter 5, we consider pair excitations caused by the harmonic modulation of the interaction, and compare our results to experimental observations.

Thesis Supervisor: Leonid S. Levitov
Title: Professor

Acknowledgments

Publications

1. "Atom-molecule coexistence and collective dynamics near a Feshbach resonance of cold fermions", R. A. Barankov and L. S. Levitov, Phys. Rev. Lett. **93**, 130403 (2004)

2. "Solitons and Rabi Oscillations in a Time-Dependent BCS Pairing Problem", R. A. Barankov, L. S. Levitov, and B. Z. Spivak, Phys. Rev. Lett. **93**, 160401 (2004)

3. "Dynamical projection of atoms to Feshbach molecules at strong coupling", R. A. Barankov and L. S. Levitov, cond-mat/0506323

4. "Dynamical Selection in Emergent Fermionic Pairing", R. A. Barankov and L. S. Levitov, cond-mat/0508215

Contents

1 Introduction **13**

1.1 Experimental background 14

1.1.1 Experiments in cold gases 14

1.1.2 Measurement of the excitation gap 17

1.1.3 Measurement of the order parameter 19

1.2 The Bardeen-Cooper-Schrieffer theory basics 21

1.2.1 The BCS ground state 21

1.2.2 The pairing amplitude 23

1.2.3 Elementary excitations 25

1.2.4 BCS theory at finite temperatures 26

1.2.5 BCS-BEC crossover theories 28

1.3 Nonequilibrium superconductivity: review of different approaches . . 29

1.3.1 Time-dependent Ginzburg-Landau equation 29

1.3.2 Boltzmann kinetic equation 31

1.3.3 Bogoliubov-de Gennes dynamical equations 33

1.4 Outline of the thesis 35

2 Pairing dynamics of cold fermions **37**

2.1 Introduction 37

2.2 BCS instability of the unpaired Fermi gas 39

2.3 Bogoliubov-de Gennes equation as a Bloch equation 46

2.4 Oscillatory solutions, analytical and numerical 50

2.5 Noise due to occupancy fluctuations 59

2.6 Spin 1/2 representation 65
2.7 Summary 67
2.8 Appendix A: Bloch and the Bogoliubov-de Gennes equation 70
2.9 Appendix B: Numerical simulation of the pairing dynamics 72

3 Collective dynamics near a Feshbach resonance of cold fermions 81
3.1 Introduction 81
3.2 Dicke model 83
3.3 Stability diagram of the degenerate Fermi gas 85
3.4 Nonlinear dynamics of the molecular state 88
3.5 Summary 91

4 Dynamical projection of atoms to Feshbach molecules at strong coupling 93
4.1 Introduction 93
4.2 Probing the pairing correlations in experiments 94
4.3 Molecular Green's function 95
4.4 Dynamics of the molecule formation 96
4.5 Asymptotic production efficiency of molecules 100
4.6 Summary 103

5 Stimulated dissociation of a paired state of cold fermions at a Feshbach resonance 105
5.1 Introduction 105
5.2 Experimental observation of the excitation spectrum 106
5.3 Atom-molecule Hamiltonian at a Feshbach resonance 108
5.4 Excitation spectrum of a non-degenerate gas 109
5.5 Excitation spectrum of a paired state 114
5.6 Summary 118

List of Figures

1-1 Bose-Einstein condensation by absorption imaging. *Left*: thermal distribution of atoms; *middle*: the bimodal distribution of atoms; *right*: almost pure condensate. From W. Ketterle and D. Pritchard group at MIT. 15

1-2 Degenerate Fermi gas by absorption imaging: (a) Absorption image of ^{6}Li atoms; (b) Density profile of the atomic cloud extracted from (a). Thomas-Fermi distribution (thin line on (b)) corresponds to low temperature $T \approx 0.05E_F$. From Z. Hadzibabic, *et al.* Phys. Rev. Lett. **91**, 160401 (2003). 16

2-1 Temperature dependence of the BCS instability growth rate γ as obtained from Eq.(2.15) for the constant density of states model (2.8), (2.9) with the coupling λ such that $\Delta_0/W = 1/5$. Note that γ coincides with the BCS gap Δ_0 at $T = 0$, up to a correction small as $(\gamma/W)^2$ at large bandwidth W. Near $T_c = \pi e^{-C}\Delta_0 \simeq 1.764\Delta_0$, the exponent γ vanishes linearly in $T_c - T$. 42

2-2 Temperature dependence of the pairing amplitude Δ for the stationary state (2.25), (2.26) obtained from the unpaired state by adiabatic increase of coupling. The equilibrium BCS gap is shown for comparison. 48

2-3 Time dependence of the pairing amplitude Δ recorded from simulation with $N = 10^5$ states (2.8), (2.9) at temperature $T = 0.7T_c$ ($\beta = 2.5\Delta_0$) with the initial conditions (2.27). The coupling constant λ was chosen to have the BCS gap $\Delta_0 = W/5$. 51

2-4 Temperature dependence of the soliton train amplitude Δ_+, obtained from the self-consistency condition (2.34) at different ratios Δ_-/Δ_+. Note that at $\Delta_- = 0$ the amplitude Δ_+ equals the BCS instability growth increment γ (see Fig.2-1), while at $\Delta_- = \Delta_+$ the result for the stationary state is reproduced (see Fig.2-2). 53

2-5 *Top panel:* Comparison of the time dependence $\Delta(t)$ obtained from BCS/Bloch dynamics (2.24), (2.20) for $N = 10^3$ spins at temperature $T = 10^{-2}\Delta_0$ (blue curve) to the analytic soliton train solution (2.28) of the same amplitude and period (green curve). The difference of the simulated and analytic $\Delta(t)$ is shown in red. (The initial conditions (2.27) and parameters W, Δ_0 are the same as in Fig.2-3.) *Lower panels:* The pair distributions of the soliton train parameters for 500 different realizations: the time lag and period (left); the period and amplitude (right). 56

2-6 Same as in Fig.2-5 for higher temperature $T = 10^{-1}\Delta_0$. The simulated time dependence $\Delta(t)$ can be accurately fitted to the analytic solution (2.28), with the distribution of the period, amplitude and time lag somewhat broader than in Fig.2-5. 57

2-7 *Top:* The phase of the pairing amplitude *versus* time for the soliton train in Fig.2-6. *Bottom:* Pairing amplitude $\Delta(t) = \Delta_x(t) + i\Delta_y(t)$ trajectory in the complex plane. The phase $\arg \Delta(t)$ is a linear function of time superimposed with noise. Each radial line in the left panel corresponds to a soliton, marked according to their order in the time sequence. Phase shift between solitons translates into rotation by a constant angle. The right panel shows the behavior near the origin, allowing to trace the order of different solitons. 59

2-8 Noise suppression at increasing number of states N. The time dependence $\Delta(t)$ recorded from a simulation at $T = 0.7T_c$ ($\beta = 2.5\Delta_0$) for $N = 10^2$, 10^3, 10^4, 10^5 states, with other parameters the same as above. 62

2-9 Temperature dependence of the soliton train amplitude as recorded from the simulation. To suppress noise, the number of levels N was gradually increased from $N = 10$ at the lowest temperature to $N = 10^5$ at the highest temperature. Analytic fit displays the single $1/\cosh$ soliton (2.35) amplitude obtained from Eq.(2.34) at $\Delta_- = 0$. 63

2-10 Stereographic projection (2.60) schematic. 71

3-1 Phase diagram of coupled atom-molecule system obtained from Eq.(3.10) for ^{40}K system [16] at particle density $n \approx 1.8 \times 10^{13}\text{cm}^{-3}$, Fermi energy $E_F = 0.35\mu$K, and coupling strength $g^2 n/E_F \approx 60\mu$K. (The coupling was estimated using the microscopic theory of Feshbach resonance developed by Falco and Stoof [47], applied to the conditions of the JILA experiment [16]). *Inset:* Effective potential schematic illustrating the behavior in the three regions. 87

3-2 *Left:* Time evolution (3.14) of fermion pair amplitudes with different energies obtained for the molecular field of a soliton train form (3.19). The Bloch sphere parametrization of pseudospin variables $r_p^{x,y,x} = \langle \sigma_p^{x,y,x} \rangle$ is used. Pseudospins precess so that each state completes a full 2π Rabi cycle per soliton. The red and blue curves correspond to the energies above and below the Fermi level. *Right:* The dependence of the trajectory center and the radius on the energy state for the states denoted by the letters on the left. 90

4-1 Molecule number N_m *vs.* the sweep rate $(\lambda^4/\alpha)^{1/3}$ at different initial detuning ν_0. The asymptotic regimes, $N_m \propto \alpha^{-1}, \alpha^{-1/3}$, correspond to slow and fast sweep. Inset: Molecular energy time dependence (4.1) with the time interval corresponding to nonadiabatic evolution marked. 103

4-2 Third power of the molecule number, N_m^3, *vs.* the inverse sweep rate $1/\alpha$. A linear fit corresponds to the predicted 1/3 power-law dependence of the molecule production during the sweep. Experimental points are taken from Fig. 5 in Ref. [16] 104

5-1 The excitation rate $S(\omega)$ *vs.* the perturbation frequency f. The solid line represents both coherent and incoherent contributions to the excitation rate in the nondegenerate case, while the dashed line corresponds to the paired state of the gas. 119

Chapter 1

Introduction

Atomic physics has been traditionally concerned with the study of one-body processes related to the structure of individual molecules and atoms. Recently, however, the experimental realization of Bose-Einstein condensation (BEC) in cold gases [1] shifted the focus of the research in this field towards the study of many-body systems, an area usually associated with condensed matter physics. It is now possible to combine powerful theoretical tools created in condensed matter physics with unique experimental precision and flexibility provided by the atomic physics.

Cold atomic gases cooled to temperatures below the degeneracy point provide a unique system in which predictions of the condensed matter physics can be tested in experiments in a precise and controllable way. In Bose-condensed gases, for example, the problem of superfluidity can be studied *quantitatively* in new physical situations based on the exactly solvable case of weakly interacting Bose gas, whereas in the study of traditional Bose superfluids such as ^{4}He only *qualitative* understanding has been accomplished.

Recent experimental progress in atomic physics also allowed to explore degenerate Fermi gases of alkali atoms with tunable interactions. The advantage of these systems over the traditional superfluids studied in condensed matter is the control over physical parameters such as the temperature, the density and the interaction strength making it possible to explore quantitatively new dynamical regimes. In these systems, one can perform time-resolved measurements on the intrinsic microscopic time scales,

and explore fundamentally new phenomena in the time dynamics of the many-body state.

The particular question we address in this thesis deals with the nonequilibrium pairing dynamics in the degenerate Fermi gas subject to the time-dependent interaction. In this introductory Chapter, we provide the experimental and theoretical background necessary to understand the relation of the thesis to the current research in this field.

This Chapter is organized as follows. In Section 1.1, we discuss the experiments in cold atomic gases related to the problem of superfluidity in Fermi system. Section 1.2 provides a brief introduction to the Bardeen-Cooper-Schrieffer theory of superconductivity. Different approaches to the problem of nonequilibrium superconductivity are reviewed in Section 1.3.

1.1 Experimental background

1.1.1 Experiments in cold gases

The interaction of two atoms in the low energy limit is described by the scattering length a defining the characteristic "size" of atoms. In the many-body system with particle density n, different interaction regimes are classified according to the ratio of the scattering length a and the interparticle distance given by $n^{-1/3}$, expressed in terms of the so-called gas parameter $n\,|a|^3$. Small value of the gas parameter, $n|a|^3 \ll 1$, when the interparticle distance is much larger than the scattering length, corresponds to weak interaction, while in the strongly interacting limit these quantities are of the same order of magnitude, i.e. $n|a|^3 \approx 1$. The properties of the many-body system are quantitatively understood in the limit of weak interaction, while the physical picture is still far from being complete in the limit of strong interaction.

Recently it has become possible to explore different interaction regimes using Feshbach resonances in interatomic scattering. Near such resonances, the physics can

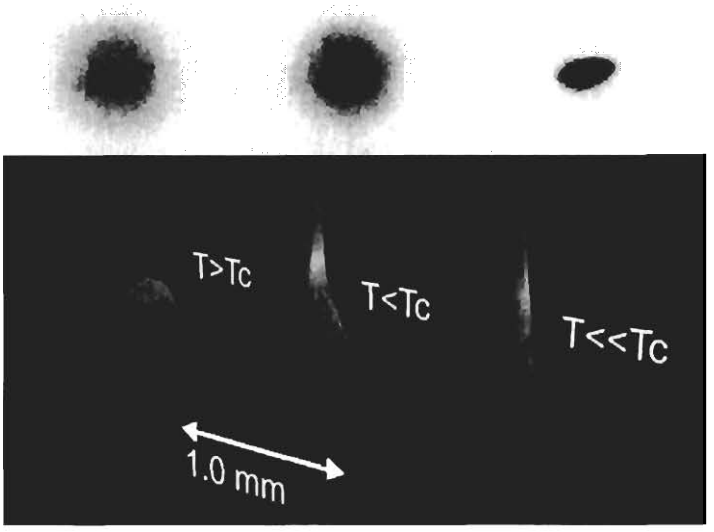

Figure 1-1: Bose-Einstein condensation by absorption imaging. *Left*: thermal distribution of atoms; *middle*: the bimodal distribution of atoms; *right*: almost pure condensate. From W. Ketterle and D. Pritchard group at MIT.

be described using a simplified picture taking into account the hyperfine coupling of atomic and molecular states. Since the molecular state has magnetic moment different from the atomic one, it is possible to change their relative position using the Zeeman splitting of the states in the external magnetic field B. Feshbach resonance corresponds to the degeneracy point of the atomic and molecular energies where hyperfine coupling causes the resonant behavior of the scattering length [2]:

$$a(B) - a_{bg} \propto \frac{1}{B_0 - B}, \tag{1.1}$$

where a_{bg} is the background scattering length far from the resonance, and B_0 is the magnetic field at the resonance. We notice that the scattering length changes the sign, being negative on the atomic side ($B > B_0$) and positive on the molecular side ($B < B_0$) of the resonance. The Feshbach resonances in interatomic scattering have been observed in ultracold alkali gases such as Na, Rb, K, and Li [3, 4, 5, 6, 7].

Cold atomic clouds are prepared in magnetic or dipole optical traps. The geometry of the parabolic trapping potential defines the shape of the cloud. The measurements

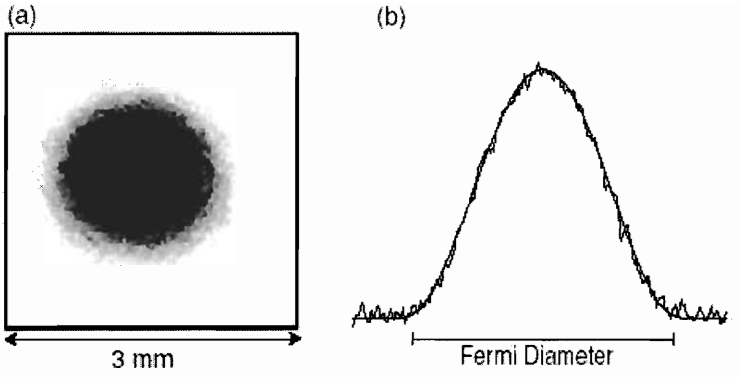

Figure 1-2: Degenerate Fermi gas by absorption imaging: (a) Absorption image of ^{6}Li atoms; (b) Density profile of the atomic cloud extracted from (a). Thomas-Fermi distribution (thin line on (b)) corresponds to low temperature $T \approx 0.05 E_F$. From Z. Hadzibabic, *et al.* Phys. Rev. Lett. **91**, 160401 (2003).

performed in these systems mainly focus on the density profile which is obtained by the resonant absorption of light as shown on Figs.1-1 and 1-2. Images obtained in this procedure correspond to the shadow on the detector cast by the expanding gas. Usually images are taken after a short period of free expansion of the gas, a restriction set by a finite resolution of the detector. The analysis of density distribution of expanding cloud allows to determine the momentum distribution of atoms.

The reliable thermometry of cold gases is one of the problems in current experiments. Presently, it is based on profile measurement and fitting it to the bimodal distribution for bosons and the thermally smeared Thomas-Fermi profile for fermions. On Fig.1-1, absorption images of Bose gas as a function of two spatial dimensions are shown. The images were taken after 6 msec of free expansion of the gas. At the temperature higher than critical, $T > T_c$, a thermal atomic cloud is visible. A bimodal distribution consisting of the thermal and condensate components appears just below the critical temperature, $T < T_c$, which transforms in almost pure condensate density distribution at very low temperatures $T \ll T_c$. In the case of Fermi gases, the fitting of the observed density profile to the Thomas-Fermi distribution is used to define temperature in experiments. An absorption image as well as the density distribution of ultracold gas of ^{6}Li atoms taken after 12 msec of free expansion are presented on

Fig.1-2 of Ref. [8]. The Thomas-Fermi density distribution shown in the thin line corresponds to low temperature, $T \approx 0.05E_F$, where E_F is the Fermi energy.

Since the state of the interacting gas is known only in the limit of weak interactions, it is hard to extract the temperature from the profile measurements in the limit of strong interactions which is presently of main interest. The difficulty can be overcome to some extent using isentropic change of the state of the system using control of the interaction via external magnetic field at a Feshbach resonance. In this method, the temperature of the system can be defined in the limit of weak interactions far from the resonance with subsequent adiabatic change of the state bringing the system to the region of interest at the resonance.

One of the goals of the current research in cold gases is the creation of Fermi superfluid. The temperature of the superfluid transition in the weak coupling regime of the Bardeen-Cooper-Schrieffer theory at low density is exponentially small, leading to unrealistic temperatures. It has been suggested [9, 10, 11, 12, 13] that the strength of attractive interactions, and therefore the critical temperature, can increase due to the resonant dependence of the interatomic scattering length at Feshbach resonances. It is expected [9, 10, 11, 12, 13] that in the vicinity of the resonance the critical temperature reaches a fraction of the Fermi temperature, E_F.

Besides difficulties associated with achieving fermion superfluidity, the detection of the pairing correlations in the Fermi gas poses a serious experimental problem. Several methods have been proposed to probe the state of Fermi gas at a Feshbach resonance. These proposals can be divided in two groups. The first one involves detection of the gap in the excitation spectrum of fermions [14, 15], while the second group looks for signatures of superfluidity [16, 17, 18, 19, 20, 21]. Below we briefly review these experiments and discuss their results.

1.1.2 Measurement of the excitation gap

In one of the recent experiments [14], a radio-frequency spectroscopy has been used to explore properties of fermionic gas of ^{6}Li atoms. An ultracold gas consisting of two hyperfine components was prepared at a Feshbach resonance. To probe the exci-

tation spectrum, a radio-frequency projection of one of the two states to the initially unoccupied third state was used. Subsequently, a selective imaging of the atom loss was performed to define the response of the system. The radio-frequency spectrum demonstrated a double-peak feature corresponding to the paired and unpaired atoms in the initial state. The energy gap in the excitation spectra, identified in this experiment, was measured against the detuning from the Feshbach resonance, temperature, and number of atoms. The quantitative description of the excitation spectrum for this experiment was provided in Ref. [22].

Another method probing the excitation spectrum of Fermi gas at a Feshbach resonance was recently realized in the JILA experiment [15]. At the resonance, the external magnetic field controls the position of the molecular level with respect to the atomic one. Perturbation of the external magnetic field causes modulation of the position of the molecular level, while strong hyperfine coupling of the levels leads to the time variation of the interaction strength. As a result, excitations are produced when the modulation frequency exceeds the dissociation energy or pair breaking threshold. The authors of Ref. [15] suggested that this method can be employed to probe the excitation gap in the Fermi gas.

Several important features have been observed in the excitation spectrum [15]. Two distinct peaks were identified at low and high perturbation frequencies, the latter being broad on the scale of the Fermi energy. The low energy peak with its maximum at twice the trap frequency was attributed to the collective excitation driven by the modulation of the interaction strength. At larger frequencies, the response of the gas increased, reaching maximum above certain threshold, and then decreasing.

On the molecular side of the Feshbach resonance, threshold frequency and the frequency of maximum response was observed to be a function of the detuning from the resonance. The threshold frequency was consistent with the dissociation energy of the molecules obtained from the one-body physics. On the atomic side of the resonance, the threshold frequency was close to zero for all detunings from the resonance. The position of the maximum response in this case was approximately twice the Fermi energy of the gas with a weak tendency to increase with the detuning.

A question was put forward in Ref. [15] about the relation of the high energy peak in the excitation spectrum to the fermionic pairing in the gas. A theoretical model that partially addresses this question is considered in Chapter 5. We find that the situation is more complex than envisioned in Ref. [15], and construct a theoretical framework that helps to understand the experimental results.

1.1.3 Measurement of the order parameter

Pairing correlations in the Fermi gas at a Feshbach resonance were probed in two recent experiments [16, 17]. The many-body atomic state was projected to Feshbach molecules using the magnetic field sweep through the resonance. To clarify the physics involved in this process, let us first consider adiabatic (sufficiently slow) sweeps of the detuning crossing the resonance from its atomic side to the molecular one. In such a process, with a slow change of the magnetic field at the resonance, the state of the cold gas continuously remains in thermal equilibrium. Regardless of the correlation properties of the initial state of the Fermi gas, at low enough temperature the final state will be the Bose-Einstein condensate of molecules. Thus, all the information about the pairing correlations in the initial state would be lost in this process.

In the opposite limit of fast magnetic sweep, the system is out of equilibrium during this process. As a result, one may expect that the pairing correlations in the initial state will be inherited by the momentum distribution of molecules in the final state, provided that the measurements are performed on a time scale shorter than the relaxation time. The correlations in the fermion superfluid state correspond to a finite probability for a pair of fermions with opposite spins to have opposite momenta. This corresponds to a special (anomalous) part in the density-density correlation function ($\hbar = 1$, volume $\mathcal{V} = 1$):

$$\langle \delta n_\uparrow (\mathbf{r})\, \delta n_\downarrow (\mathbf{r}) \rangle = \left| \sum_{\mathbf{p}} \langle a_{\mathbf{p}\uparrow} a_{-\mathbf{p}\downarrow} \rangle \right|^2 , \tag{1.2}$$

where $\delta n = n - \langle n \rangle$, and $a_{\mathbf{p}\lambda}$ is the annihilation operator of the fermion with the

momentum $\mathbf{p}$ and the spin projection λ. The average in Eq.(1.2) is taken with respect to the paired state. The correlations of fermions are related to the pairing amplitude in the BCS state, $\Delta \propto \sum_p \langle a_{\mathbf{p}\uparrow} a_{-\mathbf{p}\downarrow} \rangle$, and vanish in the normal state. As follows from Eq.(1.2), the superfluid state possesses a macroscopic number of fermion pairs with opposite spins and momenta that can turn into molecules with zero momentum, a molecular condensate (for details, see Eq.(4.22) in Chapter 4). Fast magnetic field sweep through the Feshbach resonance provides, therefore, a method to probe the pairing correlation in the initial state encoded in the final momentum distribution of molecules. We develop a theoretical model of fast projection of atomic state on molecules at Feshbach resonance in Chapter 4.

Another method to probe superfluidity in Fermi gas is based on the observation of collective excitations. In the experiment in Ref.[18], the collective excitations of a Fermi gas of ^{6}Li atoms at a Feshbach resonance were induced by the sudden change of the trapping potential. The decrease in damping of these collective modes at lower temperatures was interpreted as a signature of the superfluid transition in the system [18]. In Ref.[19], the regime of strongly interacting Fermi gas was explored using the method similar to that of Ref.[18]. In this work, the radial and axial excitation frequencies and damping rates were measured as a function of the magnetic field detuning from the Feshbach resonance. Nonmonotonic behavior of the radial frequency and increase of the damping rate at the resonance suggested a possible superfluid transition in the gas. The relation of the results of Refs. [18] and [19], which appear to contradict one another is presently not well understood.

Recent experiment [20] reported the observation of the Abrikosov vortex lattices created by stirring the strongly interacting Fermi gas at a Feshbach resonance. The rotation of the gas was induced by a laser beam, with subsequent projection of the state on the molecular condensate. Thus, this experiment combined excitation of the collective mode and the detection of the pairing correlation using fast projection technique [16, 17]. The observation of the vortex lattice in the experiment of Ref. [20] provided the first demonstration of the long-range correlations and existence of the macroscopic order parameter in strongly interacting Fermi gas.

Finally, the first measurement of the heat capacity of the Fermi gas of ^{6}Li atoms at a Feshbach resonance was recently presented [21]. One of the characteristic features of the superfluid phase transition, the specific heat jump, was found [21] to be close to the value predicted by the Bardeen-Cooper-Schrieffer theory. The observed critical temperature being a fraction of the Fermi energy, $T_c \approx 0.29E_F$, indicated that a strongly interacting regime of the BCS theory was realized.

1.2 The Bardeen-Cooper-Schrieffer theory basics

1.2.1 The BCS ground state

In this section, we summarize the main results of the Bardeen-Cooper-Schrieffer theory of superconductivity [23] in the case of neutral Fermi gases. We will consider the case of a two-component Fermi gas with attractive interaction. The many-body system of interacting fermions is described by the following Hamiltonian:

$$\mathcal{H} = \sum_{\mathbf{p},\,\sigma} \epsilon_{\mathbf{p}} a^{+}_{\mathbf{p}\sigma} a_{\mathbf{p}\sigma} - \lambda_0 \sum_{\mathbf{p},\mathbf{q},\mathbf{d}} a^{+}_{\mathbf{p+d/2}\uparrow} a^{+}_{\mathbf{-p+d/2}\downarrow} a_{\mathbf{-q+d/2}\downarrow} a_{\mathbf{q+d/2}\uparrow}, \tag{1.3}$$

where $a_{\mathbf{p}\sigma}$, $a^{+}_{\mathbf{p}\sigma}$ are the canonical fermion operators, and $\sigma = \uparrow, \downarrow$ is the generalized spin. The kinetic energy of atoms is $\epsilon_{\mathbf{p}} = \mathbf{p}^2/2m - \mu$, with μ the chemical potential. For simplicity, we consider Fermi gas with equal numbers of fermions in each spin state. The interaction constant λ_0 can be expressed through the negative scattering length a_0 in the Born approximation:

$$\lambda_0 = \frac{4\pi\hbar^2|a_0|}{m}. \tag{1.4}$$

As discussed below, a relation similar to Eq.(1.4) also holds for the physical s-wave scattering length in low energy scattering outside the Born approximation.

Let us first consider the ground state properties of the Hamiltonian (1.3). The state of the Fermi gas with attractive interaction is unstable with respect to pairing of fermions with opposite spin and momentum. It is often convenient to use the

so-called "reduced" BCS Hamiltonian, which takes into account only the processes of particle scattering with zero total momentum at energies close to E_F:

$$\mathcal{H} = \sum_{\mathbf{p},\sigma} \epsilon_{\mathbf{p}} a^+_{\mathbf{p}\sigma} a_{\mathbf{p}\sigma} - \lambda_0 \sum_{\mathbf{p},\mathbf{q}} a^+_{\mathbf{p}\uparrow} a^+_{-\mathbf{p}\downarrow} a_{-\mathbf{q}\downarrow} a_{\mathbf{q}\uparrow}. \tag{1.5}$$

Although such a simplification of the Hamiltonian may seem natural, it is fully justified only in the case of superconducting metals. The terms omitted in Eq. (1.5) are responsible for the Bogoliubov-Anderson [24, 25] collective modes that are gapped in the case of charged Fermi systems, but are present in neutral Fermi gas. In the following discussion, however, we will not encounter situations where such processes become important.

The properties of the many-particle system (1.5) can be completely understood in the thermodynamic limit. In this case, the problem of superfluidity is solved in the mean-field approximation by introducing an order parameter, a physical quantity which fully characterizes pairing in the system.

The existence of the order parameter is related to the structure of the ground state of the system. The Hilbert space of the reduced Hamiltonian is spanned by the wave functions that take into account the occupancy of the paired states. A typical wave function that corresponds to the occupied pair states has the following form:

$$|M\rangle = \prod_{\mathbf{p}\subseteq M} a^+_{\mathbf{p}\uparrow} a^+_{-\mathbf{p}\downarrow} |0\rangle, \tag{1.6}$$

where M is a subset in momentum space.

Among all possible states in the Hilbert space, there are special linear combinations of wave functions (1.6) first considered by Bardeen, Cooper and Schrieffer [26]:

$$|\Phi_{BCS}\rangle = \prod_{\mathbf{p}} \left(u_{\mathbf{p}} + v_{\mathbf{p}} a^+_{\mathbf{p}\uparrow} a^+_{-\mathbf{p}\downarrow}\right) |0\rangle, \tag{1.7}$$

with complex amplitudes $u_{\mathbf{p}}$ and $v_{\mathbf{p}}$ having a fixed relative phase independent on $\mathbf{p}$.

The wave function (1.7) can be decomposed into a linear combination with differ-

ent numbers of fermion pairs with one dominant contribution peaked at a number set by the chemical potential. The phase structure of the wave function (1.7) is evident from the form of the pairing amplitude:

$$\Psi = \lambda_0 \sum_{\mathbf{p}} \langle \Phi_{BCS} | \, a_{\mathbf{p}\downarrow} a_{-\mathbf{p}\uparrow} | \Phi_{BCS} \rangle = \lambda_0 \sum_{\mathbf{p}} u_{\mathbf{p}} v_{\mathbf{p}}^{*}. \tag{1.8}$$

Each term in the sum (1.8) has the same phase, so there is *phase coherence* of all momentum states. Since the phase of the wave function is a variable conjugate to the number operator, one can show that BCS wave function (1.7) is a coherent state. Spontaneous breaking of the symmetry of the equilibrium state is associated with an arbitrary choice of the overall phase φ of the complex pairing amplitude, $\Psi = \Delta_0 \exp(i\varphi)$.

1.2.2 The pairing amplitude

The pairing amplitude Ψ plays the role of the macroscopic order parameter in the BCS theory. The magnitude Δ_0 of the order parameter defines the equilibrium physical quantities of the superfluid state, while the phase φ is a dynamical variable in the superfluid hydrodynamics.

The ground state of the BCS Hamiltonian corresponds to the particular choice of the amplitudes $u_{\mathbf{p}}$ and $v_{\mathbf{p}}$:

$$|u_{\mathbf{p}}|^2 = \frac{1}{2}\left(1 + \frac{\epsilon_{\mathbf{p}}}{\sqrt{\epsilon_{\mathbf{p}}^2 + \Delta_0^2}}\right), \quad |v_{\mathbf{p}}|^2 = \frac{1}{2}\left(1 - \frac{\epsilon_{\mathbf{p}}}{\sqrt{\epsilon_{\mathbf{p}}^2 + \Delta_0^2}}\right). \tag{1.9}$$

Substitution of these quantities in Eq.(1.8) leads to the self-consistency equation for the pairing amplitude:

$$\Delta_0 = \frac{\lambda_0}{2} \sum_{\mathbf{p}} \frac{\Delta_0}{\sqrt{\epsilon_{\mathbf{p}}^2 + \Delta_0^2}}. \tag{1.10}$$

Eq. (1.10) has two solutions, one of which is a trivial one, $\Delta_0 = 0$. We discard it,

since the minimum of the energy corresponds to a solution with $\Delta_0 \neq 0$ (see below).

The summation over the momentum states in Eq. (1.10) leads to an ultraviolet divergence having its origin in the Hamiltonian (1.5). There, instead of the scattering potential depending on the momenta of atoms we used the low-energy Born approximation, λ_0. Since the latter does not treat appropriately the scattering at higher energies [27], one needs to consider the Lippmann-Schwinger equation for the renormalized amplitude λ that has the following operator form:

$$\lambda = \lambda_0 - \lambda_0 G_0 \lambda, \tag{1.11}$$

where we introduced the Green's function $G_0 = (E - \mathbf{p}^2/m)^{-1}$ for the two-particle scattering in the center-of-mass frame at the energy E.

Solving this equation, we express λ_0 in terms of the physical amplitude λ:

$$\lambda_0 = \lambda (1 - G_0 \lambda)^{-1}, \tag{1.12}$$

where in the low energy limit of scattering E is set equal to zero.

Substituting this expression in the self-consistency equation (1.10), one can arrive [28] at the self-consistency equation without the divergence:

$$1 = \frac{\lambda}{2} \sum_{\mathbf{p}} \left(\frac{1}{\sqrt{\epsilon_{\mathbf{p}}^2 + \Delta_0^2}} - \frac{1}{\mathbf{p}^2/2m} \right), \tag{1.13}$$

where the interaction $\lambda = 4\pi\hbar^2|a|/m$ is now expressed through the physical s-wave scattering length a.

The solution of this equation is easily found in the weak coupling limit, $\nu_0 \lambda \ll 1$, with the result:

$$\Delta_0 = \frac{8}{e^2} E_F \, e^{-1/\nu_0 \lambda}. \tag{1.14}$$

Here, $\nu_0 = m p_F / 2\pi^2 \hbar^3$ is the density of states at the Fermi energy, and $p_F = \hbar (3\pi^2 n)^{1/3}$ is the Fermi momentum for gas with the particle density $n = N/\mathcal{V}$. Further analysis [28] of fermionic interaction in the Fermi sea reduces a prefactor

in Eq.(1.14) by $(4e)^{1/3}$, and finally gives the following expression for the pairing amplitude:

$$\Delta_0 = (2/e)^{7/3} E_F e^{-1/\nu_0 \lambda}. \tag{1.15}$$

The self-consistency equation (1.13) has to be supplemented by a particle conservation constraint for the total number of fermions N:

$$N = \langle \Phi_{BCS} | \sum_{\mathbf{p},\sigma} a^+_{\mathbf{p}\sigma} a_{\mathbf{p}\sigma} | \Phi_{BCS} \rangle = 2 \sum_{\mathbf{p}} v^2_{\mathbf{p}}, \tag{1.16}$$

which in the weak coupling limit fixes the chemical potential at the Fermi energy, $\mu = E_F$.

To demonstrate that the BCS paired state has energy lower than the normal state, we calculate the corresponding energy difference:

$$E_S - E_N = -\mathcal{V}\nu_0 \Delta_0^2/2, \tag{1.17}$$

This result has simple physical interpretation. In the weak coupling limit, only the fermions in the narrow interval Δ_0 around the Fermi energy are paired. The number of such fermion pairs is roughly $\mathcal{V}\nu_0\Delta_0$, with each pair contributing negative Δ_0 to the system energy. The product, $\mathcal{V}\nu_0\Delta_0 \times (-\Delta_0)$, up to a numerical factor reproduces Eq. (1.17). The negative value of the pairing energy demonstrates that the superfluid state is energetically favorable compared to the normal one.

1.2.3 Elementary excitations

The reduced BCS Hamiltonian (1.5) can be exactly diagonalized in the thermodynamic limit. Introducing Bogoliubov creation and annihilation quasiparticle operators $\alpha_{\mathbf{p}\sigma}$,

$$\begin{aligned} \alpha_{\mathbf{p}\downarrow} &= u_{\mathbf{p}} a_{\mathbf{p}\downarrow} + v_{\mathbf{p}} a^+_{-\mathbf{p}\uparrow}, \\ \alpha_{\mathbf{p}\uparrow} &= u_{\mathbf{p}} a_{\mathbf{p}\uparrow} - v_{\mathbf{p}} a^+_{-\mathbf{p}\downarrow}, \end{aligned} \tag{1.18}$$

the BCS Hamiltonian (1.5) is brought to the diagonal form

$$\mathcal{H} = \sum_{\mathbf{p},\sigma} E_{\mathbf{p}} \alpha^{+}_{\mathbf{p}\sigma} \alpha_{\mathbf{p}\sigma}, \tag{1.19}$$

up to a constant term. Here, we introduced the excitation spectrum of the Bogoliubov quasiparticles:

$$E_{\mathbf{p}} = \sqrt{\epsilon^2_{\mathbf{p}} + \Delta^2_0}. \tag{1.20}$$

As follows from Eq.(1.20), the excitations have the pairing gap Δ_0 at the Fermi energy. The existence of the gap in the excitation spectrum makes the paired state a superfluid.

1.2.4 BCS theory at finite temperatures

The BCS Hamiltonian (1.19) expressed in terms of the Bogoliubov quasiparticle operators allows to obtain the quasiparticle distribution function $n_{\mathbf{p}}$ in the equilibrium state at finite temperatures:

$$n_{\mathbf{p}} = \frac{1}{e^{\sqrt{\epsilon^2_{\mathbf{p}} + \Delta^2(T)}/T} + 1}. \tag{1.21}$$

Validity of the mean-field approach at finite temperatures requires that thermal fluctuations of the pairing amplitude $\Delta(T)$ are small. As we will see below, this requirement is not very restrictive, and the mean-field approach breaks down only in the narrow vicinity of the critical temperature.

The account of thermal distribution of the quasiparticles in the superfluid state leads to the modification of the self-consistency equation for the pairing amplitude at finite temperatures:

$$1 = \frac{\lambda}{2} \sum_{\mathbf{p}} \left(\frac{1 - 2n_{\mathbf{p}}}{\sqrt{\epsilon^2_{\mathbf{p}} + \Delta^2(T)}} - \frac{1}{\mathbf{p}^2/2m} \right), \tag{1.22}$$

where we used the same renormalization procedure as in Eq.(1.13).

The condition $\Delta(T_c) = 0$ defines the critical temperature T_c of the superfluid phase transition:

$$T_c = \gamma \Delta_0 / \pi, \tag{1.23}$$

where $\gamma = e^C$, and $C = 0.577$ is the Euler's constant.

The dependence of the pairing amplitude $\Delta(T)$ on the temperature is illustrated in two limiting cases of low and high temperatures. At low temperatures, the pairing amplitude approaches its maximal value

$$\Delta(T) = \Delta_0 \left(1 - \sqrt{\frac{2\pi T}{\Delta_0}} e^{-\Delta_0/T} \right), \quad T \ll \Delta_0, \tag{1.24}$$

while near the critical temperature it vanishes according to the 1/2 power-law:

$$\Delta(T) = 3.06\, T_c \sqrt{1 - \frac{T}{T_c}}, \quad T_c - T \ll T_c. \tag{1.25}$$

At temperatures close to critical, the free energy difference of the superfluid and normal states goes to zero:

$$F_S - F_N = -\frac{4\pi^2}{7\zeta(3)} \mathcal{V} \nu_0 T_c^2 \left(1 - \frac{T}{T_c} \right)^2, \quad T_c - T \ll T_c. \tag{1.26}$$

This result demonstrates that the superfluid state becomes less stable as one approaches the critical temperature, and thermal fluctuations of the pairing amplitude become more pronounced. There is a temperature range

$$\left| \frac{T - T_c}{T_c} \right| \simeq \left(\frac{T_c}{E_F} \right)^4, \tag{1.27}$$

where the fluctuations dominate, and the mean-field approach is not valid. In superconducting metals, this temperature range is usually very narrow, and the fluctuation dominated region is virtually non-existent. In this respect, cold Fermi gases with tunable interaction present new possibilities to explore the strongly interacting regime with high critical temperature, $T_c \lesssim E_F$, which leads to a wide fluctuation region.

1.2.5 BCS-BEC crossover theories

Cold Fermi gases with magnetically tunable interaction (1.1) allow to study the problem of crossover from the BCS limit of weakly interacting fermions to the Bose-Einstein condensation of diatomic molecules [9, 10, 11, 12, 13].

Let us consider the Hamiltonian (1.5) where the interaction constant λ can be tuned using the external magnetic field at a Feshbach resonance (see Eq.(1.1)). As the magnetic field approaches the resonance from the atomic side, the scattering length achieves large negative values, discontinuously changing the sign at the resonance. This situation in a different physical context has been first considered by Leggett in Ref. [29].

The important observation made in Ref. [29] is that Eqs.(1.13) and (1.16) for the pairing amplitude and the total number of particles originally derived in the case of weakly interacting gas, $\lambda\nu_0 \to 0$, give intuitively correct results also in the limit $\lambda\nu_0 \to +\infty$. The qualitative properties of the crossover [29, 30] can be understood using the characteristic size of Cooper pairs given in the BCS theory by the coherence length, ξ. By dimensional analysis it can be estimated as $\xi \simeq \hbar v_F/\Delta_0$ (see also Eq.(1.32) below). The limit of weak interaction corresponds to Cooper pairs with size larger than the interparticle distance, $\xi \gg n^{-1/3}$. Strong interactions make the coherence length smaller, eventually reaching the limit of tightly bound pairs, $\xi \ll n^{-1/3}$. Energy considerations [30] support this scenario. Indeed, once the attraction of fermions becomes stronger, a bound state of two fermions forms, and it is energetically favorable for the system to form a gas of tightly bound molecules.

The calculation of the critical temperature in the strongly interacting limit [30, 31, 32] demonstrates that the transition between two limits is smooth. In Refs. [31, 32], the approach of Refs. [29, 30] was modified to include the fluctuations over the mean-field solution. The conclusion was reached that at any given coupling there was a second order phase transition from normal to superfluid state with the critical temperature being a smooth function of the coupling strength.

1.3 Nonequilibrium superconductivity: review of different approaches

1.3.1 Time-dependent Ginzburg-Landau equation

Several approaches are used to study non-equilibrium phenomena in superconducting metals. We start with the description of the so-called time-dependent Ginzburg-Landau formalism [33, 34, 35] which is a generalization of the phenomenological Ginzburg-Landau (GL) theory of superconductivity [36].

The GL free energy of a superconductor at temperatures near critical, $1-T/T_c \ll 1$, is an expansion in terms of the order parameter:

$$\mathcal{F}_{GL} = \int dV \left\{ \alpha|\Delta|^2 + \frac{\beta}{2}|\Delta|^4 + \gamma\,|-i\hbar\,\partial_{\mathbf{r}}\Delta|^2 \right\}. \tag{1.28}$$

The phenomenological parameters α, β, and γ are found in the microscopic theory [37]:

$$\alpha = \nu_0 \frac{T-T_c}{T_c}, \quad \beta = \frac{7\zeta(3)\nu_0}{8\pi^2 T_c^2}, \quad \gamma = \frac{7\zeta(3)\nu_0 v_F^2}{48\pi^2 T_c^2}, \tag{1.29}$$

where α changes the sign at the critical temperature making the superfluid state with $\Delta \neq 0$ energetically favorable compared to normal state with $\Delta = 0$.

The minimization of the free energy $\delta\mathcal{F}_{GL}/\delta\Delta^* = 0$ leads to the Ginzburg-Landau equation for the order parameter:

$$\alpha\Delta + \beta|\Delta|^2\Delta + \gamma\left(-i\hbar\partial_{\mathbf{r}}\right)^2\Delta = 0. \tag{1.30}$$

As an example, we consider spatially homogeneous solution of this equation at $T \lesssim T_c$:

$$\Delta(T) = |\alpha|/\beta = 3.06\,T_c\,(1-T/T_c)^{1/2}, \tag{1.31}$$

which coincides with the result found in the previous section, Eq.(1.25).

The Ginzburg-Landau equation (1.30) allows to study spatially non-homogeneous situations. The scale of spatial variations of the order parameter is set by the coher-

ence length:

$$\xi = \sqrt{\gamma\hbar^2/|\alpha|} = 0.84\,\xi_0(1 - T/T_c)^{-1/2}, \tag{1.32}$$

where $\xi_0 = \hbar v_F/2\pi T_c$ is the "zero-temperature" coherence length.

The simplicity of the GL approach when main physical properties of the system are formulated in terms of one physical quantity, the order parameter, calls for a generalization to the case of non-equilibrium dynamics. According to the time-dependent Ginzburg-Landau (TDGL) theory [33, 34], the deviation of the superconducting state from the equilibrium is followed by the relaxation of the order parameter back to the equilibrium. It is assumed that the rate of relaxation is proportional to the deviation from the equilibrium:

$$-\Gamma\frac{\partial\Delta}{\partial t} = \frac{\delta\mathcal{F}_{GL}}{\delta\Delta^*}, \tag{1.33}$$

where Γ is a positive constant defined in the microscopic theory.

This gives the following nonlinear relaxation equation for the order parameter:

$$-\Gamma\frac{\partial\Delta}{\partial t} = \alpha\Delta + \beta|\Delta|^2\Delta + \gamma\left(-i\hbar\partial_{\mathbf{r}}\right)^2\Delta \tag{1.34}$$

The relaxation time of the order parameter $\tau_{rel} = \Gamma/|\alpha| \propto (1 - T/T_c)^{-1}$ diverges as one approaches the critical temperature. The microscopic value of the relaxation parameter, $\Gamma = \nu_0\pi\hbar/8T_c$, found in Refs. [33, 34]. It is important to notice that the original derivation of TDGL equation in Refs. [33, 34] in the case of clean superconductors is wrong. Gorkov and Eliashberg in Ref. [35] demonstrated that TDGL theory is applicable only in superconductors with paramagnetic impurities.

Introducing the correlation length ξ and the equilibrium order parameter Δ_∞ given by Eq.(1.31), we can rewrite this equation in a convenient form:

$$\tau_{rel}\frac{\partial\Delta}{\partial t} = \Delta - \frac{|\Delta|^2}{\Delta_\infty^2}\Delta + \xi^2\partial_{\mathbf{r}}^2\Delta. \tag{1.35}$$

The microscopic derivation of the TDGL equation (1.35) is a difficult problem, and here we only discuss its validity. First, there is a restriction that stems from the applicability of the Ginzburg-Landau free energy. It is valid for temperatures close

to the critical one, but outside of the fluctuations dominated region, i.e. $(T_c/E_F)^4 \ll 1 - T/T_c \ll 1$. Second, the TDGL theory employs the order parameter as the only dynamical variable, and therefore it is necessary that both the energy spectrum and the quasiparticle distribution remain the same as in equilibrium. For this to hold, the quasiparticle relaxation has to be fast compared to the order parameter dynamics. In clean superconductors, the spectrum of quasiparticles has the excitation gap at the Fermi energy, which coincides with the pairing amplitude. Thus, the relaxation time of the order parameter and the quasiparticle relaxation time in this case are expected to be of the same order of magnitude in contradiction to the main assumption of TDGL theory. Nonetheless, if mechanisms other than collisions of quasiparticles with one another are responsible for the quasiparticle relaxation, this approach can be justified [35]. In the case of gapless superconductors, in a narrow range of paramagnetic impurities concentrations, the excitation gap is destroyed, while the order parameter still exists preserving the superconductivity in the system. As shown by Gorkov and Eliashberg [35], in this case one can derive an analog of the TDGL equation (1.35).

1.3.2 Boltzmann kinetic equation

Another approach to the non-equilibrium dynamics in superconductors is based on the Boltzmann kinetic equation that considers processes of quasiparticle relaxation.

In equilibrium, the quantum state of a superconductor is described by the complex order parameter:

$$\Psi = \Delta\, e^{i\varphi}, \tag{1.36}$$

where the magnitude Δ is defined by the self-consistency equation (1.22) with the equilibrium quasiparticle distribution function $n_{\mathbf{p}}$ given in Eq.(1.21).

The quasiparticle spectrum retains its physical meaning in the case of external perturbation, provided that its spatial variations are large on the coherence length scale with frequencies smaller than the order parameter magnitude:

$$\hbar\omega \ll \Delta, \quad q\xi \ll 1, \tag{1.37}$$

where ω is the angular frequency, and q is the wave vector of the external perturbation. Under such conditions, the low-energy superfluid dynamics is governed by order parameter phase φ, while its magnitude, Δ, is defined by the self-consistency equation (1.22) with nonequilibrium quasiparticle distribution.

In this case, the quasiparticle energy spectrum changes:

$$\tilde{E}_{\mathbf{p}} = E_{\mathbf{p}} + \mathbf{p}_s \mathbf{v}, \quad E_{\mathbf{p}} = \sqrt{\tilde{\epsilon}_{\mathbf{p}}^2 + \Delta^2}, \tag{1.38}$$

where $\tilde{\epsilon}_{\mathbf{p}} = \epsilon_{\mathbf{p}} - \delta\mu$. Here, the chemical potential shift, $\delta\mu = -\Phi - \mathbf{p}_s^2/2m$, is caused by the time dependence of the order parameter phase, $\Phi = (\hbar/2)\partial\varphi/\partial t$, and its spatial variation encoded in the superfluid momentum, $\mathbf{p}_s = (\hbar/2)\nabla\varphi$.

The Boltzmann kinetic equation for the quasiparticle distribution function can be derived in the quasiclassical limit when conditions (1.37) are satisfied:

$$\frac{\partial n_{\mathbf{p}}}{\partial t} + \frac{\partial \tilde{E}_{\mathbf{p}}}{\partial \mathbf{p}} \frac{\partial n_{\mathbf{p}}}{\partial \mathbf{r}} - \frac{\partial \tilde{E}_{\mathbf{p}}}{\partial \mathbf{r}} \frac{\partial n_{\mathbf{p}}}{\partial \mathbf{p}} + I\{n_{\mathbf{p}}\} = 0, \tag{1.39}$$

where $I\{n_{\mathbf{p}}\}$ is the collision integral describing collisions of quasiparticles.

The solution of the kinetic equation (1.39) has to be supplemented by the self-consistency equation for the pairing amplitude Δ. It can be shown that this equation has the same form (1.22) with the non-equilibrium distribution function $n_{\mathbf{p}}$ found from Eq.(1.39).

The collision integral $I\{n_{\mathbf{p}}\}$ in superconducting metals takes into account collisions of quasiparticles with impurities, phonons and with one another. The quasiparticle interaction is of main importance in the case of cold gases. It was shown by Eliashberg [38], that there are two processes of this kind: the scattering of two quasiparticles, and collisions that involve the creation or absorption of two quasiparticles. Further analysis gives the following estimates for the relaxation times corresponding to these processes. At temperatures close to critical, the rate of quasiparticle collisions

is the same as in normal metals:

$$\tau_\epsilon^{-1} \simeq \frac{T_c^2}{\hbar E_F}. \tag{1.40}$$

At low temperatures $T \ll \Delta_0$, there are two different relaxation time scales:

$$\tau_\epsilon^{-1} \simeq \frac{\Delta_0^2}{\hbar E_F} x, \quad \tilde{\tau}_\epsilon^{-1} \simeq \frac{\Delta_0^2}{\hbar E_F} x^2, \tag{1.41}$$

where we introduced the so-called dimensionless concentration of the quasiparticles, $x = \sqrt{\pi T/2\Delta_0}\, e^{-\Delta_0/T}$, a small parameter in the low temperature expansion of the pairing gap in Eq.(1.24). For processes conserving the number of quasiparticles, the relaxation time is given by τ_ϵ, while slower processes involving absorption or creation of two quasiparticles are controlled by the time scale $\tilde{\tau}_\epsilon$. The quasiparticle relaxation according to Eqs.(1.41) at low temperatures is exponentially slow, and it reaches the limit of normal metal (1.40) at the critical temperature.

The limits of applicability of Eq.(1.39) are set by the quasiclassical conditions (1.37). In addition, a requirement that the self-consistency equation (1.22) is unchanged by the nonequilibrium processes leads to the following condition on the frequency of the external perturbation [35]:

$$\hbar\omega \ll \Delta^2/T_c, \tag{1.42}$$

which is more restrictive than $\hbar\omega \ll \Delta$ at temperatures close to critical.

1.3.3 Bogoliubov-de Gennes dynamical equations

Boltzmann kinetic approach employs the concept of quasiparticle spectrum which is well-defined at low frequencies and for small deviation of the order parameter from its equilibrium value. The TDGL theory formulated at temperatures close to critical assumes that the quasiparticle relaxation is infinitely fast, which is satisfied only for gapless superconductors [35]. The kinetic equation and TDGL approach do not overlap as one approaches critical temperature: the latter assumes that distribution function of quasiparticles does not deviate from its equilibrium value, while the former

implies that such deviations are important in the non-equilibrium dynamics.

Two most important time scales that control the dynamics in superconductors are the quasiparticle relaxation time τ_ϵ defined in Eqs.(1.40) and (1.41), and the characteristics time $\tau_\Delta \simeq \hbar/\Delta_0$ associated with the dynamics of the order parameter, where Δ_0 is the BCS instability growth rate [33, 34, 39].

The main part of this thesis is the study of a new regime in the pairing dynamics of the BCS theory of superconductivity in the limit $\tau_\Delta \ll \tau_\epsilon$ when the notion of the quasiparticle spectrum looses its meaning, and neither kinetic equation nor TDGL approach is applicable. We consider the case of large deviations of the order parameter with characteristic time scale $\tau_\Delta \simeq \hbar/\Delta_0$ at low temperatures. The quasiparticle relaxation is irrelevant on the time scales that are of main interest to us. In this case, on the relatively long time interval $0 < t \lesssim \tau_{\rm el}$ the dynamics of the individual Cooper pairs plays the dominant role [39, 40] while energy relaxation can be ignored.

To study this problem, it is necessary to consider the Bogoliubov-de Gennes equations without additional assumptions similar to quasiclassical approximation used to derive the Boltzmann kinetic equation (1.39).

The wave function appropriate for the study of nonequilibrium dynamics under such conditions is a generalization of the BCS wave function (1.7) to the case of Bogoliubov amplitudes $u_{\mathbf{p}}(t)$ and $v_{\mathbf{p}}(t)$ depending on time:

$$|\Phi(t)\rangle = \prod_{\mathbf{p}} \left(u_{\mathbf{p}}(t) + v_{\mathbf{p}}(t) a^+_{\mathbf{p}\uparrow} a^+_{-\mathbf{p}\downarrow}\right) |0\rangle. \tag{1.43}$$

The Bogoliubov mean field approach, which gives a state of the form (1.43), relies on the 'infinite range' form of the pairing interaction in (1.5) owing to equal coupling strength of all $(\mathbf{p}, -\mathbf{p})$, $(\mathbf{q}, -\mathbf{q})$. Since the latter does not depend on the system being in equilibrium, one can introduce a time-dependent mean field pairing function:

$$\Delta(t) = \lambda_0(t) \sum_{\mathbf{p}} u_{\mathbf{p}}(t) v^*_{\mathbf{p}}(t). \tag{1.44}$$

The amplitudes $u_{\mathbf{p}}(t)$, $v_{\mathbf{p}}(t)$ can be obtained from the Bogoliubov-de Gennes equations

$$i\partial_t \begin{pmatrix} u_{\mathbf{p}} \\ v_{\mathbf{p}} \end{pmatrix} = \begin{pmatrix} \epsilon_{\mathbf{p}} & \Delta \\ \Delta^* & -\epsilon_{\mathbf{p}} \end{pmatrix} \begin{pmatrix} u_{\mathbf{p}} \\ v_{\mathbf{p}} \end{pmatrix}, \tag{1.45}$$

solved together with the self-consistency condition (1.44).

1.4 Outline of the thesis

In Chapter 2, we study the pairing dynamics in the normal Fermi gas triggered by the abrupt change of the interaction with the short switching time $\tau_0 \ll \tau_\Delta \ll \tau_\epsilon$. This situation formally corresponds to the time dependent interaction constant $\lambda_0(t)$ in the BCS Hamiltonian (1.5). Since the initial state of the normal Fermi gas and the BCS ground state after the switch have vanishing overlap, the system enters the non-adiabatic evolution. The time domain picture of BCS pairing buildup involves dynamics of individual pair states, self-consistently coupled to the pairing amplitude. On a time scale controlled by the quasiparticle relaxation time, the pairing amplitude is found to be an oscillatory function of time with predictable characteristics. The interplay of linear instability of the unpaired state and nonlinear interactions selects periodic soliton trains, described by the Jacobi elliptic function dn.

Cold Fermi gas at a Feshbach resonance is a promising candidate for the observation of the pairing dynamics. At the resonance, fermions coupled to molecules are unstable with respect to formation of a mixed state. In Chapter 3, we exploit the mapping of this system to the Dicke model to study the phase diagram and the non-adiabatic dynamics of the molecular field. The results are accurate in the strong coupling regime relevant for current experimental efforts.

To observe the pairing dynamics one needs a method of detection of the correlations in the Fermi gas. In Chapter 4, we develop a theory of the dynamical atom/molecule projection recently used to probe fermion pairing at a Feshbach resonance [16, 17]. An exact solution is found, predicting a 1/3 power law for molecule production efficiency at fast sweep. The results for s- and p-wave resonances are ob-

tained and compared. The predicted production efficiency agrees with experimental observations for both condensed and incoherent molecules away from saturation.

The information about the pairing gap can be extracted from the excitation spectrum. In Chapter 5, we consider cold Fermi gas subject to a magnetic detuning modulation at a Feshbach resonance. The rates of stimulated molecule dissociation and atom pair excitations are found as a function of excitation frequency and the detuning. The theory is applied to the experimental situation of Ref. [15]. The main features reported in Ref. [15] are reproduced using one-body picture with strong coupling of molecular and atomic level. It is shown that pairing in Fermi gas leads to a singularity in the excitation spectrum depending on the detuning.

Chapter 2

Pairing dynamics of cold fermions

2.1 Introduction

In this Chapter, we explore the pairing dynamics of cold fermions in the situation when BCS interaction is a function of time. As we discussed in the previous Chapter, there are three physical time scales that define the dynamical regime of pairing in cold Fermi gas. The switching time τ_0 of the interaction at a Feshbach resonance is related to the external magnetic field. The other two time scales are the quasiparticle relaxation time τ_ϵ given in Eqs.(1.40) and (1.41), and also the characteristic time $\tau_\Delta \simeq \hbar/\Delta_0$ associated with the dynamics of the order parameter, where Δ_0 is the BCS instability growth rate [33, 34, 39].

The dynamical regimes are classified according to the relation between these time scales. In the case when the switching time is much larger than both the pairing amplitude time scale and the quasiparticle relaxation time, $\max(\tau_\Delta, \tau_\epsilon) \ll \tau_0$, the system smoothly changes its state in the thermal equilibrium with the instantaneous Hamiltonian. Another situation, $\tau_\Delta \ll \tau_0 \ll \tau_\epsilon$, corresponds to the adiabatic dynamics of the system out of the thermal equilibrium at each moment of time. In the following, we will be interested in the regime when the switching time is shorter than the pairing amplitude time scale, $\tau_0 \ll \tau_\Delta \ll \tau_\epsilon$. This corresponds to the collisionless and non-adiabatic dynamics.

Cold Fermi gases are very promising for the observation of this new regime in

the pairing dynamics. The external parameters that control the interaction in these systems, such as the detuning from the Feshbach resonance, can be changed on a time scale shorter then the characteristic time scale of the pairing dynamics and the quasiparticle relaxation time.

One of the possible ways to stimulate the pairing dynamics may be realized on the atomic side of the Feshbach resonance using fast magnetic field sweep toward the resonance from some initial state. Assuming that initial and final detunings from the resonance are chosen such that the initial temperature is lower than the critical temperature in the final state, one may expect that the BCS pairing instability starts to develop after the sweep. The pairing dynamics can be observed experimentally using a method of fast magnetic field projection discussed in Chapter 4.

To assess validity of this picture in the current experiments in cold Fermi gases, we now estimate the energy scales corresponding to the pairing dynamics. The currently studied systems [16, 17, 18] are described by the non-retarded BCS pairing theory [28] which predicts $T_c \approx 0.3 E_F e^{-1/\lambda}$, $\lambda = \frac{2}{\pi} k_F |a|$, with the scattering length a having a resonance dependence (1.1) on the external magnetic field [6, 7]. To estimate the BCS parameter values, we consider magnetic fields not too close to the resonance where one can neglect the presence of the molecular field (Ref. [10, 11] and also Chapter 3) and use the weak coupling theory. At particle density $n \approx 1.8 \times 10^{13}\, cm^{-3}$ [16], which corresponds to $E_F \approx 0.35\,\mu$K, and the scattering length $a \approx -50\,$nm we obtain $T_c \approx 0.01 E_F$. Estimate of the dynamical time obtains $\tau_\Delta \simeq \hbar/\Delta_0 \approx 2\,$ms, while the quasiparticle energy relaxation time is $\tau_{\epsilon\sim\Delta} \simeq \hbar E_F/\Delta_0^2 \approx 200\,\text{ms} = 100\tau_\Delta$, consistent with weakly damped oscillations of Δ.

For simplicity, we focus on the case of a gas sample size smaller than BCS correlation length $\xi = \hbar^2 k_F/m\Delta_0$ (for the parameters listed above, $\xi \simeq 24\,\mu$m is in excess of the gas sample size [16] $L \approx 18\,\mu$m). In the 'zero-dimensional' limit $\xi \simeq L$ one can ignore aspects related with spatial dependence, such as inhomogeneous phase fluctuations and vortices.

This Chapter is organized as follows. In Section 2.2, the BCS pairing instability of the Fermi gas is analyzed at finite temperatures. Then in Section 2.3, the Bloch

equations governing the pairing dynamics are derived and their stationary states are discussed. The combination of analytic and numerical methods is used to study the nonlinear pairing dynamics in Section 2.4. The effect of the thermal noise in the initial conditions on the nonlinear pairing dynamics is discussed in Section 2.5. Spin-1/2 formulation of the problem is presented in Section 2.6. We summarize our results in Section 2.7. To provide further details, we conclude this Chapter with Appendix A discussing the relation between the Bloch and the Bogoliubov-de Gennes equations, and Appendix B containing the presentation of our numerical method and the code used to simulate the dynamics.

2.2 BCS instability of the unpaired Fermi gas

The evolution of the Fermi gas with time-varying pairing coupling can be described by the BCS Hamiltonian

$$\mathcal{H} = \sum_{\mathbf{p},\sigma} \epsilon_{\mathbf{p}} a^{+}_{\mathbf{p}\sigma} a_{\mathbf{p}\sigma} - \lambda(t) \sum_{\mathbf{p},\mathbf{q}} a^{+}_{\mathbf{p}\uparrow} a^{+}_{-\mathbf{p}\downarrow} a_{-\mathbf{q}\downarrow} a_{\mathbf{q}\uparrow} , \tag{2.1}$$

where $a_{\mathbf{p}\sigma}$, $a^{+}_{\mathbf{p}\sigma}$ are the canonical fermion operators, and $\sigma = \uparrow, \downarrow$ is generalized spin. The time dependence of λ, as well as the resulting time dependence of the system state, is assumed to be fast on the scale of quasiparticle elastic collisions and energy relaxation, τ_{el}, allowing us to ignore the latter and consider the coherent dynamics defined by (2.1). The simplest time dependence which we shall be most interested in, is described by the coupling turned on abruptly, from $\lambda(t<0) = 0$ to $\lambda(t>0) = \lambda$.

Our treatment of the problem (2.1) will focus on the time-dependent generalization of the BCS state

$$|\Psi(t)\rangle = \prod_{\mathbf{p}} \left(u_{\mathbf{p}}(t) + v_{\mathbf{p}}(t) a^{+}_{\mathbf{p},\uparrow} a^{+}_{-\mathbf{p},\downarrow} \right) |0\rangle. \tag{2.2}$$

The Bogoliubov mean field approach, which gives a state of the form (2.2), relies on the 'infinite range' form of the pairing interaction in (2.1) owing to equal coupling strength of all $(\mathbf{p}, -\mathbf{p})$, $(\mathbf{q}, -\mathbf{q})$. Since the latter does not depend on the system being

in equilibrium, one can introduce a time-dependent mean field pairing function

$$\Delta(t) = \lambda \sum_{\mathbf{p}} u_{\mathbf{p}}(t) v^*_{\mathbf{p}}(t). \tag{2.3}$$

The amplitudes $u_{\mathbf{p}}(t)$, $v_{\mathbf{p}}(t)$ can be obtained from the Bogoliubov-de Gennes equation

$$i\partial_t \begin{pmatrix} u_{\mathbf{p}} \\ v_{\mathbf{p}} \end{pmatrix} = \begin{pmatrix} \epsilon_{\mathbf{p}} & \Delta \\ \Delta^* & -\epsilon_{\mathbf{p}} \end{pmatrix} \begin{pmatrix} u_{\mathbf{p}} \\ v_{\mathbf{p}} \end{pmatrix}, \tag{2.4}$$

solved together with the self-consistency condition (2.3).

We recall that the unpaired state is a self-consistent, albeit unstable, solution of Eqs. (2.3),(2.4) with $\Delta = 0$, $T = 0$:

$$u^{(0)}_{\mathbf{p}}(t) = e^{-i\epsilon_{\mathbf{p}} t}\theta(\epsilon_{\mathbf{p}}), \quad v^{(0)}_{\mathbf{p}}(t) = e^{i\varphi_{\mathbf{p}}} e^{i\epsilon_{\mathbf{p}} t}\theta(-\epsilon_{\mathbf{p}}), \tag{2.5}$$

with $\varphi_{\mathbf{p}}$ a random phase. The stability analysis [34] shows that the deviation from the unpaired state grows as $\Delta(t) \propto e^{\gamma t} e^{-i\omega t}$, with linearized amplitudes

$$\delta u_{\mathbf{p}}(t) = \frac{\Delta(t) v^{(0)}_{\mathbf{p}}(t)}{i\gamma - 2\epsilon_{\mathbf{p}} + \omega}, \quad \delta v_{\mathbf{p}}(t) = \frac{\Delta^*(t) u^{(0)}_{\mathbf{p}}(t)}{i\gamma + 2\epsilon_{\mathbf{p}} - \omega}. \tag{2.6}$$

The growth exponent γ and the constant ω, combined into a complex number $\zeta = \omega + i\gamma$, are defined by the self-consistency condition of the linearized problem:

$$1 = \lambda \sum_{\mathbf{p}} \frac{\operatorname{sgn} \epsilon_{\mathbf{p}}}{2\epsilon_{\mathbf{p}} - \zeta}. \tag{2.7}$$

This equation has a pair of complex conjugate solutions ζ, ζ^*. From the similarity between Eq. (2.7) and the BCS gap equation one expects the exponent γ to be close to the BCS gap value Δ_0 in equilibrium, in which case the time constant $\tau_\Delta = \gamma^{-1}$ for initial pairing buildup is of the order of Δ_0^{-1}.

It will be convenient for us to introduce here the constant density of states ap-

proximation,

$$\nu(\epsilon_{\mathbf{p}}) = \begin{cases} \nu_0, & |\epsilon_{\mathbf{p}}| < \frac{1}{2}W \\ 0, & \text{else} \end{cases}, \tag{2.8}$$

used throughout this Chapter. In our numerical study we use a total $N \gg 1$ equally spaced discrete states distributed evenly in a finite size band,

$$-W/2 \leq \epsilon_{\mathbf{p}} \leq W/2, \tag{2.9}$$

with the level spacing $\delta\epsilon = W/N$. Although somewhat artificial, the model (2.9) introduces a convenient simplification due to the particle-hole symmetry. In this case, the chemical potential is locked at $\epsilon = 0$ independent of the interaction strength. As a result, the instability problem (2.15) possesses an eigenvalue with a purely imaginary $\zeta = i\gamma$, satisfying

$$1 = \lambda \sum_{\mathbf{p}} \frac{2|\epsilon_{\mathbf{p}}|}{4\epsilon_{\mathbf{p}}^2 + \gamma^2}, \tag{2.10}$$

and $\omega = 0$. Interestingly, if the bandwidth W is much larger than the BCS gap Δ_0 at $T = 0$, the value of the exponent γ obtained from (2.7) coincides with Δ_0. Indeed, Eq.(2.10) in this case gives

$$1 = 2\lambda\nu_0 \int_0^{W/2} \frac{2\epsilon d\epsilon}{4\epsilon^2 + \gamma^2} = \frac{1}{2}\lambda\nu_0 \ln \frac{W^2 + \gamma^2}{\gamma^2} \tag{2.11}$$

This equation is reminiscent of the BCS gap equation

$$1 = \frac{1}{2}\lambda \int_{-W/2}^{W/2} \frac{d\epsilon}{\sqrt{\epsilon^2 + \Delta_0^2}} = \lambda\nu_0 \sinh^{-1} \frac{W}{2\Delta_0},$$

becoming identical to it in the weak coupling limit of fermion energy band wide compared to the gap, $W \gg \gamma, \Delta_0$ [*cf.* Eq.(2.37) below]. The condition $\omega = 0$ is violated in the absence of particle-hole symmetry. The equality $\gamma = \Delta_0$ holds only at $T = 0$.

Let us briefly discuss how the analysis is modified in the case of a discrete spectrum (2.9). With the sum in Eq.(2.7) running over N levels, we obtain a polynomial of

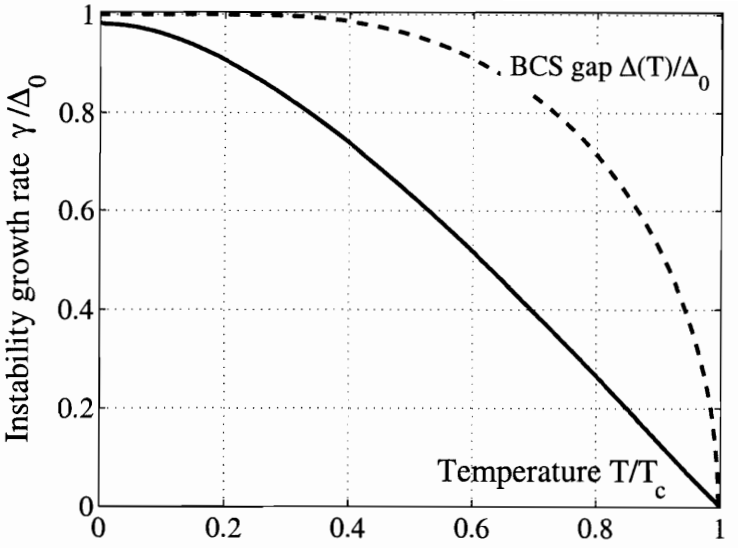

Figure 2-1: Temperature dependence of the BCS instability growth rate γ as obtained from Eq.(2.15) for the constant density of states model (2.8), (2.9) with the coupling λ such that $\Delta_0/W = 1/5$. Note that γ coincides with the BCS gap Δ_0 at $T = 0$, up to a correction small as $(\gamma/W)^2$ at large bandwidth W. Near $T_c = \pi e^{-C}\Delta_0 \simeq 1.764\Delta_0$, the exponent γ vanishes linearly in $T_c - T$.

order N, having total N roots. Simple analysis shows that $N-2$ roots are real and the remaining two are a complex conjugate pair ζ, ζ^* with values close to that obtained for continuous spectrum. Accordingly, only the normal modes corresponding to ζ, ζ^* are relevant for the instability, while the other $N-2$ modes correspond to the perturbations which do not grow and remain small. This conclusion is valid only at the times described by the linearized BCS dynamics. The situation at longer times, which is more delicate, will be discussed below.

Let us now consider the instability at finite temperature. The initial state describing Fermi gas at $T > 0$ can be tentatively chosen as

$$\prod_{\mathbf{p}} \left(u_{\mathbf{p}} + c_{\mathbf{p}} a^+_{\mathbf{p},\uparrow} + c'_{\mathbf{p}} a^+_{-\mathbf{p},\downarrow} + v_{\mathbf{p}} a^+_{\mathbf{p},\uparrow} a^+_{-\mathbf{p},\downarrow}\right) |0\rangle, \tag{2.12}$$

where $u_{\mathbf{p}}$, $c_{\mathbf{p}}$, $c'_{\mathbf{p}}$, $v_{\mathbf{p}}$ equal zero or one depending on the occupancy: $(u_{\mathbf{p}}, c_{\mathbf{p}}, c'_{\mathbf{p}}, v_{\mathbf{p}}) =$

$(1,0,0,0),...,(0,0,0,1)$. The average values are given by occupation probabilities:

$$\overline{|u_{\mathbf{p}}|^2}=(1-n_{\mathbf{p}})^2,\quad \overline{|v_{\mathbf{p}}|^2}=n_{\mathbf{p}}^2,\quad \overline{|c_{\mathbf{p}}|^2}=\overline{|c'_{\mathbf{p}}|^2}=n_{\mathbf{p}}(1-n_{\mathbf{p}}),$$

where $n_{\mathbf{p}}=1/(e^{\beta\epsilon_{\mathbf{p}}}+1)$ is the Fermi function, and the quantities $n_{\mathbf{p}}^2$, $n_{\mathbf{p}}(1-n_{\mathbf{p}})$ and $(1-n_{\mathbf{p}})^2$ describe double, single and zero occupancy probability of the two-fermion states $(\mathbf{p},-\mathbf{p})$ in the unpaired system. As we argue below, while the product state (2.12), written as a finite temperature generalization of (2.2), is not the most general fermion state, it is adequate for our problem.

The product state (2.12) is suitable for simulation, since Bogoliubov-de Gennes dynamics (2.4) couples only $u_{\mathbf{p}}$ and $v_{\mathbf{p}}$ independently for each $\mathbf{p}$, preserving the product form. At the same time, the parts of (2.12) with single occupancy are decoupled from the collisionless pair dynamics (2.1). Indeed, the Hamiltonian (2.1) gives zero when applied to singly occupied pair states $a^+_{\mathbf{k}\uparrow}|0\rangle$, $a^+_{-\mathbf{k}\downarrow}|0\rangle$, irrespective of the occupancy of other pair states. One can thus identify a subspace in the full Hilbert space, which is spanned by all combinations of pair states of occupancy zero and two. The latter have the form

$$|\psi\rangle_{\text{general}}=\prod_{\mathbf{k}}{}' a^+_{\mathbf{k}\uparrow}a^+_{-\mathbf{k}\downarrow}|0\rangle, \tag{2.13}$$

with the product taken over the states $(\mathbf{k},-\mathbf{k})$ of occupancy two whereby the states of occupancy one are excluded from the vacuum $|0\rangle$. The states (2.13) are mapped by (2.1) onto the states of a similar form, thereby defining a full representation of the Hamiltonian.

Fortunately, one can bypass the combinatorics of (2.13) and simplify the state by employing Bogoliubov mean field approach which is exact for the Hamiltonian (2.1). In the mean field framework, the general state is replaced by a product state. Indeed, since the pairing amplitude $\Delta(t)$, describing cumulative effect of all pairs, is a c-number, the dynamics (2.4) does not generate correlations between different pair states. At the same time, any correlations present at $t=0$ are dephased by the dynamics itself, described by time-dependent 2×2 evolution matrices, different for each pair $(\mathbf{p},-\mathbf{p})$. This argument, which will be refined in Sec.2.6, allows to

replace the general states (2.13) by a simpler state of the product form (2.12) with $c_{\mathbf{p}} = c'_{\mathbf{p}} = 0$. On a mean field level, the correlations between different $(\mathbf{p}, -\mathbf{p})$, $(\mathbf{k}, -\mathbf{k})$ do not matter.

The effect of Pauli blocking which eliminates the states of occupancy one can be taken into account by going back to the $T = 0$ state (2.2) with $u_{\mathbf{p}}$ and $v_{\mathbf{p}}$ chosen as

$$u^{(0)}_{\mathbf{p}}(t) = e^{-i\epsilon_{\mathbf{p}}t}(1 - n_{\mathbf{p}}), \quad v^{(0)}_{\mathbf{p}}(t) = e^{i\varphi_{\mathbf{p}}}e^{i\epsilon_{\mathbf{p}}t}n_{\mathbf{p}}, \tag{2.14}$$

with random phase $\varphi_{\mathbf{p}}$. The reduced norm $|u_{\mathbf{p}}|^2 + |v_{\mathbf{p}}|^2 = n^2_{\mathbf{p}} + (1 - n_{\mathbf{p}})^2 < 1$ reflects that at finite temperature some pair states, populated by just one particle, are decoupled from the dynamics. Near the Fermi level, at $|\epsilon_{\mathbf{p}}| \ll T$, the two-particle states with double or zero occupancy have the probability 1/4 each, so that $|u_{\mathbf{p}}|^2 + |v_{\mathbf{p}}|^2 = 1/2$. Outside this interval, $|\epsilon_{\mathbf{p}}| \geq T$, the blocking is practically absent and the norm approaches one. Below we shall use the state (2.2) with $u_{\mathbf{p}}$, $v_{\mathbf{p}}$ given by (2.14) as initial condition for the simulation.

The choice (2.14), while somewhat *ad hoc*, has an additional advantage over choosing $u_{\mathbf{p}} = 1, 0$, $v_{\mathbf{p}} = 0, 1$. With both $u_{\mathbf{p}}$ and $v_{\mathbf{p}}$ nonzero with random relative phase, the state (2.2) exhibits pairing fluctuations, providing a "seed" for the BCS instability in the simulation. The results of the latter indicate that this choice of the initial state is general enough for the instability to fully play out. As we shall see in Sec.2.6, where a spin 1/2 formulation of BCS dynamics is discussed, $u_{\mathbf{p}}$ and $v_{\mathbf{p}}$ can be understood as a two-component spinor. This means that the state of the entire system can indeed be chosen in the product form, with the initial values $u_{\mathbf{p}}$, $v_{\mathbf{p}}$ having random modulus, not just phase. This difference, however, is inessential, since the modulus of $u_{\mathbf{p}}$, $v_{\mathbf{p}}$ is quickly randomized by the dynamics itself.

Returning to the analysis of the instability, linearization of (2.4) over the finite temperature state (2.14) obtains a time-dependent perturbation of the form Eq.(2.6), and a generalization of Eq.(2.7), with $\operatorname{sgn}\epsilon_{\mathbf{p}}$ replaced by

$$\overline{|u^{(0)}_{\mathbf{p}}|^2} - \overline{|v^{(0)}_{\mathbf{p}}|^2} = 1 - 2n_{\mathbf{p}} = \tanh\frac{1}{2}\beta\epsilon_{\mathbf{p}}.$$

The resulting equation,

$$1 = \lambda \sum_{\mathbf{p}} \frac{1 - 2n_{\mathbf{p}}}{2\epsilon_{\mathbf{p}} - \zeta}, \quad \Delta(t) \propto e^{-i\zeta t}, \tag{2.15}$$

has nonzero solutions ζ, ζ^* below the BCS transition, $T < T_c$, which are purely imaginary, $\zeta, \zeta^* = \pm i\gamma$, in the case of particle-hole symmetry (2.8), (2.9). The growth exponent γ vanishes as $T \to T_c$, as shown in Fig.2-1. This can be verified by noting that Eq.(2.15) yields infinitesimally small γ at $T = T_c$, since at $\zeta = 0$ it becomes identical to the BCS equation for T_c.

Having established the form of the unstable mode (2.6) obtained from linearization, let us now estimate the time range for which this analysis is accurate. The denominator in Eq.(2.6) is larger than the numerator as long as $\Delta(t) \lesssim \gamma$, with $\gamma \approx \Delta(T)$, the BCS gap. The initial value $\eta = \Delta(t = 0)$, nonzero due to fluctuations in the unpaired Fermi system, is small in $1/N$:

$$\eta = \lambda \sum_{\mathbf{p}} u_{\mathbf{p}} v_{\mathbf{p}}^* = \lambda \sum_{\mathbf{p}} n_{\mathbf{p}}(1 - n_{\mathbf{p}}) e^{i\varphi_{\mathbf{p}}}. \tag{2.16}$$

The sum (2.16) is controlled by about $T/\delta\epsilon$ terms with $|\epsilon_{\mathbf{p}}| \lesssim T$, uncorrelated in phase. From the central limit theorem argument, we estimate $\eta \simeq \lambda\nu\sqrt{T\delta\epsilon}$ by order of magnitude. The condition $\Delta(t) \lesssim \gamma$, with exponentially growing $\Delta(t) = \eta e^{\gamma t}$, defines the time interval $0 < t \lesssim \gamma^{-1} \ln(\gamma/\eta)$ in which the evolution is described by the linearized problem.

Our aim will be to gain insight in the behavior at later times. We rely on the nondissipative character of the Bogoliubov-de Gennes dynamics (2.4),(2.3), manifest, for instance, in the energy $E = \langle \Psi(t)|\mathcal{H}|\Psi(t)\rangle$ conservation throughout the evolution. Since for the unpaired state the energy exceeds its value in the ground state by the BCS condensation energy, the equilibrium cannot be reached without collisions. Eqs. (2.4),(2.3) hold at times shorter than quasiparticle thermalization time $\tau_{\rm el}$. For temperatures away from T_c, the time $\tau_{\rm el}$, evaluated at $\epsilon \simeq \Delta_0$, is long compared to

the instability growth time,

$$\tau_{\rm el} \gg \gamma^{-1}. \tag{2.17}$$

This means that the linear instability phase is followed by a long *collisionless nonlinear phase*. Below we show that the evolution governed by Eqs. (2.4),(2.3) is described by soliton-like pulses in $\Delta(t)$. We obtain a family of exact solutions of the form of single solitons and soliton trains, and compare it with simulations.

We briefly note that the importance of coherent dynamics of individual Cooper pairs (2.2) in the time evolution of a paired state has been understood a long time ago in the context of the discussion of the validity of the time-dependent Ginzburg-Landau equation approach [33, 34, 35]. It has been pointed out by Gorkov and Eliashberg [35] that the time-dependent pairing function Δ is generally insufficient to describe the evolution. For such a description to be consistent, the pair breaking and energy relaxation must be fast compared to the time scale τ_Δ of change of Δ. This can be realized only close enough to the transition, or in superconductors with magnetic impurities [35], where the inequality (2.17) is violated. Except these special situations, however, the Cooper pairs *are not slaved* to the time-dependent $\Delta(t)$, and the dynamics of each pair has to be treated individually, via Eq. (2.4).

2.3 Bogoliubov-de Gennes equation as a Bloch equation

To analyze the nonlinear BCS dynamics we reformulate the Bogoliubov approach, bringing it to a form amenable to analytic and numerical treatment. We show that the evolution of time-dependent amplitudes $u_{\mathbf{p}}(t)$, $v_{\mathbf{p}}(t)$, governed by the Bogoliubov-de Gennes equation (2.4) with the self-consistency condition (2.3), can be cast in the form of a Bloch equation for auxiliary variables. This is achieved by by introducing a new set of variables,

$$f_{\mathbf{p}} = 2u_{\mathbf{p}}v_{\mathbf{p}}^*, \quad g_{\mathbf{p}} = |u_{\mathbf{p}}|^2 - |v_{\mathbf{p}}|^2. \tag{2.18}$$

Applied to the quantities (2.18), Eq.(2.4) gives a system of coupled equations:

$$\frac{df_{\mathbf{p}}}{dt} = -2i\epsilon_{\mathbf{p}} f_{\mathbf{p}} + 2i\Delta g_{\mathbf{p}}, \quad \frac{dg_{\mathbf{p}}}{dt} = i\Delta^* f_{\mathbf{p}} - i\Delta f_{\mathbf{p}}^*. \tag{2.19}$$

These are nothing but the Gorkov equations [41] for the Green's functions G and F. In the form (2.19), using momentum-dependent quantities $f_{\mathbf{p}}$, $g_{\mathbf{p}}$, these equations were first written by Volkov and Kogan [40].

The dynamics (2.19) is to be supplemented by the Gorkov self-consistency relation [41],

$$\Delta = \frac{\lambda}{2} \sum_{\mathbf{p}} f_{\mathbf{p}}, \tag{2.20}$$

which defines $\Delta(t)$ through the values of evolving $f_{\mathbf{p}}(t)$. The initial conditions

$$f_{\mathbf{p}}^{(0)} = 2e^{i\varphi_{\mathbf{p}}}(1 - n_{\mathbf{p}})n_{\mathbf{p}}, \quad g_{\mathbf{p}}^{(0)} = 1 - 2n_{\mathbf{p}}, \tag{2.21}$$

correspond to the unpaired Fermi gas state (2.14).

To gain insight in the behavior of Eqs.(2.19), it will be convenient to introduce the Bloch representation

$$\mathbf{r}_{\mathbf{p}} = (r_1, r_2, r_3)_{\mathbf{p}}, \quad r_1 + ir_2 = f_{\mathbf{p}}, \quad r_3 = g_{\mathbf{p}}. \tag{2.22}$$

The norm of $\mathbf{r}_{\mathbf{p}}$ is given by

$$|\mathbf{r}_{\mathbf{p}}| = \sqrt{|f_{\mathbf{p}}|^2 + g_{\mathbf{p}}^2} = n_{\mathbf{p}}^2 + (1 - n_{\mathbf{p}})^2. \tag{2.23}$$

Remarkably, after rewriting Eq.(2.19) in terms of $\mathbf{r}_{\mathbf{p}}$, it assumes the form of a Bloch equation:

$$\frac{d\mathbf{r}_{\mathbf{p}}}{dt} = 2\mathbf{b}_{\mathbf{p}} \times \mathbf{r}_{\mathbf{p}}, \tag{2.24}$$

where the "magnetic field" $\mathbf{b}_{\mathbf{p}} = -(\Delta', \Delta'', \epsilon_{\mathbf{p}})$ has time-dependent x and y component satisfying the self-consistency condition (2.20). The norm of the Bloch vectors $\mathbf{r}_{\mathbf{p}}$, given by Eq.(2.23), is less than one, which describes the effect of Pauli blocking, i.e.

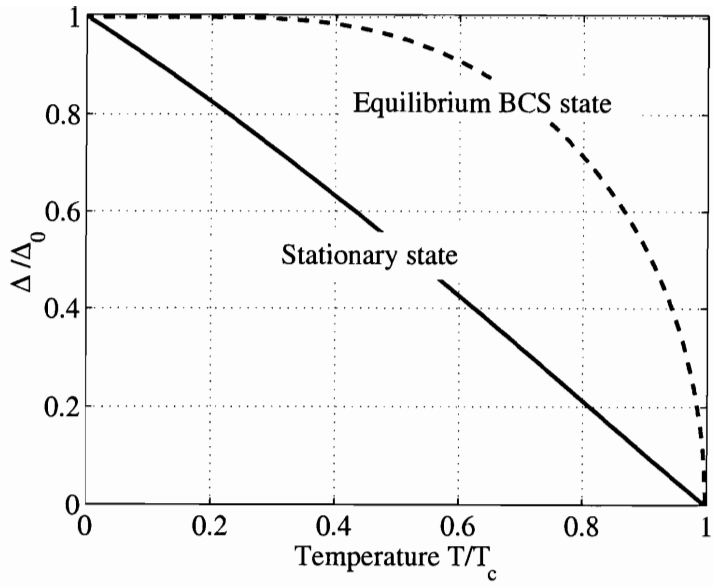

Figure 2-2: Temperature dependence of the pairing amplitude Δ for the stationary state (2.25), (2.26) obtained from the unpaired state by adiabatic increase of coupling. The equilibrium BCS gap is shown for comparison.

decoupling of the states with single occupancy from the BCS dynamics (see Sec.2.2).

Before exploring the dynamics, let us inspect the stationary states of Eq.(2.24). The latter are described by the Bloch spins aligned with the magnetic field axis, $\mathbf{l_p} = -\mathbf{b_p}/|\mathbf{b_p}|$. In this case we have

$$(l_1 + il_2)_{\mathbf{p}} = \frac{\Delta}{\sqrt{\epsilon_{\mathbf{p}}^2 + |\Delta|^2}}, \quad l_{3,\mathbf{p}} = \frac{\epsilon_{\mathbf{p}}}{\sqrt{\epsilon_{\mathbf{p}}^2 + |\Delta|^2}}, \tag{2.25}$$

and the self-consistency condition (2.20), which determines the stationary value of Δ, takes the form

$$1 = \frac{\lambda}{2} \sum_{\mathbf{p}} \frac{\tanh \frac{1}{2}\beta|\epsilon_{\mathbf{p}}|}{\sqrt{\epsilon_{\mathbf{p}}^2 + |\Delta|^2}}. \tag{2.26}$$

The numerator, $\tanh(\frac{1}{2}\beta|\epsilon_{\mathbf{p}}|) = |1-2n_{\mathbf{p}}|$, is the length of the Bloch vector $\bar{\mathbf{r}}_{\mathbf{p}}$ *averaged* over a group of levels with nearly equal energies, $|\epsilon_\alpha - \epsilon_\beta| \ll \Delta$. The averaging, applied to the initial $\mathbf{r_p}$ values (2.21), eliminates the transverse part of (2.21), containing random phases $\theta_{\mathbf{p}}$, while leaving the longitudinal part intact. The Bloch dynamics is

unitary with respect to each Bloch vector $\mathbf{r_p}$ and, in particular, is linear and preserves the norm. As a result, the averaged vectors $\bar{\mathbf{r}}_\mathbf{p}$ will evolve according to the same Bloch equations, albeit having a smaller norm $|\bar{\mathbf{r}}_\mathbf{p}| = |1 - 2n_\mathbf{p}| < |\mathbf{r_p}|$.

The equation (2.26) is different from the BCS gap equation which contains $\tanh(\frac{1}{2}\beta(\epsilon_\mathbf{p}^2 + \Delta^2)^{1/2})$ instead of $\tanh(\frac{1}{2}\beta|\epsilon_\mathbf{p}|)$, except $T = 0$, when these equations coincide since $\tanh = \pm 1$ in both cases. Thus at temperatures $0 < T < T_c$, as Fig.2-2 illustrates, Eq.(2.26) predicts the stationary value of Δ below the BCS gap scale. The temperature at which Δ vanishes coincides with the BCS critical temperature, since the condition (2.26) at $\Delta = 0$ is identical to the BCS equation for T_c.

To clarify the character of the states (2.25), (2.26), one can make the following observations. The only difference here from the BCS theory is due to incomplete equilibrium, owing to the singly occupied states being Pauli-blocked from the dynamics controlled by (2.1). Indeed, the truncated BCS Hamiltonian (2.1) accounts only for the collisionless pair dynamics, but not for single particle scattering and relaxation. The latter processes have characteristic rates set by the two-particle collisions, $1/\tau_{\rm el}$. Since $\tau_{\rm el}$ is larger than $\tau_\Delta = \gamma^{-1}$, the approach accounting only for the coherent dynamics, but not for relaxation, is valid in a relatively large time interval $0 < t \lesssim \tau_{\rm el}$.

The stationary nonequilibrium states (2.25), (2.26) can be realized when the coupling constant λ increases as a function of time slowly on the scale of τ_Δ, i.e. the condition $\tau_0 \ll \tau_\Delta$ is replaced by

$$\tau_\Delta \ll \tau_0 \ll \tau_{\rm el}.$$

In this case, each Bloch vector $\mathbf{r_p}$ follows the direction of the field $\mathbf{b_p}(t)$, maintaining constant projection on the $\mathbf{b_p}(t)$ axis equal to $1 - 2n_\mathbf{p}$ on average. During the evolution, the value $\Delta(t)$ is determined by the self-consistency condition (2.20). The amplitudes of the pair states with occupancy zero and two thereby become slaved to the adiabatic dynamics $\Delta(t)$, evolving according to (2.25), (2.26). At the same time, the amplitudes with occupancy one remain decoupled, and do not evolve at times

$t < \tau_{\rm el}$. Such a behavior can be seen as a result of the evolution which is simultaneously adiabatic in the pair sector, and totally nonadiabatic in the single particle sector.

2.4 Oscillatory solutions, analytical and numerical

Here we consider the nonlinear BCS dynamics described by the Bloch equation (2.24) and the self-consistency relation (2.20) at the times after the instability sets in. Eq. (2.24) is quite easy to simulate, since it is linear in $\mathbf{r_p}$ and is written for classical, rather than quantum variables. The initial state, Eq.(2.21), describing free fermions at a finite temperature, is

$$r_{1,\mathbf{p}}+ir_{2,\mathbf{p}} = \frac{e^{i\varphi_{\mathbf{p}}}}{2\cosh^2(\frac{1}{2}\beta\epsilon_{\mathbf{p}})},\ r_{3,\mathbf{p}} = \tanh(\tfrac{1}{2}\beta\epsilon_{\mathbf{p}}), \tag{2.27}$$

with uncorrelated phases, uniformly distributed in the interval $0 < \varphi_{\mathbf{p}} < 2\pi$. This form of initial conditions corresponds to the amplitudes $u_{\mathbf{p}}$, $v_{\mathbf{p}}$ of the form (2.14). To avoid confusion with temporal characteristics, such as the oscillation period T, hereafter we shall use the inverse temperature β, unless explicitly stated otherwise.

The dynamics (2.24), (2.20) was obtained from $3N$ coupled differential equations with the initial conditions (2.27), with N large enough to ensure proximity to the continual limit. The numerics was executed using the Runge-Kutta method with precision $O(dt^5)$. The time step dt was varied over a range of values to test numerical accuracy. We found that the step $dt = 0.01/\Delta_0$ typically provides sufficient precision over the time interval of interest.

As Fig.2-3 illustrates, a straightforward simulation generates a surprisingly regular, oscillatory time dependence $\Delta(t)$ which appears to be a periodic function of time. After initial exponential growth, controlled by the instability discussed in Sec.2.2, we observe an essentially periodic time dependence, characterized by equally spaced peaks of identical shape. We can thus define the temporal period T, the time lag τ, and the amplitude which we denote by Δ_+ for the reasons to become clear below.

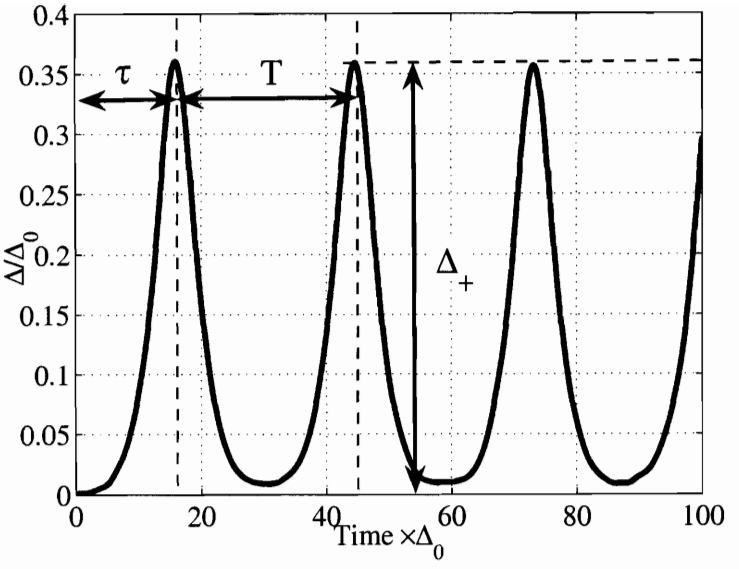

Figure 2-3: Time dependence of the pairing amplitude Δ recorded from simulation with $N = 10^5$ states (2.8), (2.9) at temperature $T = 0.7T_c$ ($\beta = 2.5\Delta_0$) with the initial conditions (2.27). The coupling constant λ was chosen to have the BCS gap $\Delta_0 = W/5$.

These notations are marked in Fig.2-3.

It might seem that the particle-hole symmetry of the density of states (2.8), (2.9) would enforce zero chemical potential, regardless of BCS interaction strength. In the simulation, however, we observe nonzero values of chemical potential due to particle-hole imbalance caused by thermal fluctuations in the initial distribution $n_{\mathbf{p}}$. The complex pairing amplitude exhibits a phase growing linearly with time, $\Delta(t) = e^{-i\varphi(t)}|\Delta(t)|$, $\varphi(t) \propto \omega t$, with ω random in sign, constant for each realization, equal twice the chemical potential. In addition, we observe noise superimposed on the linear time dependence of the phase, which we shall discuss below at the end of this section. As noted in Ref.[42], finite ω can be eliminated by a gauge transformation which shifts single particle energies by $\omega/2$, $\tilde{\epsilon}_{\mathbf{p}} = \epsilon_{\mathbf{p}} - \omega/2$, thereby making Δ real. In the Bloch equation language, this is equivalent to considering the problem in a Larmor frame rotating about the $\hat{\mathbf{z}}$ axis with frequency ω. Having this in mind, below we shall focus on the behavior of the modulus $|\Delta|$.

Interestingly, the obtained time dependence $\Delta(t)$ can be fitted extremely accu-

rately to the analytic solution found in Ref.[42] for noiseless initial conditions. The latter is given by a Jacobi elliptic function, periodic in time,

$$\Delta(t) = \Delta_+ \mathrm{dn}\,(\Delta_+(t-\tau), k), \quad k^2 = 1 - \Delta_-^2/\Delta_+^2, \tag{2.28}$$

with Δ_+ the amplitude, τ the time lag, and Δ_- the minimal value. We recall that the function $u = \mathrm{dn}\,(x,k)$ is obtained by inversion of an elliptic integral:

$$x = \int_u^1 \frac{du'}{\sqrt{(1-u'^2)(k^2-1+u'^2)}} \tag{2.29}$$

The function (2.28) satisfies the differential equation

$$(d\Delta/dt)^2 = (\Delta_+^2 - \Delta^2)(\Delta^2 - \Delta_-^2) \tag{2.30}$$

with $\Delta_\pm$ being the extremal values: $\Delta_- \leq \Delta(t) \leq \Delta_+$. The period of the function (2.28) is given by the complete elliptic integral of the 1st kind:

$$T = \frac{2}{\Delta_+} K(k) = \frac{2}{\Delta_+} \int_0^{\pi/2} \frac{d\varphi}{\sqrt{1-k^2\sin^2\varphi}}. \tag{2.31}$$

For sparse soliton trains, $T\Delta_+ \gg 1$, this expression simplifies to $T = \frac{2}{\Delta_+}\ln(4\Delta_+/\Delta_-)$.

The time dependence of the Bloch vectors $\mathbf{r}_\mathbf{p}(t)$ can be obtained from the ansatz

$$z_\mathbf{p} = A_\mathbf{p}\Delta(t) + iB_\mathbf{p}\dot{\Delta}(t), \quad r_{3,\mathbf{p}} = C_\mathbf{p}\Delta^2 - D_\mathbf{p}. \tag{2.32}$$

Eqs.(2.19) are satisfied by (2.32) provided $A_\mathbf{p} = 2\epsilon_\mathbf{p}B_\mathbf{p}$ and $B_\mathbf{p} = -C_\mathbf{p}$. The normalization condition $r_1^2 + r_2^2 + r_3^2 = 1$ thereby turns into Eq.(2.30), the same for all $\mathbf{p}$, yielding the relation between $C_\mathbf{p}$, $D_\mathbf{p}$ and $\Delta_\pm$:

$$\frac{D_\mathbf{p}^2 - 1}{C_\mathbf{p}^2} = \Delta_-^2\Delta_+^2, \quad 2\frac{D_\mathbf{p}}{C_\mathbf{p}} = 4\epsilon_\mathbf{p}^2 + \Delta_-^2 + \Delta_+^2. \tag{2.33}$$

Here $C_\mathbf{p}$ and $D_\mathbf{p}$, and likewise $A_\mathbf{p}$ and $B_\mathbf{p}$, depend on $\epsilon_\mathbf{p}$, while the quantities $\Delta_\pm$ are the same for all $\mathbf{p}$.

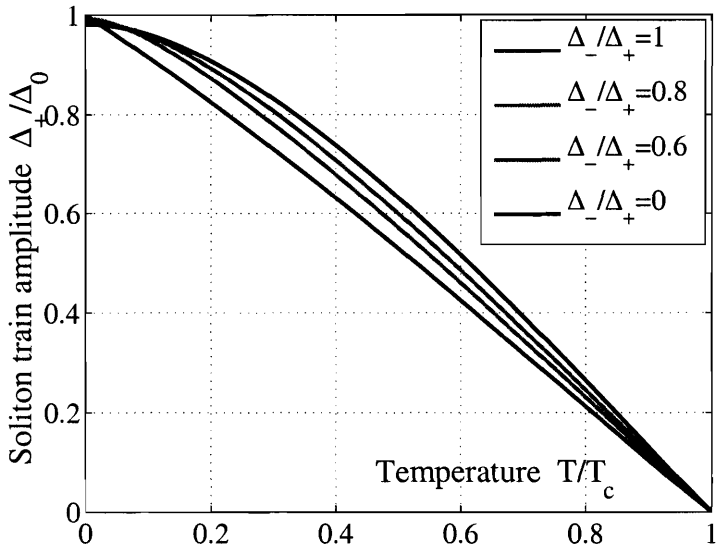

Figure 2-4: Temperature dependence of the soliton train amplitude Δ_+, obtained from the self-consistency condition (2.34) at different ratios Δ_-/Δ_+. Note that at $\Delta_- = 0$ the amplitude Δ_+ equals the BCS instability growth increment γ (see Fig.2-1), while at $\Delta_- = \Delta_+$ the result for the stationary state is reproduced (see Fig.2-2).

A special property of the ansatz (2.32) which makes it compatible with the self-consistency condition (2.20), is that $f_{\mathbf{p}} = A_{\mathbf{p}}\Delta(t)$ has the same time dependence as the left hand side of Eq.(2.20). Therefore, the self-consistency will hold at all times provided that the quantities $\Delta_\pm$ are chosen to satisfy $1 = \frac{\lambda}{2}\sum_{\mathbf{p}} |\bar{\mathbf{r}}_{\mathbf{p}}| A_{\mathbf{p}}$. Here the averaging $\bar{\mathbf{r}}_{\mathbf{p}}$ over a group of levels with close energies is performed in the same way as in the derivation of Eq.(2.26). (As above, the averaging is compatible with unitary evolution due the linear character of Bloch dynamics.) After substituting the expressions for $A_{\mathbf{p}}$ in terms of $\Delta_\pm$, and $\bar{\mathbf{r}}_{\mathbf{p}} = 1 - 2n_{\mathbf{p}}$, we obtain

$$1 = \lambda \sum_{\mathbf{p}} \frac{2\epsilon_{\mathbf{p}} \tanh(\frac{1}{2}\beta\epsilon_{\mathbf{p}})}{\left((4\epsilon_{\mathbf{p}}^2 + \Delta_-^2 + \Delta_+^2)^2 - 4\Delta_-^2\Delta_+^2\right)^{1/2}}. \tag{2.34}$$

The role of this equation is similar to the BCS gap equation. The only difference is that it fixes one of the two constants $\Delta_\pm$, leaving the other one free.

The motivation to consider this particular solution can be seen from the behavior

of the elliptic integral (2.29) at $\Delta_- = 0$. In this case, we obtain a single soliton

$$\Delta(t) = \frac{\Delta_+}{\cosh \Delta_+(t-\tau)}. \tag{2.35}$$

At large negative time, Eq.(2.35) describes exponential growth of Δ. Furthermore, Eq.(2.34) at $\Delta_- = 0$ is identical to the condition (2.15) for the instability growth rate, so that $\Delta_+ = \gamma$. Thus the single soliton solution (2.35) describes the nonlinear evolution following the linear instability regime. The nonmonotonic behavior of $\Delta(t)$, first growing and then decreasing to zero, can be understood as a result of energy mismatch of the BCS ground state and the unpaired state: energy conservation in the collisionless dynamics prevents system to evolve to the ground state with lower energy.

Remarkably, while these solutions appear to be very special, they are robust in the presence of noise. Below we study the instability of Fermi gas at finite temperature, and find that the time dependence survives thermal fluctuations in the initial state. The reason for such a behavior is owing to the property of BCS instability, discussed in Sec.2.2, to develop through a single unstable mode. As a result, only the fluctuation in the initial state along the unstable direction is amplified by BCS dynamics, while other fluctuations remain small, providing a selection mechanism for the solutions (2.34).

Returning to the analysis of soliton trains (2.28), we note that the ratio $r = \Delta_-/\Delta_+$ controls the inter-soliton time separation. Different regimes can be qualitatively understood by noting that Δ varies in the interval $\Delta_- \leq \Delta(t) \leq \Delta_+$. For r increasing from 0 to 1, the soliton train period T decreases, making the solitons overlap stronger and gradually merge, turning into weak harmonic oscillations with frequency $2\Delta_+$ as Δ_- approaches Δ_+ (see Fig. 1 of Ref.[42]).

As a function of temperature, the quantity Δ_+ varies from the value close to the BCS gap Δ_0 at $T = 0$, to zero at $T = T_c$ (see Fig.2-4). At $\Delta_- \ll \Delta_+$, Eq. (2.34) turns into Eq. (2.7) which, as we found above, defines the amplitude of a single soliton (2.35). In the opposite limit, $\Delta_- \to \Delta_+$, Eq. (2.34) coincides with Eq.(2.26) for the

stationary state.

To understand the behavior of Δ_+ in more detail, let us analyze the self-consistency condition (2.34) for the symmetric band of states (2.9). We first consider zero temperature, when $\tanh \frac{1}{2}\beta\epsilon = \operatorname{sgn}\epsilon$. The integral (2.34), evaluated using variable substitution $x = 4\epsilon^2$, gives

$$\begin{aligned} &\frac{1}{2}\int_0^{W^2} \frac{dx}{\sqrt{(x+\Delta_+^2+\Delta_-^2)^2 - 4\Delta_+^2\Delta_-^2}} \\ &= \cosh^{-1}\frac{W^2+(r^2+1)\Delta_+^2}{2r\Delta_+^2} - \ln\frac{1}{r}. \end{aligned} \tag{2.36}$$

Substituting this in Eq. (2.34) and solving it, we obtain

$$\Delta_+^2 = \frac{W^2}{2(e^{1/\lambda} - r^2 e^{-1/\lambda})\sinh\frac{1}{\lambda}}, \tag{2.37}$$

where here and below the density of states is absorbed in the coupling, $\lambda\nu_0 \to \lambda$. At $r = 1$ we recover the BCS gap for the symmetric band (2.9), $\Delta_0 = W/2\sinh\frac{1}{\lambda}$. At $r < 1$ we obtain a value somewhat below Δ_0, the difference being small as $(1-r^2)e^{-2/\lambda}\Delta_0$. This explains small departure from Δ_0 seen in Figs.2-1,2-4 at $T = 0$, as well as its absence in Fig.2-2.

The simulated dynamics $\Delta(t)$ appears to be periodic (or very close to it) over the entire time interval of the simulation. A nearly perfect fit to $\Delta(t)$, as illustrated in Figs.2-5,2-6, is provided by the elliptic function (2.28) with the same period and amplitude. The numerical and analytic functions are found to agree to accuracy better than 10^{-4} for $\beta = 100/\Delta_0$ (Fig.2-5 inset, top panel) and 10^{-3} for $\beta = 10/\Delta_0$ (Fig.2-6 inset, top panel).

While each realization $\Delta(t)$ is essentially a perfectly periodic function of time of the form (2.28), the parameters such as the period T, the time lag τ, and the amplitude Δ_+ exhibit significant variations from one realization to another. To explore this phenomenon, we generated a large number (500) of different realizations, and for each of them determined the values T, τ and Δ_+ from fitting to the elliptic function (2.28). Figs.2-5,2-6 display the resulting pair distributions as a set of points in the

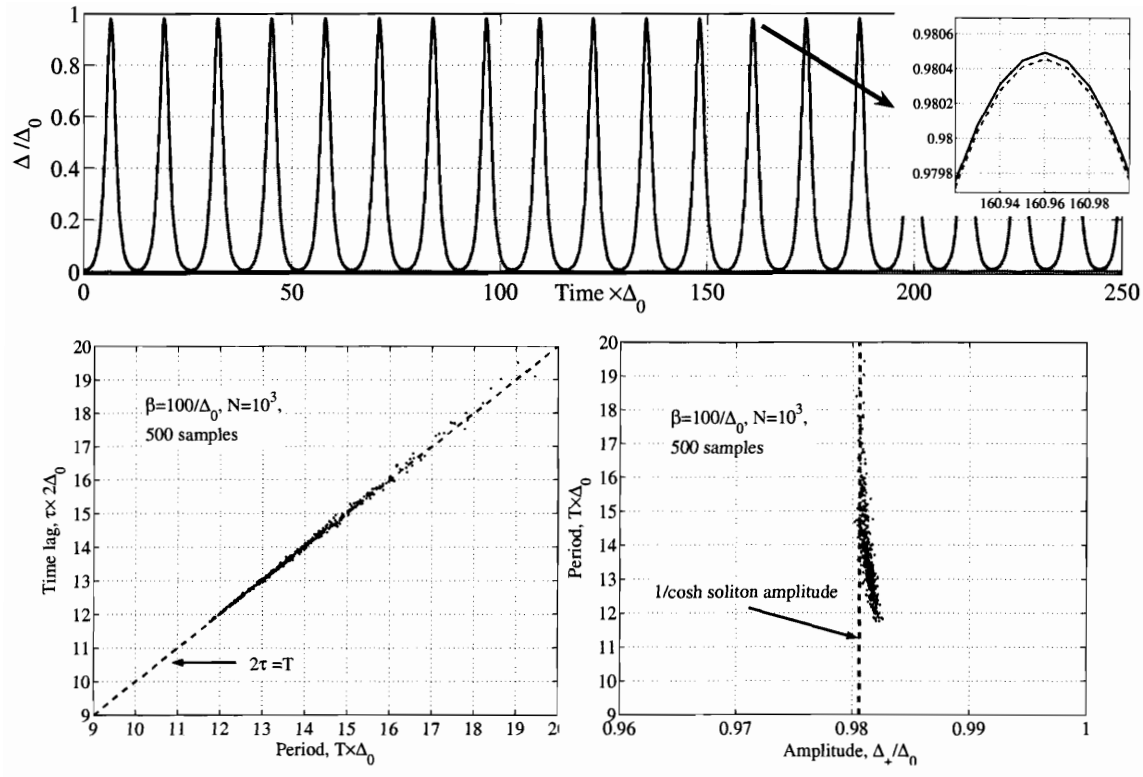

Figure 2-5: *Top panel:* Comparison of the time dependence $\Delta(t)$ obtained from BCS/Bloch dynamics (2.24), (2.20) for $N = 10^3$ spins at temperature $T = 10^{-2}\Delta_0$ (blue curve) to the analytic soliton train solution (2.28) of the same amplitude and period (green curve). The difference of the simulated and analytic $\Delta(t)$ is shown in red. (The initial conditions (2.27) and parameters W, Δ_0 are the same as in Fig.2-3.) *Lower panels:* The pair distributions of the soliton train parameters for 500 different realizations: the time lag and period (left); the period and amplitude (right).

(T, τ) and (T, Δ_+) planes, one point per realization.

These results lead to a number of interesting observations. First, as one would expect, the distribution is less noisy at lower temperature (Fig.2-5). Second, while at $\beta = 10/\Delta_0$ the points are scattered over a 2d region, at $\beta = 100/\Delta_0$ each distribution collapses on a 1d curve, indicating a specific relation between T, τ and Δ_+ at the lower temperature.

The pair distribution of the period and the time lag tends to cluster around the straight line

$$\tau = T/2. \tag{2.38}$$

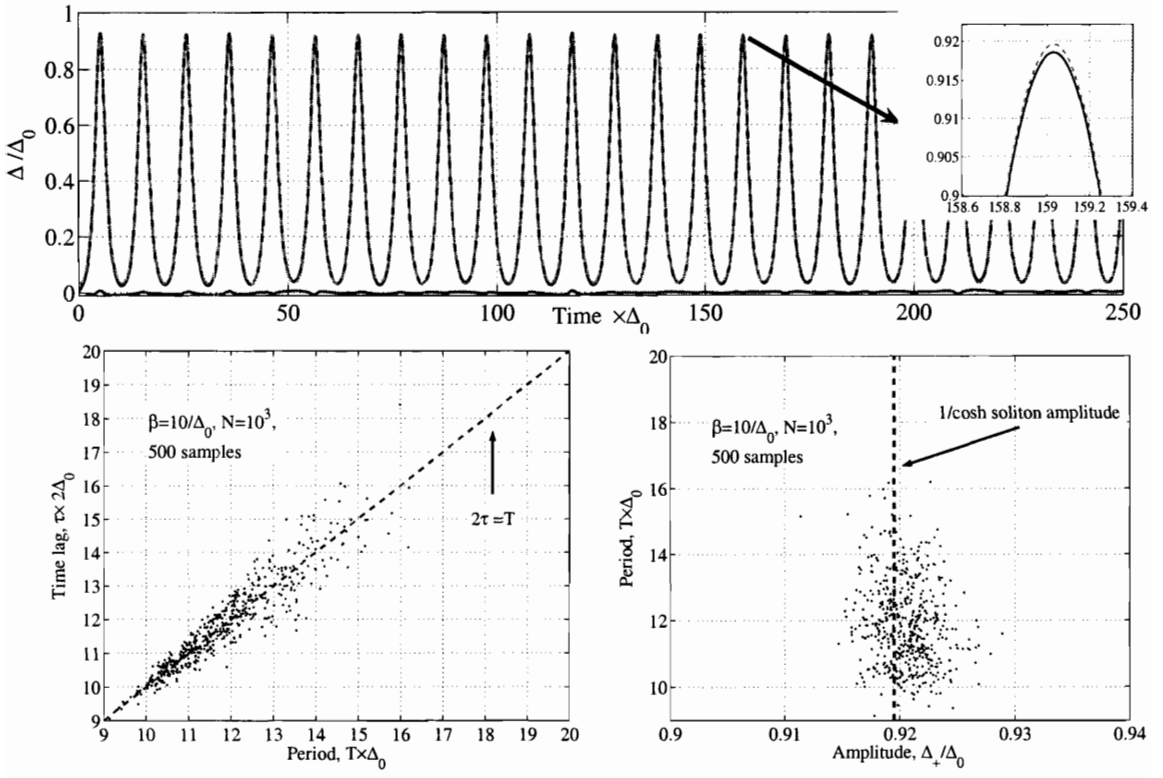

Figure 2-6: Same as in Fig.2-5 for higher temperature $T = 10^{-1}\Delta_0$. The simulated time dependence $\Delta(t)$ can be accurately fitted to the analytic solution (2.28), with the distribution of the period, amplitude and time lag somewhat broader than in Fig.2-5.

This can be understood from the linear stability analysis of Sec.2.2. Indeed, there we found that the linearized BCS problem has only two eigenvalues outside the unit circle, $\zeta = \omega + i\gamma$ and $\zeta^* = \omega - i\gamma$. The projections of the initial unpaired state on these two vectors are close by order of magnitude. Now, let us take into account that the elliptic function (2.28) at large period $T\Delta_+ \gg 1$ represents a train of well-separated $1/\cosh$ solitons (2.35):

$$\Delta(t) = \sum_n \frac{\Delta_+}{\cosh \Delta_+(t - t_n)} + O(e^{-\gamma T}), \quad \Delta_+ = \gamma, \tag{2.39}$$

$t_n = nT + \tau$. In between the solitons this function is given by a sum of exponential

tails of the nearest solitons:

$$\Delta(t_n \lesssim t \lesssim t_{n+1}) = \gamma(e^{-\gamma(t-t_n)} + e^{\gamma(t-t_{n+1})}).$$

The amplitudes of the two terms, taken at some t in the interval (t_n, t_{n+1}), should match the ζ, ζ^* projections of the initial state for the numerical and analytical solution to coincide. Since the terms $e^{-\gamma(t-t_n)}$, $e^{\gamma(t-t_{n+1})}$ are equal at the midpoint $t_0 = \frac{1}{2}(t_n + t_{n+1})$, the time t defined by the matching condition must be close to t_0. This suggests that the time lag τ should indeed be close to half a period, with the product $(2\tau - T)\gamma$ of order one and random in sign. This conclusion is consistent with our observations at different temperatures (Figs.2-5,2-6).

To complete the description of the behavior of Δ, obtained in simulation, here we analyze the phase dynamics. The phase $\varphi = \arg\Delta(t)$ recorded in the simulation exhibits an approximately linear time dependence, as illustrated in Fig.2-7. As discussed above, in a system with perfect particle-hole symmetry one expects the chemical potential to be pinned to the band center, in which case the condition $d\varphi/dt = 2\mu = 0$ would make the phase time-independent. The observed linear behavior can be explained by particle-hole imbalance due to fluctuations of particle distribution $n_{\mathbf{p}}$ in the initial state. These fluctuations result in nonzero chemical potential of random sign. The fluctuations in μ caused by random occupancy will be estimated in Sec.2.5, Eq.(2.46.ii). The magnitude and temperature dependence of the fluctuations is found to be consistent with observations.

The noise superimposed on the linear time dependence $\varphi(t)$ has several interesting features. First, the fluctuations about the linear dependence show no sign of phase diffusion, since $\delta\varphi$ does not grow. Instead, they can be described as a periodic, or quasiperiodic, arrangement of steps connected by kinks. By comparing to Fig.2-6 which depicts $|\Delta|$ for this simulation, we see that each step is associated with a soliton, while the kinks occur in between the solitons. This behavior can be partially understood by analyzing the trajectory $\Delta(t)$ in a complex plane, displayed in Fig.2-7. Each radial straight line in this plot corresponds to a soliton, making it apparent that

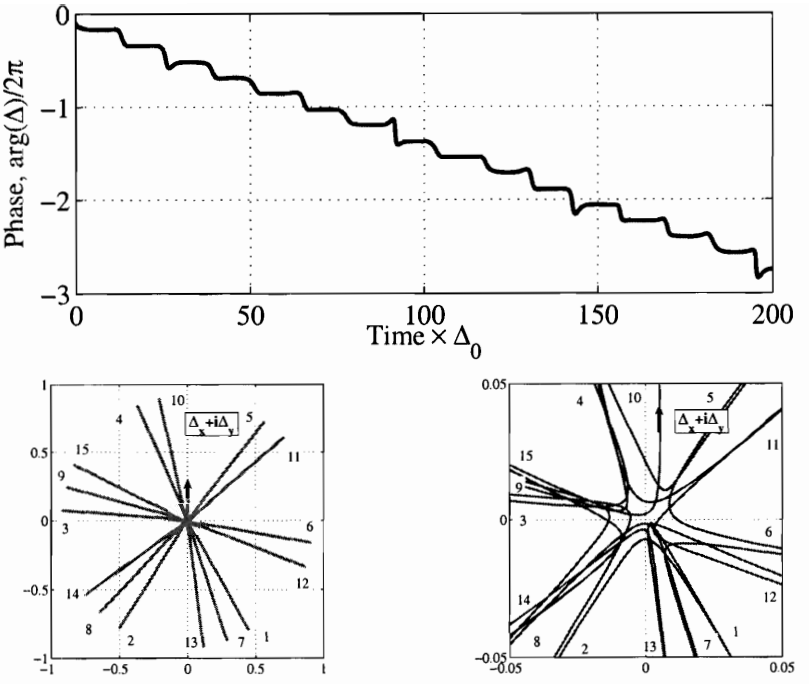

Figure 2-7: *Top:* The phase of the pairing amplitude *versus* time for the soliton train in Fig.2-6. *Bottom:* Pairing amplitude $\Delta(t) = \Delta_x(t) + i\Delta_y(t)$ trajectory in the complex plane. The phase $\arg\Delta(t)$ is a linear function of time superimposed with noise. Each radial line in the left panel corresponds to a soliton, marked according to their order in the time sequence. Phase shift between solitons translates into rotation by a constant angle. The right panel shows the behavior near the origin, allowing to trace the order of different solitons.

the phase variation occurs mainly in between the solitons. Interestingly, the deviation of the phase time dependence from linear does not lead to noticeable deviation in $|\Delta|$ from the elliptic function time dependence.

2.5 Noise due to occupancy fluctuations

The robustness of the elliptic function (2.28) accompanied by sometimes significant variations of the parameters T, τ and Δ_+ among different realizations may seem surprising. To get insight into the origin of this behavior we consider variations in the initial conditions, which can be attributed to fluctuations of the pair states occupancy (2.12) at $t = 0$. The latter is due to thermodynamic fluctuations of fermion occupancy $n_{\mathbf{p}}$, and can be interpreted more intuitively as temperature fluctuations.

The first thing we note is that the existence of the soliton solutions, as well as their analytic form, is not dependent upon the details of the energy distribution $n_{\mathbf{p}}$, provided the state is unpaired, i.e. there is no coherence in the amplitudes $u_{\mathbf{p}}$, $v_{\mathbf{p}}$ at different $\mathbf{p}$. The main difference arising for the more general distribution is possible lack of particle-hole symmetry relative to E_F. In this case, the pairing interaction shifts the chemical potential which manifests itself as a time-dependent phase factor $e^{-i\omega t}$ multiplying $\Delta(t)$. As discussed in Ref.[42], this can be taken into account by a gauge transformation which shifts single particle energies by $\omega/2$. In the transformed problem, only the modulus $|\Delta|$ varies with time, with its functional form still given by the elliptic function (2.28). The parameters $\Delta_{\pm}$ and ω satisfy algebraic self-consistency equations [42] with $\tanh \frac{1}{2}\beta\epsilon_{\mathbf{p}}$ replaced by $1 - 2n_{\mathbf{p}}$.

The variation in the period T can be linked to the fluctuations in the initial state projection on the unstable mode (2.6). Denoting this projection η, we can write for it a distribution of Porter-Thomas form [43],

$$P(|\eta| = x) = 2ux \exp(-ux^2), \tag{2.40}$$

The latter describes fluctuations of individual components of a random complex vector in a high dimensional space, with the parameter u being a function of the vector norm statistics. In our case, the effective dimensionality can be estimated as a ratio of temperature to the level spacing, $d \simeq 1/\beta\delta\epsilon = N/(\beta W)$. To relate η to the period T, we write the time-dependent Δ at the times described by linear instability as $\Delta(t) \propto \eta e^{\gamma t}$. The corresponding time range can be estimated from the condition $\Delta(t) \lesssim \Delta_+ \simeq \gamma$, giving $t = \gamma^{-1} \ln \gamma/\eta$. The time t is close to the phase lag τ which, for the reasons discussed above, is approximately equal to $\frac{1}{2}T$.

Porter-Thomas distribution predicts order of magnitude fluctuations with typical $\eta \sim u^{-1/2}$. This translates into fluctuations of $T = 2\gamma^{-1} \ln \gamma/\eta$ about its mean value with the dispersion independent of u. Indeed, Figs.2-5,2-6 indicate that a ten-fold increase in temperature, while reducing the period, has little effect on its fluctuations.

To see whether the randomness in the initial state, and specifically in the occu-

pancy $n_{\mathbf{p}}$, can explain the fluctuations in Δ_+ recorded in Figs.2-5,2-6, we consider instability of a particular initial unpaired state (2.12). Eq.(2.15) gives an equation for the instability exponent:

$$1 = \lambda \sum_{\mathbf{p}} \frac{g_{\mathbf{p}}}{2\epsilon_{\mathbf{p}} - \zeta}, \quad g_{\mathbf{p}} = |u_{\mathbf{p}}^{(0)}|^2 - |v_{\mathbf{p}}^{(0)}|^2, \tag{2.41}$$

with microscopic non-averaged $u_{\mathbf{p}}^{(0)}$, $v_{\mathbf{p}}^{(0)}$ taking values zero or one with the probabilities $p_{|u_{\mathbf{p}}|^2=1} = (1 - n_{\mathbf{p}})^2$, $p_{|v_{\mathbf{p}}|^2=1} = n_{\mathbf{p}}^2$ [see Eq.(2.12)].

The fluctuation $\delta g_{\mathbf{p}}$ causes deviation $\delta\zeta$ from the average value $\zeta = i\gamma$. Linearization of (2.41) gives

$$\delta\zeta \sum_{\mathbf{p}} \frac{\bar{g}_{\mathbf{p}}}{(2\epsilon_{\mathbf{p}} - i\gamma)^2} = -\sum_{\mathbf{p}} \frac{\delta g_{\mathbf{p}}}{2\epsilon_{\mathbf{p}} - i\gamma} \tag{2.42}$$

with $\bar{g}_{\mathbf{p}} = \tanh \frac{1}{2}\beta\epsilon_{\mathbf{p}}$. We see that both the real and the imaginary part of $\delta\zeta = \delta\zeta' + i\delta\zeta''$ are nonzero, due to the parts of the distribution fluctuation $\delta g_{\mathbf{p}}$ even and odd relative to E_F. The imaginary part $\delta\zeta''$ gives fluctuation in the instability growth exponent γ. The real part $\delta\zeta'$ can be associated with a shift of the chemical potential due to particle-hole imbalance in the pair sector.

We estimate the magnitude of the fluctuations for low temperature $T \ll \Delta_0 \simeq \gamma$, when Eq.(2.42) is reduced to

$$\delta\zeta = \frac{i}{\gamma} \sum_{\mathbf{p}} (2\epsilon_{\mathbf{p}} - i\gamma)\delta g_{\mathbf{p}}. \tag{2.43}$$

Separating the real and imaginary part, we obtain

$$\langle \delta\zeta''^2 \rangle = \delta\epsilon \sum_{\mathbf{p}} \frac{4\epsilon_{\mathbf{p}}^2}{\gamma^2} \langle \delta g_{\mathbf{p}}^2 \rangle, \quad \langle \delta\zeta'^2 \rangle = \delta\epsilon \sum_{\mathbf{p}} \langle \delta g_{\mathbf{p}}^2 \rangle. \tag{2.44}$$

Here the second moment $\langle \delta g_{\mathbf{p}}^2 \rangle$ is given by

$$\begin{aligned} \langle \delta g_{\mathbf{p}}^2 \rangle &= \overline{(|u_{\mathbf{p}}^{(0)}|^2 - |v_{\mathbf{p}}^{(0)}|^2)^2} - (\overline{|u_{\mathbf{p}}^{(0)}|^2} - \overline{|v_{\mathbf{p}}^{(0)}|^2})^2 \\ &= (1 - n_{\mathbf{p}})^2 + n_{\mathbf{p}}^2 - (1 - 2n_{\mathbf{p}})^2 = 2n_{\mathbf{p}}(1 - n_{\mathbf{p}}). \end{aligned} \tag{2.45}$$

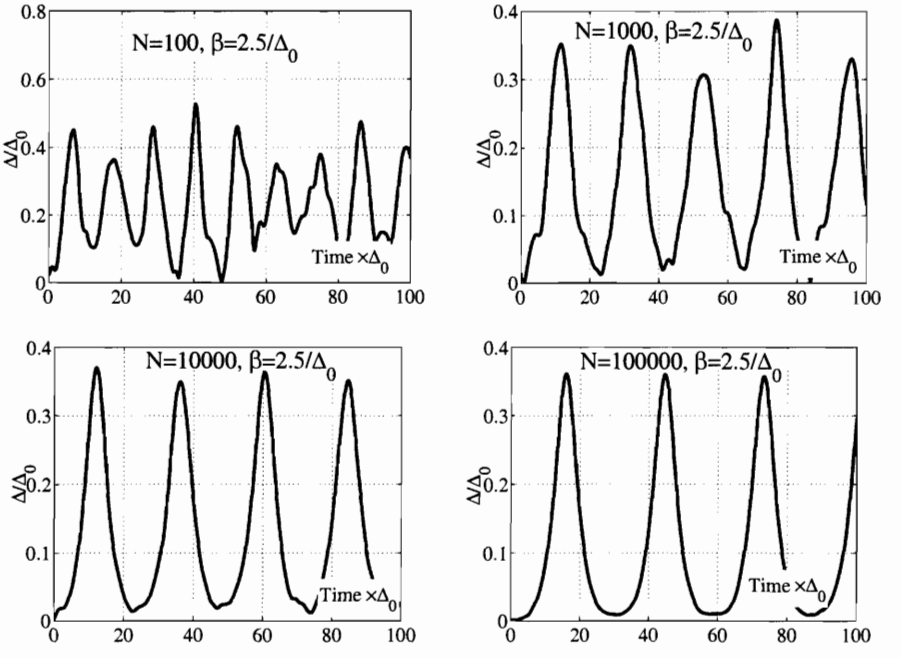

Figure 2-8: Noise suppression at increasing number of states N. The time dependence $\Delta(t)$ recorded from a simulation at $T = 0.7T_c$ ($\beta = 2.5\Delta_0$) for $N = 10^2$, 10^3, 10^4, 10^5 states, with other parameters the same as above.

To obtain an order of magnitude estimate, we note that the fluctuations $\delta g_{\mathbf{p}}$ are of order one at $|\epsilon_{\mathbf{p}}| \lesssim T$ and exponentially small at $|\epsilon_{\mathbf{p}}| \gg T$. Thus we find

$$\text{(i)} \quad \langle \delta\zeta''^2 \rangle \simeq \frac{T^3}{\gamma^2}\,\delta\epsilon, \quad \text{(ii)} \quad \langle \delta\zeta'^2 \rangle \simeq T\,\delta\epsilon, \tag{2.46}$$

where $\delta\epsilon = W/N$ is the level spacing.

The $T^{3/2}$ temperature dependence of the fluctuation in γ, Eq.(2.46.i), can be compared to the distributions of the amplitude Δ_+ presented in Figs. 2-5,2-6. As we demonstrated above, Δ_+ is numerically close to γ, becoming equal to it in the limit of well-separated solitons (see Fig.2-4). According to the $T^{3/2}$ law, a ten-fold increase in temperature from $\Delta_0/100$ to $\Delta_0/10$ should lead to the dispersion in γ increase by a factor of 30, which is indeed close to the increase in Δ_+ dispersion seen in Figs. 2-5,2-6.

The noise, which quickly grows as a function of temperature, Eq.(2.46), can be

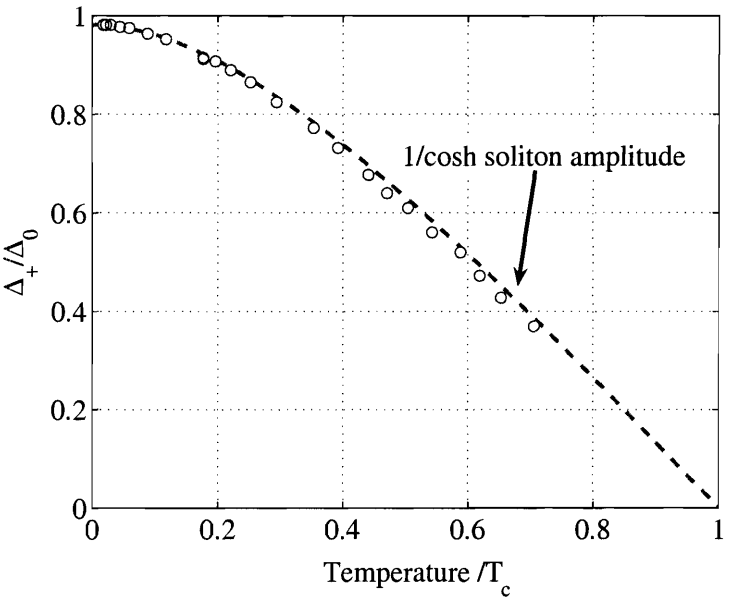

Figure 2-9: Temperature dependence of the soliton train amplitude as recorded from the simulation. To suppress noise, the number of levels N was gradually increased from $N = 10$ at the lowest temperature to $N = 10^5$ at the highest temperature. Analytic fit displays the single $1/\cosh$ soliton (2.35) amplitude obtained from Eq.(2.34) at $\Delta_- = 0$.

suppressed by reducing the level spacing $\delta\epsilon = W/N$. The dramatic effect of level spacing on noise is illustrated in Fig.2-8 which presents the time dependent $\Delta(t)$ at a relatively high temperature $T = 0.7T_c$ for several values of the number of levels N. We observe that the noise, at this temperature significant at small N, decreases at large N, with the time dependence assuming the elliptic function form (2.28). As demonstrated in Fig.2-9, the soliton train amplitude, recorded at N large enough to minimize noise, follows very closely the analytic temperature dependence, Eq.(2.34). The value of N required to reduce noise to the level at which the behavior (2.34) is revealed, grows as a function of temperature. While at $T = 0$ as few levels as $N = 10$ is quite sufficient, we find that N increases rapidly as T_c is approached.

To analyze the noise at T close to T_c, we again consider fluctuations in the instability growth rate, given by Eq.(2.42). At these temperatures, since γ is linear in $T_c - T$ near T_c, we have $\gamma \ll T$. In this case, the sum $\sum_{\mathbf{p}} \bar{g}_{\mathbf{p}}(2\epsilon_{\mathbf{p}} - i\gamma)^{-2}$ in (2.42)

equals

$$4i\gamma \sum_{\mathbf{p}} \frac{\epsilon_{\mathbf{p}} \bar{g}_{\mathbf{p}}}{((2\epsilon_{\mathbf{p}})^2 + \gamma^2)^2} = \frac{i\pi}{8}\beta$$

After averaging over fluctuations $\delta g_{\mathbf{p}} = g_{\mathbf{p}} - \bar{g}_{\mathbf{p}}$, we obtain

$$\langle |\delta\zeta|^2 \rangle = \left(\frac{8T}{\pi}\right)^2 \delta\epsilon \sum_{\mathbf{p}} \frac{\langle \delta g_{\mathbf{p}}^2 \rangle}{(2\epsilon_{\mathbf{p}})^2 + \gamma^2}. \tag{2.47}$$

Using the expression (2.45) for $\langle \delta g_{\mathbf{p}}^2 \rangle$ at $|\epsilon_{\mathbf{p}}| \ll T$, we have

$$\langle |\delta\zeta|^2 \rangle = \left(\frac{8T}{\pi}\right)^2 \delta\epsilon \sum_{\mathbf{p}} \frac{\langle \delta g_{\mathbf{p}}^2 \rangle}{(2\epsilon_{\mathbf{p}})^2 + \gamma^2} = \frac{16T^2}{\pi\gamma}\delta\epsilon. \tag{2.48}$$

By inspecting the right hand side of Eq.(2.42) we find that the fluctuations in $\delta\zeta''$, the instability growth rate, dominate at T close to T_c, while the fluctuations in $\delta\zeta'$, the chemical potential, are smaller by a factor γ/T. Thus Eq.(2.48) gives an estimate for the fluctuations in γ and, by the argument used above, also provides an estimate of the noise in the soliton train amplitude Δ_+.

The condition necessary for the noise (2.48) to be small, $|\delta\zeta| \ll \gamma$, translates into

$$N \gg \frac{16T^2 W}{\pi\gamma^3}. \tag{2.49}$$

We see that the minimal level number required to suppress noise grows as $(T_c - T)^{-3}$ near the transition. The fast growth is consistent with the results of simulation presented in Figs. 2-8,2-9.

The level number N, which so far was taken to be arbitrary, can be related to other parameters as follows. For a system of size L smaller than the BCS correlation length $\xi = \hbar v_F/\Delta$, which corresponds to a tightly trapped cold gas, N is of the order of the total particle number. This can also be written as a relation of N and particle Fermi momentum: $N \simeq (Lp_F/2\pi\hbar)^3$.

In an infinite system, or in a system of size larger than ξ, one can define an effective N equal to the number of particles in the correlation volume, $N \simeq (\xi p_F/2\pi\hbar)^3 \approx (E_F/\Delta)^3$. Comparing this to the inequality (2.49), with the identifications $W = E_F$,

$\gamma \simeq \Delta \propto T_c - T$, we obtain a condition $E_F^2 \gg T^2$, nonrestrictive in the entire interval $0 < T < T_c$. Other requirements for the mean field approach are also nonrestrictive: (i) The detuning from transition, $T_c - T$, must be outside the fluctuation region, very narrow at weak coupling; (ii) The collisionless regime condition $\tau_\Delta \ll \tau_{\rm el}$ requires that $T_c - T$ is outside the region described by the time-dependent Ginzburg-Landau equation [35], which is also quite narrow. From this one can conclude that the mean field approach, validated by (2.49), remains accurate in an infinite system, at least for spatially uniform solutions.

It is not inconceivable that the mean field theory, known to work well in equilibrium at weak coupling, is also valid for the dynamical problem with generic spatially varying Δ. However, an understanding of this question can only be achieved after the role of spatial fluctuations in the BCS instability is clarified [44]. Here most interesting are spatial fluctuations of the phase of Δ, and the properties of vortices, which presently are not understood. If the characteristic length scale of phase fluctuations is of order or larger than the correlation length ξ, which seems likely to be the case, the dynamics of the modulus $|\Delta|$ can be obtained in a local approximation, using the results of this work and ignoring spatial dependence.

2.6 Spin 1/2 representation

In Sec.2.3 we derived Bloch equations (2.24) from Bogoliubov-de Gennes equations for $u_{\mathbf{p}}$ and $v_{\mathbf{p}}$, by rewriting them in the form of Gorkov equations for $g_{\mathbf{p}} = |u_{\mathbf{p}}|^2 - |v_{\mathbf{p}}|^2$, $f_{\mathbf{p}} = 2u_{\mathbf{p}}v_{\mathbf{p}}^*$, and then recognizing that these quantities form a three-component Bloch vector. To gain more insight, here we demonstrate a different approach in which spin 1/2 operators and Bloch dynamics appear on an earlier stage. Following Anderson [24], we define pseudospins associated with individual Cooper pair states, by assigning 'Pauli spin' operators $\sigma_{\mathbf{p}}^{\pm} \equiv \frac{1}{2}(\sigma_{\mathbf{p}}^x \pm i\sigma_{\mathbf{p}}^y)$ to each pair of fermion states with opposite momenta as follows

$$\sigma_{\mathbf{p}}^+ = a_{\mathbf{p}\uparrow}^+ a_{-\mathbf{p}\downarrow}^+ , \quad \sigma_{\mathbf{p}}^- = a_{-\mathbf{p}\downarrow} a_{\mathbf{p}\uparrow} , \tag{2.50}$$

and $\sigma^z_{\mathbf{p}} \equiv [\sigma^+_{\mathbf{p}}, \sigma^-_{\mathbf{p}}] = a^+_{\mathbf{p}\uparrow} a_{\mathbf{p}\uparrow} - a_{-\mathbf{p}\downarrow} a^+_{-\mathbf{p}\downarrow}$. This allows to represent the BCS problem (2.1) as an ensemble of interacting spins:

$$\mathcal{H} = \sum\nolimits'_{\mathbf{p}} \epsilon_{\mathbf{p}} \sigma^z_{\mathbf{p}} - 2\lambda \sum\nolimits'_{\mathbf{p},\mathbf{q}} \sigma^+_{\mathbf{p}} \sigma^-_{\mathbf{q}}, \tag{2.51}$$

where $\sum'_{\mathbf{p}}$ means a sum over the pairs of states $(\mathbf{p}, -\mathbf{p})$. Since all the spins interact with each other equally, the mean field theory here is exact, just like for the BCS problem. The mean field Hamiltonian for each spin is

$$\mathcal{H}_{\mathbf{p}} = \mathbf{b}_{\mathbf{p}} \cdot \sigma_{\mathbf{p}}, \quad \mathbf{b}_{\mathbf{p}} = (-\Delta', -\Delta'', \epsilon_{\mathbf{p}}) \,. \tag{2.52}$$

Here the z component of the effective field $\mathbf{b}_{\mathbf{p}}$, given by the single particle energy, is spin-specific, while the transverse components, the same for all the spins, satisfy

$$\Delta \equiv \Delta' + i\Delta'' = \lambda \sum_{\mathbf{p}}{}' \langle \sigma^+_{\mathbf{p}} \rangle. \tag{2.53}$$

This dynamical self-consistency relation for time-dependent Δ and $\sigma^+_{\mathbf{p}}$ is identical to the Gorkov equation (2.20). In the ground state each spin is aligned with $\mathbf{b}_{\mathbf{p}}$, and the spins form a texture near the Fermi surface [24], given by Eq.(2.25), with spin rotation described by the Bogoliubov angle.

The dynamical problem of interest takes the form of a Bloch equation for the spins,

$$\dot{\sigma}_{\mathbf{p}} = i[\mathcal{H}_{\mathbf{p}}, \sigma_{\mathbf{p}}] = 2\mathbf{b}_{\mathbf{p}} \times \sigma_{\mathbf{p}} \tag{2.54}$$

with the field $\mathbf{b}_{\mathbf{p}}$ defined self-consistently by (2.52),(2.53). Eq. (2.54), linearized about the texture state, describes collective excitations of a superconductor with frequency 2Δ [40, 24]. Linearized about the unpaired state, Eq. (2.54) describes the BCS instability (2.7).

The Hilbert space for the spin Hamiltonian (2.51) can be constructed in a standard fashion, using the states

$$\{\sigma_{\mathbf{p}}\} = |... \uparrow\downarrow\downarrow\uparrow\downarrow ...\rangle \tag{2.55}$$

as basis vectors, where $\sigma_{\mathbf{p}} = \uparrow, \downarrow$ correspond to the fully occupied and empty pair states. The pair states having fermionic occupancy one are to be excluded as they are decoupled from the dynamics (2.51). The Hilbert space spanned by the states (2.55) provides a full representation of the Hamiltonian (2.51).

The spin states (2.55), which are identical to the many-body pair states (2.13), provide the most general description of the problem. Here one can note, however, that the mean field relation (2.53) eliminates dynamical coherence of different spins. This allows to simplify the state, replacing (2.55) by a product state

$$|\psi\rangle = \bigotimes_{\mathbf{p}} \begin{pmatrix} v_{\mathbf{p}} \\ u_{\mathbf{p}} \end{pmatrix} . \tag{2.56}$$

Comparing this to the fermionic product states (2.2), (2.12), we see that the spinor components $u_{\mathbf{p}}$, $v_{\mathbf{p}}$ are identical to Bogoliubov amplitudes, since the Bogoliubov-de Gennes dynamics (2.4) is equivalent to the Bloch dynamics (2.54).

One can reduce the spin 1/2 Bloch equations (2.54) to the Bloch equations (2.24) for classical vectors $\mathbf{r}_{\mathbf{p}}$ used above as follows. Each pair state $(\mathbf{p}, -\mathbf{p})$ participates in the product (2.56) with the probability $n_{\mathbf{p}}^2 + (1 - n_{\mathbf{p}})^2$, and is excluded with the probability $2n_{\mathbf{p}}(1 - n_{\mathbf{p}})$. Since the Bloch equation (2.54) is linear in $\sigma_{\mathbf{p}}$, it takes the same form when $\sigma_{\mathbf{p}}$ is replaced by its expectation value $\mathbf{r}_{\mathbf{p}} = \langle \sigma_{\mathbf{p}} \rangle$. One can include the probability of having occupancy 0 or 2 is the expectation value, which makes the norm of $\mathbf{r}_{\mathbf{p}}$ equal $n_{\mathbf{p}}^2 + (1 - n_{\mathbf{p}})^2$, in agreement with Eq.(2.23). Thus we see that the spin formulation is indeed equivalent to the fermionic formulation employed above.

2.7 Summary

This work demonstrates that the unpaired fermionic state, after being suddenly presented with pairing interaction, develops a BCS instability which triggers oscillations of the pairing amplitude and other quantities. The oscillations are periodic in time and are not damped as long as particle collisions do not play a role. The oscillatory behavior comes quite naturally, given that without collisions the system cannot lower

its energy to that of the BCS ground state.

What comes as a surprise, however, is that the oscillations have predictable characteristics despite thermal noise in the initial conditions. The time-dependent pairing amplitude is described by the soliton train solutions of Jacobi elliptic function dn form [42] in which only the parameters such as the period, amplitude and time lag depend on the initial conditions. The explanation for such a behavior can be traced to the physics of the BCS instability. In the latter, when linearization over the unpaired state is analyzed, only one mode exhibits instability, while other modes correspond to the perturbations that do not grow. As a result, in the evolution of a generic unpaired fermion state only the perturbation along the unstable direction is amplified by the instability, selecting the special elliptic function as a time dependence. The accuracy to which the special solution is selected is controled by the strength of fluctuations in the initial state, due to finite temperature and level spacing.

The selection phenomenon may appear counterintuitive. Here it is instructive to make comparison to the results of Ref.[45] which employs the integrability of the BCS problem to study time-dependent solutions. The large family of solutions obtained in Ref.[45] could leave one under impression that they all are equally relevant for the evolution of a generic state, which does not agree with the results of our simulation and analytic arguments. Instead, as we have seen above, some solutions are singled out by the dynamics, while others are not. This peculiar situation illustrates that knowing the general solution of a nonlinear problem is not necessarily helpful in identifying the special solution relevant for the physical system in which a selection mechanism is at work.

Let us also comment on some issues of interest not considered in this work. One has to do with energy relaxation, left out of the analysis of collisionless BCS dynamics. The relaxation processes relevant for cold gasses are due to elastic collisions involving two particle scattering. The rate of such processes, estimated above as $\tau_{\rm el}^{-1}$, is small compared to the typical frequency of oscillations $\omega \sim \Delta/\hbar$, allowing for undamped oscillations over a relatively long time interval $0 < t \lesssim \tau_{\rm el}$. While proper treatment of relaxation can only be obtained with the help of quantum kinetic theory, one

can account for it heuristically [42] by inserting a Landau-Lifshitz term in the Bloch equation (2.24), changing $\mathbf{b_p}$ to

$$\mathbf{b}'_{\mathbf{p}} = \mathbf{b_p} - \frac{1}{\tau_{\rm el}} \mathbf{l_p} \times \mathbf{r_p},$$

where $\mathbf{l_p} = \mathbf{b_p}/|\mathbf{b_p}|$. The resulting evolution exhibits damped oscillations converging to the BCS ground state asymptotically at large times $t \gg \tau_{\rm el}$.

We note that Volkov and Kogan [40], who investigated the weak oscillation regime, found nonexponential decay of lianearized oscillations, interpreted as collisionless damping [33, 40] caused by mixing of the oscillations of Δ with quasiparticle states slightly above the gap.

Another phenomenon of interest is related with spatial fluctuations. Our discussion focused on the dynamics in a system of finite size, of order or smaller than the correlation length, in which we considered spatially uniform $\Delta(t)$, neglecting the spatial dependence altogether. In an infinite system, one expects the emergent pairing dynamics to exhibit phase fluctuations and vortices simultaneously with the oscillations of the modulus $|\Delta|(t)$ similar to that studied above. If the phase fluctuations occur at distances larger than the correlation length and the vortices are dilute, one can use the estimates made at the end of Sec.2.5 to argue that the modulus $|\Delta|$ will oscillate in a pretty much the same way as in the spatially uniform situation. However, more work will be needed to clarify this.

In this Chapter we studied fermionic pairing in a system with time-dependent pairing interaction. We analyze the situation when the pairing builds up after the interaction has been abruptly turned on. Theoretical analysis, supported by numerical simulations, predicts a stage of exponential growth, described by BCS instability of the unpaired Fermi gas, followed by periodic oscillations described by collisionless nonlinear BCS dynamics. We consider spatially uniform situation relevant for systems of small size, and find that:

(i) In the collisionless approximation, at times shorter than the energy relaxation time, the oscillations are undamped;

(ii) The time dependence of the pairing amplitude is obtained from an exact solution of the nonlinear BCS problem [42], a periodic soliton train described by the Jacobi elliptic function dn, with parameters depending on the microscopic initial conditions;

(iii) The robustness of the elliptic function behavior is explained by a dynamical selection process, in which the BCS instability acts to amplify the initial perturbation in a specific unstable mode of the system, generating a time dependence with predictable characteristics;

(iv) The fluctuations of the amplitude, period and time lag of the soliton train can be accounted for by occupation probability fluctuations in the initial state.

2.8 Appendix A: Bloch and the Bogoliubov-de Gennes equation

Here we present yet another derivation of the Bloch equation (2.24), starting from the evolution of time-dependent amplitudes $u_{\mathbf{p}}(t)$, $v_{\mathbf{p}}(t)$. Let us consider the Bogoliubov-de Gennes equation (2.4) with the self-consistency condition (2.3). By introducing a new variable $w_{\mathbf{p}} = u_{\mathbf{p}}/v_{\mathbf{p}}$, the pair of linear differential equations (2.4) is reduced to a single nonlinear equation of Riccati form,

$$i\partial_t w_{\mathbf{p}} = 2\epsilon_{\mathbf{p}} w_{\mathbf{p}} + \Delta(t) - \Delta^*(t) w_{\mathbf{p}}^2 \tag{2.57}$$

which was analyzed in Ref.[46]. The self-consistency condition (2.3), rewritten in terms of $w_{\mathbf{p}}(t)$, becomes

$$\Delta(t) = \lambda \sum_{\mathbf{p}} Q_{\mathbf{p}} \frac{w_{\mathbf{p}}(t)}{1 + |w_{\mathbf{p}}(t)|^2}, \tag{2.58}$$

where

$$Q_{\mathbf{p}} = |u_{\mathbf{p}}|^2 + |v_{\mathbf{p}}|^2 \tag{2.59}$$

is the norm of $(u_{\mathbf{p}}, v_{\mathbf{p}})$, conserved by the dynamics (2.4).

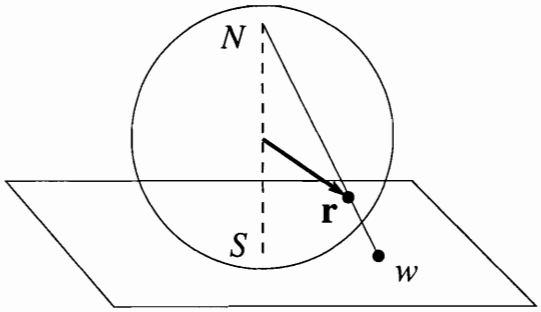

Figure 2-10: Stereographic projection (2.60) schematic.

The initial value $w_{\mathbf{p}}$ corresponding to the unpaired Fermi gas (2.14) is $w_{\mathbf{p}}^{(0)} = e^{i\varphi_{\mathbf{p}}}(1-n_{\mathbf{p}})/n_{\mathbf{p}} = e^{\beta\epsilon_{\mathbf{p}}+i\varphi_{\mathbf{p}}}$, with the phases $\varphi_{\mathbf{p}}$ random and uncorrelated for different $\mathbf{p}$. For $(u_{\mathbf{p}}, v_{\mathbf{p}})$ of the form (2.14) we have

$$Q_{\mathbf{p}} = n_{\mathbf{p}}^2 + (1-n_{\mathbf{p}})^2$$

The factor $Q_{\mathbf{p}} < 1$ describes the effect of Pauli blocking which was discussed in Sec.2.3.

The next step is to perform a reverse stereographic projection of the complex variable w, mapping it onto the unit sphere $r_1^2 + r_2^2 + r_3^2 = 1$ as follows:

$$r_1 + ir_2 = \frac{2w}{|w|^2+1}, \quad r_3 = \frac{|w|^2-1}{|w|^2+1} \tag{2.60}$$

(see Fig.2-10). The dynamics (2.57), written in terms of $z = r_1 + ir_2$ and r_3, gives

$$\frac{dz}{dt} = -2i\epsilon_{\mathbf{p}} z + 2i\Delta r_3, \quad \frac{dr_3}{dt} = i\Delta^* z - i\Delta z^*. \tag{2.61}$$

After rewriting Eq.(2.61) in terms of $\mathbf{r}_{\mathbf{p}} = (r_1, r_2, r_3)_{\mathbf{p}}$, we again obtain the Bloch equation (2.24), $\dot{\mathbf{r}}_{\mathbf{p}} = 2\mathbf{b}_{\mathbf{p}} \times \mathbf{r}_{\mathbf{p}}$, with the "magnetic field" $\mathbf{b}_{\mathbf{p}} = -(\Delta', \Delta'', \epsilon_{\mathbf{p}})$.

The self-consistency condition (2.58) takes the form

$$\Delta = \frac{\lambda}{2}\sum_{\mathbf{p}} Q_{\mathbf{p}} z_{\mathbf{p}}. \tag{2.62}$$

The difference in the form of the self-consistency relations (2.62 and (2.20) is due to the difference in normalization of $\mathbf{r_p}$ here and in Sec.2.3. Here we have $|\mathbf{r_p}| = 1$, while in Sec.2.3 we had $|\mathbf{r_p}| = n_\mathbf{p}^2 + (1 - n_\mathbf{p})^2 < 1$ which is precisely the factor $Q_\mathbf{p}$ needed to account for the difference in the norm.

2.9 Appendix B: Numerical simulation of the pairing dynamics

For our numerical analysis we used Bloch dynamical equations (2.24) for the pseudospin variable together with the self-consistency equation for the order parameter Δ. The pseudospins are numbered by the energy state in the range of an appropriate energy bandwidth W centered at the Fermi level. The magnitude of the equilibrium order parameter Δ has to be chosen such that the energy states involved in the dynamics fall into the bandwidth W, and no other states get excited. Simple physical considerations convince that only states with energies of the order of the equilibrium gap Δ_0 participate in the dynamics. The typical ratio of the equilibrium order parameter to the bandwidth $\Delta/W = 0.2$ used in our numerical calculations is enough to ensure the consistency of the simulation.

The numerical simulation of the pairing dynamics of cold fermions was programmed using Matlab (©The Mathworks, Inc.). This choice is justified by highly effective algorithms for matrix operations implemented in Matlab, since the dynamical equations have simple vector structure in both energy and time domain.

To study the dynamics in the thermodynamic limit we choose the number of states in the bandwidth $W = 10$ to be $N = 1000 - 100000$ which gives for the level spacing $\delta\epsilon = W/N = 0.01 - 0.0001$. The choice of the level spacing in this range is sufficient to ensure that both the energy intervals of the order parameter Δ_0 and the temperature $0.01\Delta_0 < T < T_c$ enclose large number of states.

The initial state of the pseudospins, Eq.(2.21), we used in the simulations, de-

scribes free fermions at a finite temperature:

$$r_{1,\mathbf{p}}+ir_{2,\mathbf{p}} = \frac{e^{i\varphi_{\mathbf{p}}}}{2\cosh^2(\frac{1}{2}\beta\epsilon_{\mathbf{p}})},\ r_{3,\mathbf{p}} = \tanh(\tfrac{1}{2}\beta\epsilon_{\mathbf{p}}), \tag{2.63}$$

with uncorrelated phases, uniformly distributed in the interval $0 < \varphi_{\mathbf{p}} < 2\pi$. Such initial conditions correspond to the amplitudes $u_{\mathbf{p}}$, $v_{\mathbf{p}}$ of the form (2.14).

To study the dynamics one needs to solve $3 \times N$ differential equations simultaneously. Inspection of the Bloch equations provides us with $N + 1$ integrals of motion. First N integrals of motion fix the norm of the Bloch vector $|\mathbf{r}| = const$ for every energy state. An additional integral of motion is obtained after summing up the Bloch equations for the third component of the Bloch vector which gives $\sum_{\mathbf{p}}(r_3)_{\mathbf{p}} = const$.

The integration of $3 \times N$ differential equations is performed using the fourth order Runge-Kutta method with precision $O(dt^5)$. The time step is fixed through the integration, and we find that value $dt = 0.01/\Delta_0$ provides sufficient precision for all our calculations. We implement the Runge-Kutta algorithm in the Matlab programming language instead of using the standard program provided with Matlab to have more flexibility over the different parameters and better control over the precision of the calculation.

The form of the order parameter dynamics for initial conditions Eq.(2.21) can be fitted with high accuracy by the elliptical function dn with three parameters: the amplitude Δ_+, the period T, and the time lag τ. The thermal noise in the initial conditions leads to the variation of these parameters for different realizations. For every realization we extract the corresponding parameters from the fit and then plot the pair distributions. The statistics presented in Figs.(2-5), and (2-5) is obtained for 500 realizations.

Below we describe the MatLab code used to simulate the pairing dynamics. The comments along the code are written in **boldface** font.

MATLAB CODE: BCS PAIRING DYNAMICS SIMULATION OF THE BLOCH EQUATIONS

START OF THE CODE

$clear\ all;$

The energy band centered at the Fermi surface

(in case of superconductors, it is $2 \times \omega_{Debay}$:)

$band = 10;$

We assume the uniform distribution of states.

The number of energy states inside the energy band:

$N = 1000;$

The energy of a state, $p^2/2m - E_F$, within the energy band:

$Bz = (2 * (1 : N) - N - 1)/(N - 1) * band/2;$

The equilibrium gap Δ_0:

$Delta0 = 2; D0 = Delta0;$

The energy step:

$step = band/(N - 1);$

Calculation of the coupling constant g corresponding to Δ_0 :

$S = 0;$

$for\ j = 1 : N$

$x = (j - 0.5) * step;$

$S = S + step/sqrt(D0\text{^}2 + Bz(j)\text{^}2);$

$end;$

Dimensionless coupling constant g:

$g = 2/S;$

Energy step multiplied by the dimensionless coupling constant g:

$G = g * band/(N - 1)$

Time interval of integration:

$T = 20/D0$

Time step of integration:

$dt = 0.01/D0;$

The relaxation constant $gamma$

(no relaxation corresponds to $gamma = 0$**):**

$gamma = 0.0$

Chemical potential (Fermi energy)

(large values correspond to the particle-hole symmetry):

$mu = 1E + 20 * band/(2 * 0.49);$

Start of the initial spin distribution on the energy axis.

$nx = zeros([1, N]); ny = zeros([1, N]); nz = zeros([1, N]);$

We consider spin distribution of the non-interacting Fermi gas

at finite temperature T**, parameterized by** $beta = 1/T$**:**

$beta = 10/D0;$

Random angle uniformly distributed on a circle:

$theta = zeros([1, N]);$

$theta = rand(1, N) * 2 * pi;$

Spin distribution:

$nx = cos(theta)./(2 * cosh(beta * Bz/2).\hat{}2);$

$ny = sin(theta)./(2 * cosh(beta * Bz/2).\hat{}2);$

$nz = tanh(beta * Bz/2);$

End of the initial spin distribution on the energy axis.

Auxiliary energy variable, $Hz = 2 \times (p^2/2m - E_F)$**:**

$Hz = zeros([1, N]);$

$Hz = band * (2 * (1 : N) - N - 1)/(N - 1);$

Energy dependent density of states

(equal to 1 **in the case of the particle-hole symmetry):**

$Dos = sqrt(1 + Hz/(2 * mu));$

Effective magnetic field acting on spins:

$Hx = G * nx * Dos';$

$Hy = G * ny * Dos';$

Number of time iterations during the integration:

$Nit = round(T/dt);$

It is convenient to change the sign of the time step:

$dt = -abs(dt);$

The initial components of the pairing amplitude divided by the equilibrium gap (e.g. dimensionless):

$Deltax = zeros([1, Nit]); Deltay = zeros([1, Nit]);$

$Delta = zeros([1, Nit]);$

$Deltax(1) = Hx/2/D0;$

$Deltay(1) = Hy/2/D0;$

$Delta(1) = sqrt(Hx\text{^}2 + Hy\text{^}2)/2/D0;$

Total z-component of the spin (conserved quantity):

$Deltaz = zeros([1, Nit]);$

$Deltaz(1) = G * nz * Dos'/2/D0;$

START OF THE 4th ORDER RUNGE-KUTTA

FIRST ITERATION

Auxiliary variables necessary for the time integration:

$kx1 = zeros([1, N]); ky1 = zeros([1, N]); kz1 = zeros([1, N]);$

$kx2 = zeros([1, N]); ky2 = zeros([1, N]); kz2 = zeros([1, N]);$

$kx3 = zeros([1, N]); ky3 = zeros([1, N]); kz3 = zeros([1, N]);$

$kx4 = zeros([1, N]); ky4 = zeros([1, N]); kz4 = zeros([1, N]);$

Effective magnetic field acting on spins:

$$Hx = G * nx * Dos'; Hy = G * ny * Dos';$$

$$Bx = Hx + gamma * (nz * Hy - ny. * Hz);$$

$$By = Hy + gamma * (nx. * Hz - nz * Hx);$$

$$Bz = Hz + gamma * (ny * Hx - nx * Hy);$$

$$kx1 = nz. * By - ny. * Bz;$$

$$ky1 = nx. * Bz - nz. * Bx;$$

$$kz1 = ny. * Bx - nx. * By;$$

$$Hx = G * (nx + dt * kx1/2) * Dos'; Hy = G * (ny + dt * ky1/2) * Dos';$$

$$Bx = Hx + gamma * (nz * Hy - ny. * Hz);$$

$$By = Hy + gamma * (nx. * Hz - nz * Hx);$$

$$Bz = Hz + gamma * (ny * Hx - nx * Hy);$$

$$kx2 = By. * (nz + dt * kz1/2) - (ny + dt * ky1/2). * Bz;$$

$$ky2 = (nx + dt * kx1/2). * Bz - Bx. * (nz + dt * kz1/2);$$

$$kz2 = Bx. * (ny + dt * ky1/2) - By. * (nx + dt * kx1/2);$$

$$Hx = G * (nx + dt * kx2/2) * Dos'; Hy = G * (ny + dt * ky2/2) * Dos';$$

$$Bx = Hx + gamma * (nz * Hy - ny. * Hz);$$

$$By = Hy + gamma * (nx. * Hz - nz * Hx);$$

$$Bz = Hz + gamma * (ny * Hx - nx * Hy);$$

$$kx3 = By. * (nz + dt * kz2/2) - (ny + dt * ky2/2). * Bz;$$

$$ky3 = (nx + dt * kx2/2). * Bz - Bx. * (nz + dt * kz2/2);$$

$$kz3 = Bx. * (ny + dt * ky2/2) - By. * (nx + dt * kx2/2);$$

$$Hx = G * (nx + dt * kx3) * Dos'; Hy = G * (ny + dt * ky3) * Dos';$$

$$Bx = Hx + gamma * (nz * Hy - ny. * Hz);$$

$$By = Hy + gamma * (nx. * Hz - nz * Hx);$$

$$Bz = Hz + gamma * (ny * Hx - nx * Hy);$$

$kx4 = By. * (nz + dt * kz3) - (ny + dt * ky3). * Bz;$

$ky4 = (nx + dt * kx3). * Bz - Bx. * (nz + dt * kz3);$

$kz4 = Bx. * (ny + dt * ky3) - By. * (nx + dt * kx3);$

END OF THE FIRST ITERATION

THE RUNGE-KUTTA INTEGRATION

Start of the integration cycle

$for\ j = 2 : Nit$

$nx = nx + dt/6 * (kx1 + 2 * kx2 + 2 * kx3 + kx4);$

$ny = ny + dt/6 * (ky1 + 2 * ky2 + 2 * ky3 + ky4);$

$nz = nz + dt/6 * (kz1 + 2 * kz2 + 2 * kz3 + kz4);$

CALCULATION OF THE PAIRING AMPLITUDE:

$Deltax(j) = G * nx * Dos'/2/D0;$

$Deltay(j) = G * ny * Dos'/2/D0;$

$Delta(j) = sqrt(Deltax(j)\text{^}2 + Deltay(j)\text{^}2);$

$Deltaz(j) = G * nz * Dos'/2/D0;$

$Hx = G * nx * Dos'; Hy = G * ny * Dos';$

$Bx = Hx + gamma * (nz * Hy - ny. * Hz);$

$By = Hy + gamma * (nx. * Hz - nz * Hx);$

$Bz = Hz + gamma * (ny * Hx - nx * Hy);$

$kx1 = By. * nz - ny. * Bz;$

$ky1 = nx. * Bz - Bx. * nz;$

$kz1 = Bx. * ny - By. * nx;$

$Hx = G * (nx + dt * kx1/2) * Dos'; Hy = G * (ny + dt * ky1/2) * Dos';$

$Bx = Hx + gamma * (nz * Hy - ny. * Hz);$

$By = Hy + gamma * (nx. * Hz - nz * Hx);$

$Bz = Hz + gamma * (ny * Hx - nx * Hy);$

$kx2 = By. * (nz + dt * kz1/2) - (ny + dt * ky1/2). * Bz;$

$ky2 = (nx + dt * kx1/2). * Bz - Bx. * (nz + dt * kz1/2);$

$kz2 = Bx. * (ny + dt * ky1/2) - By. * (nx + dt * kx1/2);$

$Hx = G * (nx + dt * kx2/2) * Dos'; Hy = G * (ny + dt * ky2/2) * Dos';$

$Bx = Hx + gamma * (nz * Hy - ny. * Hz);$

$By = Hy + gamma * (nx. * Hz - nz * Hx);$

$Bz = Hz + gamma * (ny * Hx - nx * Hy);$

$kx3 = By. * (nz + dt * kz2/2) - (ny + dt * ky2/2). * Bz;$

$ky3 = (nx + dt * kx2/2). * Bz - Bx. * (nz + dt * kz2/2);$

$kz3 = Bx. * (ny + dt * ky2/2) - By. * (nx + dt * kx2/2);$

$Hx = G * (nx + dt * kx3) * Dos'; Hy = G * (ny + dt * ky3) * Dos';$

$Bx = Hx + gamma * (nz * Hy - ny. * Hz);$

$By = Hy + gamma * (nx. * Hz - nz * Hx);$

$Bz = Hz + gamma * (ny * Hx - nx * Hy);$

$kx4 = By. * (nz + dt * kz3) - (ny + dt * ky3). * Bz;$

$ky4 = (nx + dt * kx3). * Bz - Bx. * (nz + dt * kz3);$

$kz4 = Bx. * (ny + dt * ky3) - By. * (nx + dt * kx3);$

End of the integration cycle.

end;

END OF THE RUNGE-KUTTA INTEGRATION.

END OF THE 4th ORDER RUNGE-KUTTA.

Now we plot the results of the calculation:

$t = T * D0/Nit * (0 : Nit - 1);$

$odin = ones(1, Nit);$

$plot(t, Delta, '-b', 'LineWidth', 2); hold\ on;$

$plot(t, odin, '-g', 'LineWidth', 2);$

$xlabel('Time \times \Delta_0')$

$ylabel('$Absolute value of the pairing amplitude, $|\Delta(t)|/\Delta_0')$

$grid\ on;$

END OF THE CODE

Chapter 3

Collective dynamics near a Feshbach resonance of cold fermions

3.1 Introduction

Cold Fermi gas at a Feshbach resonance can be used to explore the non-equilibrium pairing dynamics discussed in Chapter 2. Here, we study properties of cold fermions resonantly coupled to Feshbach molecules.

The physics near the resonance in a macroscopic system is sensitive to the effects of quantum statistics. In particular, at positive detuning from the resonance molecules can coexist with fermions [10, 11, 47, 48], stabilized by Pauli blocking of molecular decay into the states below the Fermi level. The stability and properties of the mixed state depend on the interaction effects. Below we argue that the interactions greatly enhance stability of the atom-molecule mixture, and lead to molecules and atom pairs hybridizing to form a coherent state. We address the problem of molecules interacting with atoms by mapping it onto the Dicke problem [49] of two-level systems coupled to a Bose field. This problem, being exactly solvable [50], allows to describe the experimentally relevant regime of strong coupling. In the Feshbach resonance case,

the two-level systems represent fermion pair states which can be occupied or empty, while the Bose field represents molecules.

The coupling to molecules at positive detuning from Feshbach resonance enhances pairing interaction between fermions, which is expected to stimulate BCS superfluidity [9, 10, 11, 12, 13, 47, 48]. In addition, as noted by Holland *et al.* [10] and Timmermans *et al.* [11], the strong coupling BCS condensation, with the critical temperature up to a fraction of E_F, may depend on the presence of molecular field. This conclusion was strengthened by a microscopic analysis carried out by Ohashi and Griffin [12], by Milstein *et al.* [13], who refine the approach of Ref. [10]. Bruun and Pethick [48] studied noncondensed molecules coexisting with the Fermi gas at positive detuning using an effective theory of strong coupling formulated in terms of low energy parameters. It was noted that strong many-body effects exist even for detuning well above the Fermi energy. The important role of molecular field at positive detuning has been reemphasized recently by Falco and Stoof [47], who argued that a BCS-BEC crossover takes place in this region.

Here we focus on the effects of molecule-atom hybridization and develop an approach allowing to handle this problem in the strong coupling regime. This is of interest, since the experiment deals with systems where the atom-molecule coupling, measured in the Fermi energy units, is very large. We will see that molecule-atom mixing occurs in this situation in the range of detuning much larger than the Fermi energy, i.e. on the energy scale very different from that of fermionic condensate. The energy scale for the latter, set by the pairing interaction strength, expected to reach $0.2\,E_F$ at best [13], is much smaller than the atom-molecule interaction. Thus accurate results can be obtained with the help of a simple analysis which ignores direct pairing interaction between fermions, and relies on the exact solution of the atom-molecule dynamics.

Below we analyze stability of fermions with respect to molecule formation, and obtain a phase diagram. There is a fairly wide region around the resonance, spanning both positive and negative detuning, were atoms and molecules coexist, forming a coherent state. At strong coupling, this region has width of the order of $g^2 n/E_F$,

a quantity which different estimates [47, 48] put between few tens and few hundred E_F for current experiments [16, 18, 17]. Also, we exploit the Dicke problem solution to obtain nonlinear oscillations of the molecular field, in which population coherently oscillates between molecular and atomic components. The results of stability analysis are verified by comparing to the exact solution and to the thermodynamic ground state properties.

This Chapter is organized as follows. In Section 3.2, we map the system of resonantly coupled atoms and molecules on the Dicke model of quantum optics. The stability analysis of the degenerate Fermi gas at a Feshbach resonance is carried out in Section 3.3. The integrability of the Dicke model is exploited in Section 3.4 to study the nonlinear dynamics of the molecular state. We summarize our results in Section 3.5.

3.2 Dicke model

We consider the problem of a Fermi gas interacting with molecules in a single mode approximation which takes into account only the lowest energy molecular state:

$$\mathcal{H} = \sum_{p,\alpha} \frac{p^2}{2m} a^+_{p,\alpha} a_{p,\alpha} + g \sum_p \left(b^+ c_p + \text{h.c.} \right) + \omega b^+ b \tag{3.1}$$

with a_p, a_p^+ and b, b^+ the atom and molecule operators, α the fermion spin, and ω the energy of a molecule. The atom pair creation and annihilation operators $c_p = \frac{1}{\sqrt{2}} \left(a_{-p\downarrow} a_{p\uparrow} + a_{p\downarrow} a_{-p\uparrow} \right)$, $c_p^+ = \frac{1}{\sqrt{2}} \left(a^+_{p\uparrow} a^+_{-p\downarrow} + a^+_{-p\uparrow} a^+_{p\downarrow} \right)$ describe pairs of fermions in a spin singlet state that undergo conversion into molecules at Feshbach resonance. The approximation (3.1) is justified by the analysis below which finds that the energy gained by a formation of a mixed atom-molecule state, with all molecules occupying one state, is large compared to E_F, which allows to limit consideration to a single molecular state.

The utility of the single mode approximation (3.1) is that it turns a difficult many-body problem into a well-known exactly solvable problem. The mapping is achieved

by identifying the pair operators c_p, c_p^+ with pseudospin Pauli operators [24]

$$c_p = \sigma_p^- \equiv \frac{1}{2}(\sigma_p^x - i\sigma_p^y), \quad c_p^+ = \sigma_p^+ \equiv \frac{1}{2}(\sigma_p^x + i\sigma_p^y) \tag{3.2}$$

and noting that their product gives the particle number operator $n_p = a_p^+ a_p$ in the subspace of the many-body Hilbert space in which both states p and $-p$ are simultaneously filled or empty, $2c_p^+ c_p \equiv n_p + n_{-p} = 0, 2$. More formally, defining $\sigma_p^z = [\sigma_p^+, \sigma_p^-]$, one verifies that the standard Pauli spin commutation relations hold:

$$[\sigma_p^+, \sigma_p^z] = -2\sigma_p^+, \quad [\sigma_p^-, \sigma_p^z] = 2\sigma_p^- \tag{3.3}$$

This enables one to bring the Hamiltonian (3.1) to the form containing the spin variables only,

$$\mathcal{H} = \sum_p{}' \left(\frac{p^2}{2m}\sigma_p^z + gb\sigma_p^+ + gb^+\sigma_p^- \right) + \omega b^+ b \tag{3.4}$$

where the sum is taken over singlet pair states with momenta p and $-p$. We note that the states with $n_p + n_{-p} = 1$, with only one of the p and $-p$ particle states filled and the other one empty, are decoupled and do not participate in the dynamics defined by (3.4). The reason for this decoupling is that these states have not enough particles to form a molecule, but also one particle too many to contribute to molecule dissociation.

The spin-boson problem (3.4) is the Dicke model of quantum optics [49, 50, 51]. Hepp and Lieb [50] found that the Hamiltonian (3.4) is integrable, and constructed exact many-body states. Besides the total particle number

$$N = 2b^+ b + \sum_p \left(1 + \sigma_p^z\right) \tag{3.5}$$

there are also infinitely many nontrivial conserved quantities underpinning the exact solubility.

The problem (3.4) resembles in many ways the BCS pairing problem. The latter is also integrable, which allows to obtain the full energy spectrum, and to construct

nontrivial conserved quantities in a closed form [52]. In fact, the above pseudospin trick has its roots in the BCS problem, where it was invented by Anderson [24] as an interpretation of Bogoliubov mean field theory.

3.3 Stability diagram of the degenerate Fermi gas

Here we employ the Hamiltonian (3.4) to assess stability of the Fermi gas with respect to molecule formation. The spin dynamics described by (3.4) is of the Bloch form, $\dot{\sigma} = i[\mathcal{H}, \sigma] = 2\mathbf{h}_p \times \sigma$, with an effective magnetic field $\mathbf{h}_p = (gb', gb'', p^2/2m)$, where $b = b' + ib''$ is a c-number describing the molecular state in macroscopic limit.

The Bloch equations of motion for the spin components $\sigma_p^{\pm}$, σ_p^z and b take the form

$$i\dot{\sigma}_p^+ = -(p^2/m)\sigma_p^+ + gb\sigma_p^z, \quad i\dot{\sigma}_p^- = (p^2/m)\sigma_p^- - gb\sigma_p^z \tag{3.6}$$

$$i\dot{\sigma}_p^z = 2gb\sigma_p^+ - 2gb^*\sigma_p^-, \quad i\dot{b} = g{\sum_p}' \sigma_p^- + \omega b \tag{3.7}$$

From a mathematical standpoint, Eqs.(3.6),(3.7) describe collective dynamics of a Bloch spin 1/2 ensemble, with the coupling between the spins provided by the 'magnetic field' $\mathbf{h}_p$ transverse components which depend on the spin variables via an equation for b. Physically, the transverse spin components $\sigma_p^{\pm}$ characterize coherence between the filled and unfilled pair state, while σ_p^z describes the number of pairs.

Since the field b is a c-number, the operator equations (3.6),(3.7) are linear, and thus the spin operators expectation values are subject to evolution equations of the form identical to (3.6),(3.7). In the absence of molecules, we have $b = 0$, and all the spins are aligned in the $\pm z$ direction, with probabilities determined by occupation of pair states: $\langle \sigma_p^z \rangle = p_\uparrow - p_\downarrow = n_p^2 - (1-n_p)^2 = 2n_p - 1$, where $n_p = (e^{\beta(p^2/2m-\mu)} + 1)^{-1}$ in thermal equilibrium. This state, containing only fermions but no molecules, $\langle b \rangle = \langle \sigma_p^{\pm} \rangle = 0$, is stationary for the problem (3.6),(3.7).

To assess stability with respect to molecule formation, we linearize Eqs.(3.6),(3.7), introducing $\delta\sigma_p^-, \delta b \propto e^{-i\lambda t}$, $\delta\sigma_p^+, \delta b^* \propto e^{i\lambda^* t}$. From the coupled linear equations for

$\delta\sigma_p^-$ and δb we obtain the eigenvalue equation

$$\lambda = \omega + g^2 \sum_p \frac{\langle \sigma_p^z \rangle}{p^2/m - \lambda} \tag{3.8}$$

To make the formally divergent sum over p well-behaved, following Ohashi and Griffin [53], we renormalize ω by subtracting the term $\delta\omega = g^2 \sum_p (p^2/m)^{-1}$. The shift $\omega \to \omega - \delta\omega$ brings the position of the Feshbach resonance to $\omega = 0$ for zero particle density, while Eq.(3.8) transforms to

$$\lambda = \omega + g^2 \sum_p \left(\frac{2n_p - 1}{p^2/m - \lambda} + \frac{1}{p^2/m} \right) \tag{3.9}$$

with the sum now converging at large p.

The solution of Eq.(3.9) can be real or complex, depending on the value of ω. Complex-valued $\lambda = \lambda' + i\lambda''$ indicates an instability, with λ'' describing the instability growth rate. Numerical analysis of the solutions of Eq.(3.9) and simple analytic arguments reveal that (i) the real part λ' is a monotonic function of ω; (ii) the instability occurs in an interval $\omega_0 < \omega < \omega_1$ with the threshold values $\omega_{0,1}$ being a function of temperature.

The values $\omega_{0,1}$ can be inferred by noting that the complex λ becomes real at $\omega = \omega_{0,1}$, which gives the condition $\lambda'' = 0$. When does Eq.(3.9) admit real solutions? This is possible for $\lambda \leq 0$, as well as for $\lambda = 2\mu$, since $2n_p - 1$ changes sign at $p = p_F$. (For all positive λ except $\lambda = 2\mu$ the residue $\langle \sigma_p^z \rangle = 2n_p - 1$ generates a finite imaginary part of λ.) With $\lambda = 0,\ 2\mu$ one obtains

$$\begin{aligned} \omega_0 &= -g^2 \sum_p \frac{2n_p}{p^2/m} \\ \omega_1 &= 2\mu + g^2 \sum_p \left(\frac{1 - 2n_p}{p^2/m - 2\mu} - \frac{1}{p^2/m} \right) \end{aligned} \tag{3.10}$$

This indicates that atoms are stable at $\omega > \omega_1$, metastable at $\omega < \omega_0$, and at $\omega_0 < \omega < \omega_1$ can exist only in a state coherently mixed with the molecules (Fig. 3-

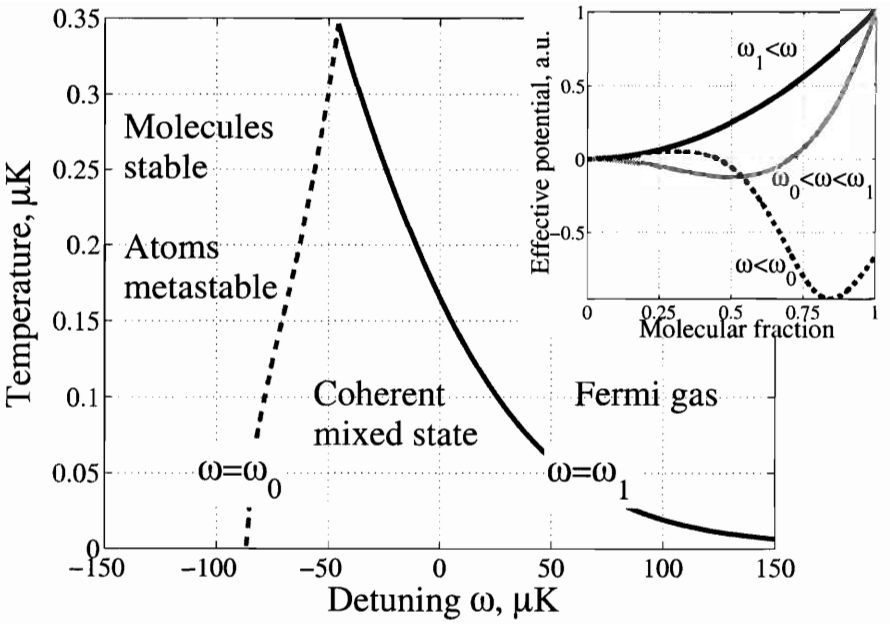

Figure 3-1: Phase diagram of coupled atom-molecule system obtained from Eq.(3.10) for ^{40}K system [16] at particle density $n \approx 1.8\times10^{13}\text{cm}^{-3}$, Fermi energy $E_F = 0.35\mu$K, and coupling strength $g^2n/E_F \approx 60\mu$K. (The coupling was estimated using the microscopic theory of Feshbach resonance developed by Falco and Stoof [47], applied to the conditions of the JIlA experiment [16]). *Inset:* Effective potential schematic illustrating the behavior in the three regions.

1). We note that, since $\omega_0 < 0$ and $\omega_1 > 2\mu$, coexistence is favored by interaction. Moreover, at strong interaction, the detuning range where coexistence takes place becomes very large: $\Delta\omega \simeq g^2n/E_F \gg E_F$.

The upper temperature at which $\omega_0 = \omega_1$ is determined by the condition $\mu(T) = 0$. For a two-species Fermi gas of total particle density n one has $n = 2\sum_p n_p(\mu = 0) = 0.0972(m/\beta)^{3/2}$ which gives $T_* = 0.9885\,E_F$. Interestingly, at low temperature $T \ll T_*$, the instability is pushed to higher detuning, $\omega_1 = 2\mu + g^2\nu\ln(\mu/T)$, due to a BCS-like log divergence at the Fermi level $p = p_F$.

It is instructive to look at the JILA experiment parameters (Fig. 3-1). The estimate of coupling $\Delta\omega = g^2n/E_F \simeq 60\mu\text{K} \approx 8\,\text{MHz}$ gives a typical energy gained by the system via molecules and atom pairs hybridization, which is much larger than E_F. This leads to pair size in the mixed state $\sim \hbar/(2m\Delta\omega)^{1/2}$ much smaller than fermion wavelength p_F^{-1}. This indicates that the kinetic energy of atoms *and molecules* does

not play a significant role, justifying the single mode approximation.

3.4 Nonlinear dynamics of the molecular state

Nonlinear dynamics at instability can be found with the help of the mapping to Bloch spins. Defining $r_p^{\pm} = \langle \frac{1}{2}(\sigma_p^x \pm i\sigma_p^y) \rangle$, $r_p^z = \langle \sigma_p^z \rangle$, and rescaling $gb \to b$, we write

$$i\dot{r}_p^- = (p^2/m) r_p^- - b r_p^z \,, \quad i\dot{r}_p^z = 2b r_p^+ - 2b^* r_p^- \tag{3.11}$$

$$i\dot{b} = \omega b + g^2 \sum_p r_p^- \tag{3.12}$$

Since the norm is preserved by Bloch time evolution, $|\mathbf{r}_p|^2 = 4r_p^- r_p^+ + (r_p^z)^2$ is conserved for each spin. We apply rotation,

$$r_p^- \to e^{-i\eta t} r_p^- \,, \quad r_p^+ \to e^{i\eta t} r_p^+ \,, \quad b \to e^{-i\eta t} b \tag{3.13}$$

with the value η to be determined later. This is equivalent to shifting $p^2/m \to \epsilon_p = p^2/m - \eta$ and $\omega \to \omega - \eta$.

The resulting problem possesses real-valued solutions which can be obtained from the standard ansatz [54]

$$r_p^- = A_p b + i B_p \dot{b} \,, \quad r_p^z = D_p - C_p b^2 \tag{3.14}$$

Substituting this into Eqs.(3.11),(3.12), from the real part of the equation or r_p^- and from the the equation or r_p^z one finds the relations between the ansatz parameters $A_p = \epsilon_p B_p$, $C_p = 2B_p$ while the imaginary part of the equation or r_p^- generates a set of equations

$$B_p \ddot{b} + \epsilon_p b - b(D_p - C_p b^2) = 0 \tag{3.15}$$

The constant of motion $|\mathbf{r}_p|^2 = 4r_p^- r_p^+ + (r_p^z)^2$ provides a first integral of Eq.(3.15):

$$4\left(\epsilon_p^2 b^2 + \dot{b}^2\right) + \left(2b^2 - D_p/B_p\right)^2 = B_p^{-2} |\mathbf{r}_p|^2 \tag{3.16}$$

where we expressed A_p and C_p through B_p.

Evidently, since the function $b(t)$ is the same for all spins, the dependence on p has to drop out of Eq.(3.16), giving a single equation for b of the form

$$\dot{b}^2 = (b^2 - b_-^2)(b_+^2 - b^2), \quad b_- < b_+ \tag{3.17}$$

which is possible with the following choice of constants:

$$D_p/B_p - \epsilon_p^2 = b_-^2 + b_+^2, \quad D_p^2 - |\mathbf{r}_p|^2 = 4b_-^2 b_+^2 B_p^2 \tag{3.18}$$

These equations determine the modulus of B_p and D_p only. The sign has to be determined from initial conditions: $\operatorname{sgn} B_p = \operatorname{sgn} D_p = \operatorname{sgn} r_p^z$,

The solution of Eq. (3.17) is an elliptic function $b(t) = \operatorname{dn}(t, \kappa^2)$ with $\kappa^2 = 1 - b_-^2/b_+^2$ [55], oscillating periodically between b_- and b_+. At $b_- \ll b_+$, the solution is approximately given by a train of weakly overlapping solitons

$$b(t) = \sum_n \frac{\gamma}{\cosh \gamma(t - t_n)}, \quad t_n = \tau n, \tag{3.19}$$

where each soliton in Eq.(3.19) is a solution of Eq. (3.17) with $b_- = 0$, $b_+ = \gamma$. On Fig. 3-2, the pseudospin dynamics of Eqs.(3.14) on a Bloch sphere is illustrated.

The quantities $b_\pm$ and the frequency η must be determined from the equation for b. One verifies that Eq.(3.12) is consistent with the ansatz (3.14) and obtains

$$\begin{aligned} 1 &= g^2 \sum_p \frac{r_p^z}{\sqrt{\left(\epsilon_p^2 + b_-^2 + b_+^2\right)^2 - 4b_-^2 b_+^2}}, \\ \omega &= \eta - g^2 \sum_p \left(\frac{\epsilon_p r_p^z}{\sqrt{\left(\epsilon_p^2 + b_-^2 + b_+^2\right)^2 - 4b_-^2 b_+^2}} + \frac{1}{p^2/m} \right), \end{aligned} \tag{3.20}$$

Here $r_p^z = 2n_p - 1$ corresponds to the energy distribution n_p of fermions which depends on the initial state. For the parameters used in Fig. 3-1, by order of magnitude we estimate $\gamma, \tau^{-1} \simeq g^2 n/E_F \approx 8\,\mathrm{MHz}$. This is much faster than typical energy

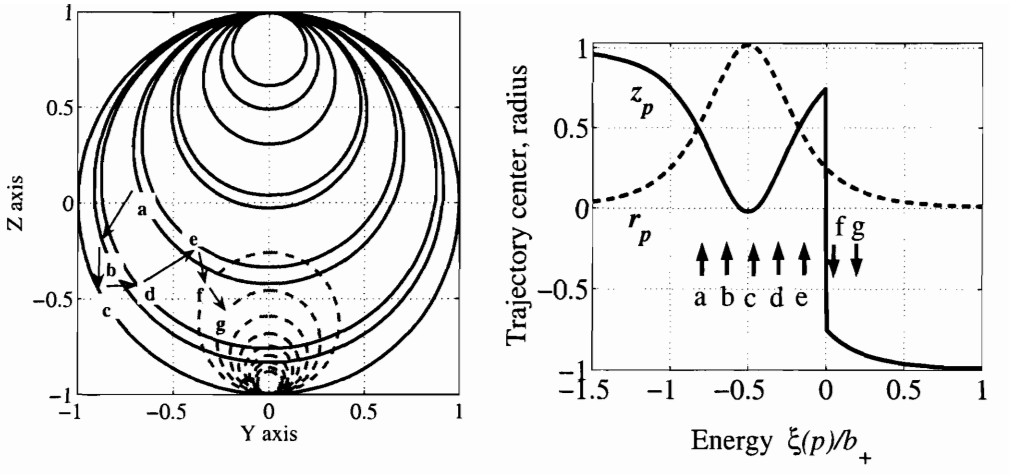

Figure 3-2: *Left:* Time evolution (3.14) of fermion pair amplitudes with different energies obtained for the molecular field of a soliton train form (3.19). The Bloch sphere parametrization of pseudospin variables $r_p^{x,y,x} = \langle \sigma_p^{x,y,x} \rangle$ is used. Pseudospins precess so that each state completes a full 2π Rabi cycle per soliton. The red and blue curves correspond to the energies above and below the Fermi level. *Right:* The dependence of the trajectory center and the radius on the energy state for the states denoted by the letters on the left.

relaxation rates, which justifies ignoring relaxation effects in the dynamics.

The properties at equilibrium can be understood by considering the limit $b_- \to b_+ = b_0$, when oscillations are absent. The energy distribution n_p can be easily obtained in the pseudospin picture, taking into account that each spin is presented with a tilted field $\mathbf{h}_p = (b_0, 0, p^2/2m - \mu)$ which gives $n_p = 1/\left(1 + e^{\beta|\mathbf{h}_p|}\right)$. The molecular field b_0 in the ground state is determined by

$$\omega = \eta + g^2 \sum_p \left(\frac{1 - 2n_p}{\sqrt{\epsilon_p^2 + 4b_0^2}} - \frac{1}{p^2/m} \right) \tag{3.21}$$

along with the constraint $N = 2b_0^2/g^2 + 2\sum_p n_p$.

Here we use Eq.(3.21) to verify the above stability analysis. To determine when the atoms can be stable with respect to hybridizing with molecules, we set $b_0 = 0$ and immediately recover Eq.(3.9) for the instability exponent λ. The difference, however, is that η defined by Eq.(3.21) is real, while λ is complex. Atoms' stability is thus

indeed equivalent to the existence of a real-valued solution of Eq.(3.9). One possibility to have such a solution is to set $\eta = 2\mu$, which eliminates the log divergence in (3.21) at $\epsilon_p = 0$. The other possibility is to have $\mu, \eta \leq 0$. Put together with the properties of equilibrium state at finite b_0, this confirms the above estimate of the coexistence region (3.10) and the conclusion that pure atom state is metastable at the detuning $\omega < \omega_0$.

3.5 Summary

In summary, we studied the properties of the degenerate Fermi gas interacting with molecules near Feshbach resonance and demonstrated that molecule-atom mixing occurs in this situation in the range of detuning much larger than the Fermi energy. The characteristic energy scales make the Dicke model approximation that ignores molecular dispersion as well as the BCS fermion pairing effects accurate enough. We explored the stability diagram of the Fermi gas and found that there is a fairly wide region around the resonance, spanning both positive and negative detuning, were atoms and molecules coexist, forming a coherent state. This region has width of the order of $g^2 n/E_F$, a quantity which different estimates [47, 48] put between few tens and few hundred E_F for current experiments [16, 18, 17]. Also, we used the Dicke problem solution to obtain nonlinear oscillations of the molecular field, in which population coherently oscillates between molecular and atomic components.

Chapter 4

Dynamical projection of atoms to Feshbach molecules at strong coupling

4.1 Introduction

As we demonstrated in Chapter 3, fermionic atoms resonantly coupled to molecules at a Feshbach resonance are unstable with respect to formation of the mixed state in the wide detuning range around the resonance with critical temperatures up to the degeneracy temperature of Fermi gas. Cold fermions in these systems are expected to be in the paired many-body state similar to that of the BCS theory of superconductivity [9, 10, 11]. The experimental detection of the state is an important topic of current research. In this Chapter, we consider fast magnetic field projection of atomic state to Feshbach molecules, and demonstrate that this method allows to probe the pairing correlations in the initial state of Fermi gas.

This Chapter is organized as follows. In Section 4.2, we discuss the projection experiments [16, 17] probing the pairing correlations in Fermi gas at the Feshbach resonance. The properties of a single molecule resonantly coupled to atoms are described in Section 4.3. General formalism that allows to study the dynamics of the

molecule formation for linear sweeps is considered in Section 4.4. To apply these results to the experimental situation of Ref. [16], in Section 4.5 we find the asymptotic expressions for the molecule production for linear sweeps starting on the atomic side of the resonance, and compare our calculation to the experimental observations. In Section 4.6, we summarize our results.

4.2 Probing the pairing correlations in experiments

An interesting method of atomic state projection on to the Feshbach molecules using the magnetic field sweep through the resonance was employed in the recent experiments [16, 17]. The sweep could be made very fast compared to typical fermion time scales, such as the collision frequency or inverse Fermi bandwidth and pairing energy gap, making the process a "snapshot probe" with regard to the collective fermion processes. Since the system is out of the equilibrium during this process, one may expect that the pairing correlations in the initial state will affect the momentum distribution of molecules in the final state, provided that the measurements are performed on a time scale shorter than the relaxation time.

There is an important aspect in the molecular dynamics during the sweep. On a single particle level, broad Feshbach resonances studied in Refs. [16, 17], exhibit strong atom-molecule coupling in a relatively wide detuning range. In this sense, the sweep speed [16, 17] corresponds to essentially adiabatic atom/molecule conversion, slow on the scale of the resonance width. For example, in the JILA experiment [16], the Feshbach resonance width $\Delta B \simeq 10\,\mathrm{G}$ translates into $\Delta\nu \simeq 180\,\mathrm{MHz}$ in detuning frequency, while the characteristic time of the magnetic field sweep, $\tau_* = (dt/d\nu)^{1/2} \simeq 1\,\mu\mathrm{s}$, is about 10^2 times longer than $\Delta\nu^{-1}$. A similar estimate applies to the MIT fast projection experiment [17]. Somewhat paradoxically, the fermions involved in this "slow" molecule formation are the same whose many-body state is being analyzed by the dynamical "snapshot" projection. Thus a correct physical picture of the molecular state swept through the resonance must combine the adiabatic single-particle and the "snapshot" many-body aspects in a seamless way.

Continuing efforts to use atom/molecule projection as investigative tool call for better understanding of the driven molecular state. The Landau-Zener model [56, 57], which fits the data well near saturation [58], focuses on the adiabatic aspects, ignoring molecule dissociation into the continuous spectrum of atom pairs on the fermionic side of the resonance. The dynamical mean field approach [59, 60, 61, 62, 63, 64, 65, 66], which can be justified for bosons in the atomic BEC regime, lacks firm foundation in the fermion case. Recently, the many-body state overlap models [67, 68, 69, 70] were put forward. While providing some guidance, these approaches do not account for the experimentally relevant situation of broad resonance [16, 17] when the "snapshot" many-body projection is slow on the scale of individual molecule formation.

We describe the molecules swept through the resonance using a time-dependent Green's function which fully accounts free relative motion of the atoms associating to form molecules. While our method is quite general and applicable to Feshbach resonances with any angular momentum, here we focus, for the sake of concreteness, on the s-wave case. We consider the evolution from equilibrium at $\nu = \nu_0$, followed by an abrupt linear sweep:

$$\nu(t) = \begin{cases} \nu_0, & t < 0 \\ \nu_0 - \alpha t, & t > 0 \end{cases} \tag{4.1}$$

with α the sweep rate. The generalization to the p-wave resonances [71, 72, 73, 74, 75] will be straightforward (see below).

4.3 Molecular Green's function

Let us recall the form of the two-channel Hamiltonian [2], describing pairs of fermions binding to form molecules at the resonance:

$$\mathcal{H} = \mathcal{H}_a + \mathcal{H}_m + \sum_{\mathbf{p},\mathbf{p}'} \left(g b^+_{\mathbf{p}+\mathbf{p}'} a_{\mathbf{p}\uparrow} a_{\mathbf{p}'\downarrow} + \text{h.c.} \right) \tag{4.2}$$

with $\mathcal{H}_a = \sum_{\mathbf{p}\sigma} \frac{p^2}{2m} a^+_{\mathbf{p}\sigma} a_{\mathbf{p}\sigma}$, $\mathcal{H}_m = \sum_{\mathbf{k}} (\nu + \frac{k^2}{4m}) b^+_{\mathbf{k}} b_{\mathbf{k}}$, and $a_{\mathbf{p}\sigma}$, $b_{\mathbf{k}}$ the atom and molecule operators, σ the spin ($\hbar = 1$). The detuning ν is determined by the molecule and two-atom Zeeman energy difference, $\nu = \Delta\mu\,(B - B_0)$.

The single molecule Green's function, obtained from Dyson equation [48], has the form

$$G(\omega, k) = \frac{1}{\tilde{\omega} - \nu - \Sigma(\tilde{\omega})}, \quad \tilde{\omega} = \omega - \frac{k^2}{4m} + i0, \tag{4.3}$$

where $\Sigma(\omega) = \lambda(-\omega)^{1/2}$ is the self-energy describing molecule dissociation (s-wave), which arises after integrating over the 3d density of atom pair states $N(\epsilon) \propto \epsilon^{1/2}$ along with a suitable ultraviolet regularization [27].

For time-independent ν, the molecular state dressed by atom pairs, is described by the Green's function pole:

$$G_0(\omega) = \frac{Z(\omega)}{\omega - \omega(k) + i0} \tag{4.4}$$

with $\omega(k)$ given by $\tilde{\omega} - \Sigma(\tilde{\omega}) = \nu$. Near the resonance, at $|\nu| \ll \Delta E_* = \lambda^2$, neglecting ω compared to $\Sigma(\omega)$, one obtains molecular energy quadratic in detuning:

$$\omega(k) = -(\nu/\lambda)^2 + k^2/4m. \tag{4.5}$$

At $\nu < 0$, Eq.(4.5) gives the energy of molecules, while at $\nu > 0$ it describes a resonance in the two-fermion scattering mediated by virtual molecules [76]. The residue Z defines the bare molecule weight in the physical molecule state, $Z^{-1}(\omega) = dG^{-1}/d\omega = 1 + \frac{\lambda}{2}(-\tilde{\omega})^{-1/2}$, which varies from zero to one across the resonance, at $-\Delta E_* \lesssim \nu < 0$. At relatively small detuning, $|\nu/\Delta E_*| \ll 1$, Z increases linearly: $Z(\omega) \approx 2|\nu|/\lambda^2$.

4.4 Dynamics of the molecule formation

To investigate molecule formation at the resonance, we consider the Green's function for the problem with time-dependent detuning $\nu(t)$. In this case, due to nonlocal

character of Σ in the time domain, the molecule evolution is described by an integral-differential equation [62, 63]

$$\left(i\partial_t - \nu(t) - \tfrac{k^2}{4m}\right) b_k(t) - \int \Sigma_k(t,t') b_k(t') dt' = \eta_k(t) \tag{4.6}$$

with $\eta_k(t) = g\int e^{-ikx}\psi_\uparrow(x,t)\psi_\downarrow(x,t)d^3x$ the pairing field, and $\psi_\sigma(x,t) = \sum_p a_{p,\sigma}e^{ipx-i\epsilon_p t}$. Here the self-energy is

$$\Sigma_k(t>t') = \int \Sigma_k(\tilde{\omega})e^{-i\omega(t-t')}\frac{d\omega}{2\pi} = \frac{ae^{-i\frac{k^2}{4m}(t-t')}}{(t-t')^{3/2}}, \tag{4.7}$$

$a = \frac{\lambda}{2\sqrt{i\pi}}$, and $\Sigma(t<t')$ vanishes due to the causality.

The pairing field η, which acts as a source in Eq.(4.6), should be taken as a c-number for the condensed molecules (with $k = 0$), and as an operator for the incoherent molecules. Generally, its correlation function includes both the coherent and incoherent parts:

$$\langle \bar{\eta}_{k,\omega}\eta_{k,\omega}\rangle = (2\pi)^4|\eta_0|^2\delta(\omega-\mu)\delta(k) + K(\omega,k), \tag{4.8}$$

where η_0 describes a finite amplitude for two fermions to have opposite momenta in the paired state, with $\mu \lesssim 2E_F$ the chemical potential of a pair, and $K(\omega,k) = \langle\langle \bar{\eta}_{k,\omega}\eta_{k,\omega}\rangle\rangle$ the dynamical pair correlator which is nonzero even for ideal Fermi gas. We first consider the coherent molecule production, treating both $\eta = \eta_0 e^{-i\mu t}$ and $b(t)$ as c-numbers. The incoherent pair source $K(\omega,k)$ will be discussed subsequently below.

Finding the time-dependent Green's function is a nontrivial mathematical problem, here solved exactly using an idea similar to that of the Wiener-Hopf method. The important time scale, characterizing the adiabaticity of the sweep (see Fig. 4-1 inset), is found to be

$$\tau_0 = \left(\hbar\lambda^2/\alpha^2\right)^{1/3}, \quad \lambda = g^2m^{3/2}/4\pi\hbar^3, \tag{4.9}$$

with g the atom-molecule coupling (see Eq.(4.2)), and m the atom mass. The time

scale τ_0 can also be inferred, as noted by Altman and Vishwanath [70], from the adiabaticity condition $\dot{\omega} \lesssim \omega^2$ for the time-dependent molecule energy $\hbar\omega$.

The evolution problem (4.6) is non-elementary due to nonlocality of $\Sigma(t,t')$. Our approach employs an idea similar to that used in the Wiener-Hopf method. We first handle an auxiliary problem in which the linear sweep $\nu(t) = \nu_0 - \alpha t$ extends from $-\infty$ to ∞, and then modify the solution to describe the situation of interest (4.1).

The auxiliary problem in question is to find $b(t)$, $-\infty < t < \infty$, which obeys a linear integral-differential equation

$$(\hat{\omega} - \nu_0 - \Sigma(\hat{\omega}) + \alpha t)\, b(t) = \eta(t)\,, \quad \hat{\omega} = i\partial_t \tag{4.10}$$

with a source term $\eta(t)$ of a generic form. It is convenient to go to Fourier representation, in which $t = -i\partial_\omega$ and the problem is reduced to an ordinary differential equation $(\omega - \Sigma(\omega) - \nu_0 - i\alpha\partial_\omega)\, b(\omega) = \eta(\omega)$ for $b(\omega) = \int e^{i\omega t} b(t) dt$. Solution of this equation, first order in ∂_ω, is found using the gauge transformation $b(\omega) \to e^{i\varphi(\omega)} b(\omega)$ with the phase φ satisfying

$$-\alpha\varphi'(\omega) = D_0(\omega) \equiv \omega - \Sigma(\omega) - \nu_0. \tag{4.11}$$

This problem is solved by the function

$$b(\omega) = -i\alpha^{-1} e^{i\varphi(\omega)} \int_\omega^{+\infty} e^{-i\varphi(\omega')} \eta(\omega') d\omega'. \tag{4.12}$$

To verify (4.12), one can compare its behavior to that of $b(\omega) = Ce^{i\varphi(\omega)}$, the solution to the homogeneous problem (4.10). For ω large and positive, since $(-\omega - i0)^{1/2} = -i\sqrt{\omega}$, we obtain the asymptotic behavior $D_0 \approx i\lambda\omega^{1/2}$, $\varphi \approx -i(2/3)\,(\tau_0\omega)^{3/2}$, $e^{\pm i\varphi} \propto e^{\pm a\omega^{3/2}}$ ($a = (2/3)\tau_0^{3/2}$). Thus, $C = 0$ is required to eliminate exponential growth. Indeed, the asymptotic behavior of the integral in (4.12) at large positive ω is non-exponential: $\int_\omega^{+\infty} e^{-i\varphi(\omega')} \eta(\omega') d\omega' \approx e^{-i\varphi(\omega)} \eta(\omega)/\varphi'(\omega)$. (For any physical source, $\eta(\omega \to \infty)$ is algebraic.) At the same time, the behavior at large negative ω does not require special attention: φ is real at $\omega < 0$, and so the exponentials $e^{\pm i\varphi}$ oscillate as $e^{\pm ia(-\omega)^{3/2}}$

without giving rise to "dangerous" asymptotic behavior. Notice, that the adiabaticity time scale, τ_0, naturally appeared in the phase dynamics, as we discussed before.

Now, having found the solution for the sweep spanning the entire range $-\infty < t < +\infty$, let us consider the sweep trajectory (4.1). In this case, it is convenient to represent the function $b(t)$ as a sum $b_<(t) + b_>(t)$, with $b_{>,<}(t)$ nonzero only at $t \geq 0$ ($t \leq 0$), respectively, obtained by restricting $b(t)$ on the half-line $t \geq 0$ ($t \leq 0$). Then the evolution equation, in operator form written as $(\hat{\omega} - \nu(t) - \Sigma(\hat{\omega}))\, b(t) = \eta(t)$, can be represented as

$$\hat{D}_0 b_< + (\hat{D}_0 + \alpha\hat{t}) b_> = \eta_< + \eta_> \tag{4.13}$$

with $\eta_{>,<} = \theta(\pm t)\eta(t)$ having the same meaning as $b_{>,<}(t)$, and $\hat{D}_0 \equiv D_0(\hat{\omega})$ defined in Eq.(4.11).

Let us project the terms on the left hand side on the regions $t \geq 0$, $t \leq 0$, taking into account the constraints due to causality. The integral operator Σ acts only forward, not backward in time, the property explicit in Eq.(4.7). Thus the function $\left(D_0(\hat{\omega}) + \alpha\hat{t}\right) b_>$ is nonzero only at $t > 0$, while the function $D_0(\hat{\omega}) b_<$ has both the $t > 0$ and the $t < 0$ parts. This observation allows to write the problem as two separate problems for $b_{>,<}(t)$ as follows:

$$\left[\hat{D}_0 b_<\right]_< = \eta_<\,, \quad (\hat{D}_0 + \alpha\hat{t}) b_> + \left[\hat{D}_0 b_<\right]_> = \eta_>, \tag{4.14}$$

where $[...]_{<,>}$ denotes the part of the function at $t > 0$ ($t < 0$), with zero value on the opposite half-line. Now, we can solve the first equation for $b_<$ and substitute the result in the second equation, which (after some algebra) can be brought to the form

$$(\hat{D}_0 + \alpha\hat{t}) b_> = \hat{D}_0 \left[\hat{D}_0^{-1}\eta\right]_> . \tag{4.15}$$

We note that $b_>$ and the function on the right-hand side are both nonzero only at $t > 0$. This allows to treat this equation as Eq.(4.10), formally extending the linear time dependence αt to negative t. Using the above result, we obtain the answer in

Fourier representation of the form (4.12) with η replaced by

$$\tilde{\eta}(\omega) = \hat{D}_0 \left[\hat{D}_0^{-1}\eta\right]_> = D_0(\omega)\int \frac{D_0^{-1}(\omega')\eta(\omega')}{\delta - i(\omega-\omega')}\frac{d\omega'}{2\pi}.$$

Now, let us consider the source $\eta(t) = \eta_0 e^{-i\mu t}$, describing coherent fermion pairs with the chemical potential $\mu/2$ per particle. In this case, $\eta(\omega) = 2\pi\eta_0\delta(\omega-\mu)$ and $\tilde{\eta}(\omega) = D_0^{-1}(\mu)\eta_0 D_0(\omega)/(\delta - i(\omega-\mu))$. Inserting $\tilde{\eta}$ in Eq.(4.12), and using the identity $(\delta - i(\omega-\mu))^{-1} = \int_0^\infty e^{i(\omega-\mu)\tau}d\tau$, we find a closed form representation

$$b(\omega) = \frac{A\eta_0}{\delta - i(\omega-\mu)} + \Delta b(\omega), \tag{4.16}$$
$$\Delta b(\omega) = iA\eta_0 e^{i\varphi(\omega)}\int_0^\infty e^{-i\mu\tau}\tau\int_\omega^{+\infty} e^{i\omega'\tau - i\varphi(\omega')}d\omega' d\tau$$

with $A = D_0^{-1}(\mu)$. (To obtain (4.16), we transformed the integral over ω' by writing $D_0(\omega') = \alpha d(\omega'\tau - \varphi(\omega'))/d\omega' - \alpha\tau$ and integrating by parts.) Since the first term of (4.16) gives the would be $b(\omega)$ in the absence of the sweep, $\Delta b(\omega)$ describes the effect of the sweep.

4.5 Asymptotic production efficiency of molecules

Now, let us analyze the asymptotic behavior of $b(t) = \int e^{-i\omega t}b(\omega)d\omega/2\pi$ at large positive $t \gg \tau_0, \nu_0/\alpha$. In this case, the integral over ω is controlled by large negative ω, which can be seen with the help of the stationary phase approximation. Indeed, the saddle point ω_* of $-\omega t + \varphi(\omega)$, obtained from $\varphi' = t$, at $t \to +\infty$ implies $\omega \to -\infty$. With that in mind, we obtain the asymptotic for $b(t)$ by setting the lower integration limit in Eq.(4.16) at $\omega = -\infty$, leading to the central result of this work:

$$\Delta b(t) = -\frac{A\eta_0}{2\pi i}F^*(t)\int_0^\infty e^{-i\mu\tau}\tau F(\tau)d\tau, \tag{4.17}$$
$$F(t) = \int_{-\infty}^{+\infty} e^{i\omega' t - i\varphi(\omega')}d\omega'. \tag{4.18}$$

The qualitative behavior of $F(t)$ can be analyzed using the stationary phase approximation. We obtain $F(t) = \sqrt{-2\pi i/\varphi''(\omega_*)}e^{i\omega_*\tau - i\varphi(\omega_*)}$, where the stationary phase equation for ω_*, given by $D_0(\omega_*) + \alpha t = 0$, has a real solution $\omega_* = -(t-t_0)^2/\tau_0^3$ only for $t > t_0 = \nu_0/\alpha$. Relating the curvature φ'' and the Green's function residue, $-\alpha\varphi'' = D_0' = Z^{-1}$, yields the asymptotic form

$$F(t > t_0) = (2\pi i \alpha Z(\omega_*))^{1/2} e^{-i(t-t_0)^3/3\tau_0^3} \tag{4.19}$$

with $Z(\omega_*) = 2\alpha(t-t_0)/\lambda^2$. (The self-energy-dominated $D_0(\omega) = -\nu_0 - \Sigma(\omega)$, appropriate for broad s-wave Feshbach resonance, was used in the above estimates.) Thus $F(t)$ grows as $(t-t_0)^{1/2}$ and oscillates at $(t-t_0)/\tau_0 \gg 1$, decreasing exponentially at $t - t_0 < 0$.

To apply Eq.(4.17) to the experimental situation we take into account that $\mu \ll \hbar/\tau_0, \hbar/t_0$. (Indeed, $\mu \lesssim 2E_F$, with $E_F = 0.35\,\mu\mathrm{K} = 50\,\mathrm{KHz}$ in Ref. [16].) We evaluate the integral in (4.17) using the stationary phase form (4.19):

$$\Delta b(t) = (2\alpha Z(t))^{1/2} A \eta_0 e^{i(t-t_0)^3/3\tau_0^3}(C_1 t_0 + C_2 \tau_0)\,, \tag{4.20}$$

$C_1 = (i/3)^{1/2}\Gamma(1/2)$, $C_2 = (i/3)^{1/6}\Gamma(5/6)$. The asymptotic number of molecules at time t is evaluated as $N_m^{(0)} = |\Delta b(t)|^2$ (see Fig.4-1). The fast and slow sweep regimes can be identified: at $t_0 \ll \tau_0$ we obtain $N_m \propto \alpha^{-1/3}$, while at $t_0 \gg \tau_0$ we have $N_m \propto \alpha^{-1}$.

The incoherent molecule production can be studied in a similar manner. Using the operator η_k as a source in (4.7), and averaging over its dynamical correlations (4.8) we obtain the molecule momentum distribution

$$N_m(k) = \sum_\omega \left| \frac{A}{2\pi} F^*(t) \int_0^\infty e^{-i\omega\tau} \tau F(\tau) d\tau \right|^2 K(\omega, k). \tag{4.21}$$

with $A = D_0^{-1}(\omega)$. As a function of frequency, K is nonzero at $\omega \lesssim 2E_F$. At $E_F \ll \hbar/\tau_0, \hbar/t_0$, the expression $|...|^2$ is ω-independent, as above. Factoring it out,

we conclude that the condensed and incoherent molecule production efficiencies are identical. The molecule condensate fraction is then expressed through the fermion pair fraction:

$$\frac{N_m^{(0)}}{N_m^{(0)} + \sum_k N_m(k)} = \frac{|\langle \psi_\uparrow(x)\psi_\downarrow(x)\rangle|^2}{\langle \hat{n}_\uparrow(x)\hat{n}_\downarrow(x)\rangle} \tag{4.22}$$

$\hat{n}_\sigma(x) = \bar{\psi}_\sigma(x)\psi_\sigma(x)$. We note that the incoherent contribution exists even in the absence of pairing. For ideal fermions at density n, we have $\sum_\omega K(\omega, k) = \frac{1}{2}g^2 n(1-u)^2(1+u/2)\theta(1-u)$, $u = k/2p_F$, which corresponds to a broad molecule momentum distribution with $k \leq 2p_F$.

As we have seen, different regimes arise depending on the relation between τ_0 and ν_0/α, the time it takes the sweep to reach the resonance (Fig. 4-1). The atom-to-molecule transformation takes place at times less than τ_0 after crossing the resonance, where the evolution is nonadiabatic. At later times, the molecules, dressed by atom pairs, evolve adiabatically. For a fast sweep, $\alpha\tau_0 \gg \nu_0$, the number of produced molecules scales with the sweep rate as $\alpha^{-1/3}$, while for slower sweep, $\alpha\tau_0 \ll \nu_0$, the number of molecules scales as α^{-1}.

These results agree with the molecular number and condensate production efficiency reported by JILA group [16]. The sweep speeds $|dt/dB| \approx 10 - 80\,\mu$s/G [16] correspond to $\nu_0/\alpha \approx 1 - 100\,\mu$s with $\nu_0 = 0.1 - 1\,$G in the magnetic field units. The characteristic atom-molecule coupling $\lambda^2 \approx 1\,$GHz gives the adiabaticity time $\tau_0 \approx 10 - 20\,\mu$s depending on the sweep speed. Thus with $0.2 < \alpha\tau_0/\nu_0 < 10$ both the fast and the slow regimes are realized. Indeed, the molecule number obtained for different sweep speeds below saturation (see Fig. 5 in Ref. [16] displaying the data for $\nu_0 = 0.12\,$G) can be fitted quite accurately with the 1/3 power law dependence, $N_m \propto |dt/dB|^{1/3}$, in agreement with our results (see Fig.(4-2)). Also reasonable, by the order of magnitude, is the predicted total number of produced molecules. Our conclusions regarding the incoherent molecule production channel are consistent with the observed independence of the condensate fraction [16] of the sweep speed. We obtain the same production efficiency for condensed and incoherent molecules (Eq.(4.22)), except near saturation.

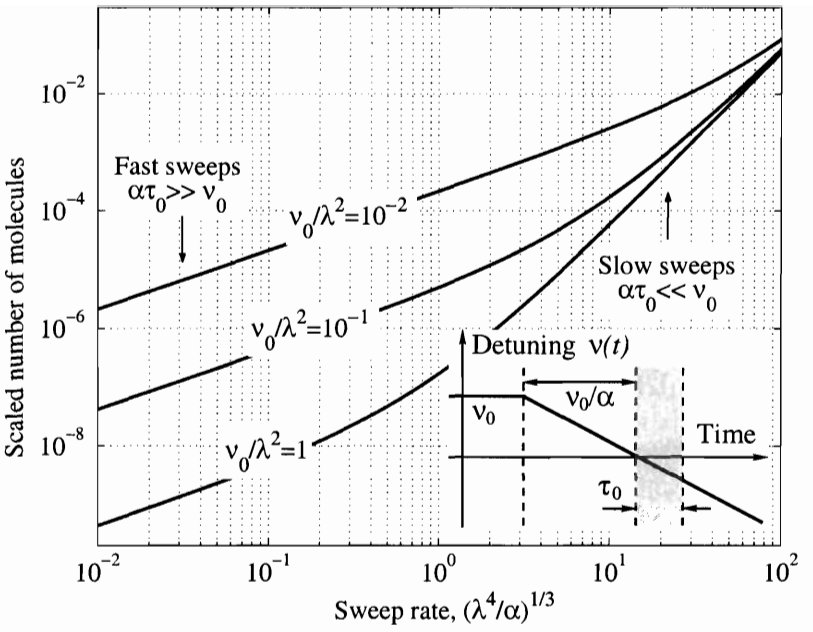

Figure 4-1: Molecule number N_m *vs.* the sweep rate $(\lambda^4/\alpha)^{1/3}$ at different initial detuning ν_0. The asymptotic regimes, $N_m \propto \alpha^{-1}$, $\alpha^{-1/3}$, correspond to slow and fast sweep. Inset: Molecular energy time dependence (4.1) with the time interval corresponding to nonadiabatic evolution marked.

4.6 Summary

In summary, molecule production at Feshbach resonance is considered as a many-body problem for which the exact Green's function is obtained using Wiener-Hopf method. The theory is applied to the s-wave and p-wave resonances. The slow and fast sweep regimes are identified in the s-wave case, controled by the adiabaticity time scale (4.9). The predicted power law 1/3 for the molecule production, as well as the total molecule number, are found to be in agreement with observations away from saturation [16]. The independence of the produced condensate fraction on the sweep rate observed at fast sweep [16] is also explained by this theory.

The approach presented above yields accurate results for the atom/molecule projection in a wide range of sweep rates, fast and slow, as long as the times τ_0, t_0 are short on the scale of E_F. The only limitation stems from the assumption of a steady source, which describes the situation when the fraction of atoms converted into molecules is small. The depletion effects, which are different for the condensed

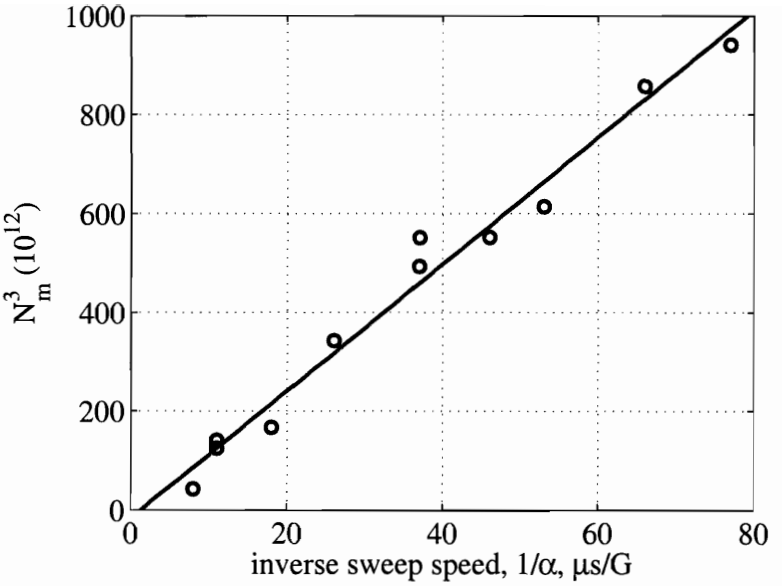

Figure 4-2: Third power of the molecule number, N_m^3, *vs.* the inverse sweep rate $1/\alpha$. A linear fit corresponds to the predicted 1/3 power-law dependence of the molecule production during the sweep. Experimental points are taken from Fig. 5 in Ref. [16]

and incoherent molecules, can be incorporated in the framework of a quantum kinetic equation.

The above method is applicable to the p-wave Feshbach resonance case, with the essential modification in the self-energy form $\Sigma(\omega) \propto (-\omega)^{3/2}$ [73, 74]. This self-energy is an irrelevant perturbation near the resonance, so we have the atom/molecule conversion time $\tau_0 = \alpha^{-1/2}$ and $Z = 1$, as for weak coupling. Thus one can use $D_0(\omega) = \omega - \nu_0$ in (4.11), yielding the result identical to (4.17) with

$$F(t) = \int e^{i\omega(t-t_0)+i\omega^2/2\alpha} d\omega = (2\pi i\alpha)^{1/2} e^{-i\alpha(t-t_0)^2/2}.$$

The number of produced molecules, both condensed and incoherent, scales as inverse sweep rate α^{-1}. The production is less efficient than in the s-channel case due to weaker coupling at resonance.

Chapter 5

Stimulated dissociation of a paired state of cold fermions at a Feshbach resonance

5.1 Introduction

In this Chapter, we consider the excitation spectrum of cold fermions coupled to the molecular state at a Feshbach resonance.

Cold Fermi gases at a magnetically tuned Feshbach resonance in interatomic scattering are expected [10, 11] to host a superfluid state with an order parameter similar to that in the Bardeen-Cooper-Schrieffer (BCS) theory of superconductivity. Fermion pairing in this system is stimulated by coupling of atomic and molecular states [10, 11], enhanced near a Feshbach resonance. The critical temperature of such superfluid state is predicted to reach a fraction of the Fermi energy [10, 11, 12], the temperature already achieved in current experiments which would allow detection of fermionic pairing.

The information about the pairing gap can often be inferred from the excitation spectrum. In a paired state with the excitation gap Δ, the binding energy of a Cooper pair can be released by absorbing the energy quantum $\hbar\omega \geq 2\Delta$. In the

case of superconducting metals, coupling of electrons to crystal lattice and electromagnetic field was employed in the experiments on acoustic attenuation and infrared radiation absorption [77, 78]. In these experiments, the absorption at frequency ω in the superconducting state with the gap Δ creates quasiparticles and, therefore, is only possible above a threshold frequency, $\hbar\omega \geq 2\Delta$. The observation of the threshold frequency in absorption was one of the first tests of the microscopic foundations of the BCS theory [23].

Similar method can be utilized to study the excitation spectrum of cold gases. At a Feshbach resonance, the external magnetic field controls the detuning of molecules with respect to atoms. Perturbation of the external magnetic field causes modulation of molecular energy, while strong hyperfine coupling to the atoms results in the variation of the interaction strength. As a result, excitations are produced if the modulation frequency exceeds the dissociation energy or the pair breaking threshold in the many-body state. Thus, the dependence of the latter on the detuning from the resonance can be extracted from the excitation spectrum.

This Chapter is organized as follows. In Section 5.2, we discuss the excitation spectrum observed in Ref. [15]. Then, in Section 5.3 the Hamiltonian describing the atom-molecule coupling at a Feshbach resonance is presented. We obtain the excitation spectrum in non-degenerate gas in Section 5.4. We extend this calculation to the case of a BCS-like paired state of the Fermi gas in Section 5.5. Finally, we summarize our results in Section 5.6.

5.2 Experimental observation of the excitation spectrum

The excitation spectrum of Fermi gas of ^{40}K atoms at a Feshbach resonance was recently probed in the JILA experiment [15]. The gas of atoms was trapped in a shallow optical trap, and the uniform time-dependent magnetic field applied at different detunings from the resonance produced energetic atoms escaping the trap.

The evaporation rate was measured as a function of the frequency and the detuning. Several important features have been observed in the excitation spectrum. Two distinct peaks were identified at low and high perturbation frequencies, the latter being broad on the scale of the Fermi energy. Low energy peak with its maximum at twice the trap frequency was attributed to the collective excitation driven by the modulation of the interaction strength. At larger frequencies, the response of the gas increased and achieved its maximum above certain threshold. The fall off of the response above the maximum could be well described by a power-law dependence $\omega^{-3/2}$.

On the molecular side of the resonance, threshold frequency and the frequency of maximum response were observed to be a function of the detuning. The threshold frequency was consistent with the dissociation energy of the molecules obtained from the one-body physics. On the atomic side of the resonance, the threshold frequency was close to zero for all detunings. The position of the maximum response in this case was approximately twice the Fermi energy of the gas with a weak tendency to increase with the detuning.

These observations have led [15] to the question about the relation of the high energy peak in the excitation spectrum to the fermionic pairing in the gas. To clarify the relative importance of the one-body and many-body effects in the interpretation of the experimental results, we calculate the excitation spectrum of the Fermi gas caused by a small modulation of the external magnetic field.

We start with a detailed discussion of the excitation of the Fermi gas in the low density limit when effects of the quantum statistics can be neglected and the one-body physics becomes dominant. We show that all main features observed in the experiment can be reproduced in this limit:

(i) The dependence of the threshold frequency and position of the maximum response on detuning as well as the power-law, $\omega^{-3/2}$, at high perturbation frequencies on the molecular side of the resonance;

(ii) On the atomic side of the resonance, at positive detuning, while the one-body physics does not support a stable molecular state, only the processes involving virtual

molecular states contribute to the atom pairs excitation. The resulting excitation spectrum has no threshold frequency and is described by a broad peak with the position weakly depending on the detuning from the resonance with a power-law tail $\omega^{-3/2}$.

We also discuss the modification of the excitation spectrum when many-body effects associated with pairing of fermions are taken into account. On the atomic side of the Feshbach resonance, pairing effects are manifest in a singularity at the energy $\hbar\omega \approx 2|\Delta|$, with the order parameter Δ depending on the detuning from the resonance. On the molecular side, a weaker singularity at a higher energy $\hbar\omega = 2(\Delta^2 + w_0^2)^{1/2}$ where w_0 is the detuning from the resonance, emerges in the spectrum.

5.3 Atom-molecule Hamiltonian at a Feshbach resonance

To study the system of atoms coupled to molecules at a Feshbach resonance, we use two-channel Hamiltonian describing atoms of mass m and molecules of mass $2m$ which undergo mutual conversion:

$$\mathcal{H} = \sum_{\mathbf{k}} \omega_k b_{\mathbf{k}}^+ b_{\mathbf{k}} + \sum_{\mathbf{p},\lambda} \xi_p a_{\mathbf{p}\lambda}^+ a_{\mathbf{p}\lambda} + g \sum_{\mathbf{p},\mathbf{k}} \left(b_{\mathbf{p}} a_{\mathbf{k}+\mathbf{p}/2\uparrow}^+ a_{-\mathbf{k}+\mathbf{p}/2\downarrow}^+ + \text{h.c.} \right), \tag{5.1}$$

where $a_{\mathbf{p}\lambda}^+$ and $b_{\mathbf{k}}^+$ are atom and molecule creation operators. Here, λ labels the internal states, which we refer to as spin 1/2. The kinetic energies of atoms and molecules are given by:

$$\xi_p = p^2/2m, \quad \omega_k = k^2/4m + w_0 \tag{5.2}$$

where the detuning w_0 is defined by the Zeeman splitting of the molecular and atomic states, $w_0 = \Delta\mu\,(B - B_0)$, with the magnetic moment $\Delta\mu$.

In the above Hamiltonian (5.1), we neglected the atomic interaction energy as well as the interaction of molecules. To justify this model we notice that for a Fermi

gas of particle density $n \approx 10^{13}\text{cm}^{-3}$ [16, 17, 15], the typical coupling energy $g\sqrt{n}$ is much larger than the Fermi energy E_F which makes atom-molecule coupling at the Feshbach resonance a dominant physical process in the current experiments.

In the JILA experiment [15], the modulation of the external magnetic field B caused harmonic oscillations in the position of the molecular level w_0:

$$w(t) = w_0 + \delta w \cos(\omega t + \varphi), \quad \delta w \ll |w_0|, \tag{5.3}$$

where ω is the angular frequency of the perturbation, and δw is its amplitude.

While modulation (5.3) does not couple directly to the atoms, the atom-molecule coupling described by the last term in (5.1) makes excitation of atom pairs possible.

5.4 Excitation spectrum of a non-degenerate gas

Let us consider the excitation spectrum of the gas neglecting the degeneracy effects. There are two main mechanisms of energy absorption:

(i) At negative detunings (on the molecular side of the resonance) and temperatures lower than the molecular binding energy, stable molecules exist. In this case, the modulation of the external magnetic field changes the Zeeman splitting between atomic and molecular state while the hyperfine interaction leads to the dissociation of the molecules with a rate depending on the perturbation frequency. This mechanism involving the dissociation of molecules is of main importance at negative detunings.

(ii) At positive detunings, molecular state is unstable, and the first order process discussed above is nonexistent. In this case, the perturbation of the magnetic field affects atoms through second order processes involving creation of virtual molecular state during two-atom scattering. Such processes give the main contribution to the excitation spectrum on the atomic side of the Feshbach resonance, although they also present on its molecular side.

To calculate the absorption spectrum, we need to define the molecule Green's function. For one molecule the Green's function $D(\epsilon, k) = \int e^{i\epsilon t}(-i)\langle \mathrm{T} b_k(t) b_k^+(0)\rangle dt$

can be found from the Dyson equation with the self-energy part describing molecule dissociation into two atoms:

$$\begin{aligned} D(\epsilon,k) &= \frac{1}{D_0^{-1}(\epsilon,k)-\Sigma(\epsilon,k)}, \\ \Sigma(\epsilon,k) &= ig^2\sum_{\epsilon',\mathbf{p}} G_0(\epsilon'_+,\mathbf{p}_+)G_0(-\epsilon'_-,-\mathbf{p}_-) \end{aligned} \tag{5.4}$$

with $\epsilon'_\pm = \epsilon' \pm \epsilon/2$, $\mathbf{p}_\pm = \mathbf{p} \pm \mathbf{k}/2$, and D_0, G_0 the free particle Green's functions of a molecule and an atom without interaction:

$$D_0(\epsilon,k) = \frac{1}{\epsilon-\omega_k+i\delta}, \quad G_0(\epsilon,p) = \frac{1}{\epsilon-\xi_p+i\delta}. \tag{5.5}$$

Here, the energy of an atom and a molecule are correspondingly $\xi_p = p^2/2m$ and $\omega_k = k^2/4m + w_0$.

The Green's function of a single atom is not changed by the interaction because it always involves destruction or creation of two atoms. Thus, in the dilute limit we obtain $G(\epsilon,k) = G_0(\epsilon,k)$.

Evaluating Σ, we obtain

$$D(\epsilon,k) = \frac{1}{\epsilon-\omega_k-\alpha_m g^2\sqrt{-\epsilon+k^2/4m}+i\delta}, \tag{5.6}$$

where $\alpha_m = m^{3/2}/4\pi\hbar^3$ arises after evaluating the integral over p using the 3d density of states $N(\epsilon) \propto \epsilon^{1/2}$ along with a suitable regularization [76].

The spectral weight of the molecular Green's function $\mathrm{Im}D$ has two parts, resonant and continuous, representing the molecular and two-fermion contributions:

$$\mathrm{Im}D(\epsilon,k) = F_m(\epsilon,k) + F_{2a}(\epsilon,k), \tag{5.7}$$

$$F_m(\epsilon,k) = -Z\pi\delta(\tilde{\epsilon}-\epsilon_0)\theta(-\tilde{\epsilon})\theta(-w_0), \tag{5.8}$$

$$F_{2a}(\epsilon,k) = -\frac{\alpha_m g^2\sqrt{\tilde{\epsilon}}}{(\tilde{\epsilon}-w_0)^2+\alpha_m^2 g^4\tilde{\epsilon}}\theta(\tilde{\epsilon}). \tag{5.9}$$

Here, $\tilde{\epsilon} = \epsilon - k^2/4m$, and ϵ_0 is the molecular energy defined by the pole of $D(\epsilon,k)$ at

$w_0 \leq 0$. The corresponding spectral weight Z is given by the residue of this pole:

$$\epsilon_0 = -\frac{1}{4}\left(\sqrt{\alpha_m^2 g^4 + 4|w_0|} - \alpha_m g^2\right)^2, \quad Z = \frac{\sqrt{-\epsilon_0}}{\sqrt{-\epsilon_0} + \alpha_m g^2/2}.$$

Resonant contribution in the spectral weight is zero at positive detuning. The pole in $D(\epsilon, k)$ exists only at negative detuning, so at $w_0 > 0$ contribution to $\mathrm{Im}D(\epsilon, k)$ comes from two-fermion part F_{2a} only.

Now we need to extend the above results, so far derived for a single molecule, to a system in thermodynamic equilibrium. We use the standard Matsubara Green's functions approach in which, to account for finite particle density, chemical potentials of molecules and fermions are introduced: $\xi_\pm = \mathbf{p}_\pm^2/2m - \mu$, $w_0 \to w_0 - 2\mu$. The value of μ must be found from the total particle number $N = 2N_m + N_a$, where

$$N_m = \lim_{\delta \to 0} D(\tau = -\delta, \mathbf{r} = 0), \quad N_a = 2 \lim_{\delta \to 0} G(\tau = -\delta, \mathbf{r} = 0), \tag{5.10}$$

where τ is the imaginary time. In what follows, we will need the retarded Green's functions at finite temperature which can be obtained by the analytic continuation of Matsubara functions from positive frequencies. For molecules,

$$D^R(\epsilon, k) = \frac{1}{(D_0^R(\epsilon, k))^{-1} - \Sigma^R(\epsilon, k)} \tag{5.11}$$

with the regularized [76] self energy part

$$\Sigma^R(\epsilon, k) = \frac{g^2}{2} \sum_{\mathbf{p}} \left(\frac{\tanh(\beta\xi_+/2) + \tanh(\beta\xi_-/2)}{\epsilon - \xi_+ - \xi_- + i0} + \frac{2m}{p^2} \right). \tag{5.12}$$

The system is probed by oscillatory magnetic field which modulates the detuning energy w_0 according to Eq.(5.3). The excitation rate can be evaluated using the Golden Rule ($\hbar = 1$):

$$S(\omega) = 2\pi \sum_{m,n} \delta(E_m - E_n - \omega) |\langle m|V_\omega|n\rangle|^2 \rho_n, \tag{5.13}$$

where the excitation operator is bilinear, $V_\omega = \delta w/2 \sum_p b_p^+ b_p$.

To analyze transitions in a many-body system, it is convenient to relate the Golden Rule transition rate $S(\omega)$ with the imaginary part of a two-particle Green's function $\mathcal{K}(\omega)$ [79]:

$$S(\omega) = (\delta w/2)^2 \, 2\mathrm{Im}\mathcal{K}(\omega)/(1 - e^{-\beta\omega}). \tag{5.14}$$

After standard analytic continuation of Matsubara functions, and evaluating the sum over discrete frequencies, one obtains

$$\mathrm{Im}\mathcal{K}(\omega) = \sum_{\epsilon, \mathbf{k}} \mathrm{Im}D^R(\epsilon + \omega, k) \, \mathrm{Im}D(\epsilon, k) \left(\coth \frac{\epsilon}{2T} - \coth \frac{\epsilon + \omega}{2T} \right). \tag{5.15}$$

Taking into account the two contributions to $\mathrm{Im}D^R$, we find $S(\omega) = S_{m\to 2a}(\omega) + S_{2a\to 2a}(\omega)$ where

$$\begin{aligned} S_{m\to 2a}(\omega) &= (\delta w)^2 \sum_{\mathbf{k}} \pi Z g^2 \theta(-w_0) |D^R(\epsilon_0(k) + \omega, k)|^2 n_P(\epsilon_0(k)) \, \nu_2(\epsilon_0(k) + \omega), \\ S_{2a\to 2a}(\omega) &= (\delta w)^2 \sum_{\epsilon, \mathbf{k}} \pi^2 g^4 |D^R(\epsilon + \omega, k)|^2 |D^R(\epsilon, k)|^2 \nu_2(\epsilon + \omega) \, \nu_2'(\epsilon) \end{aligned} \tag{5.16}$$

with $\epsilon_0(k) = \epsilon_0 + k^2/4m$. Here ν_2 and ν_2' are the two-particle and two-hole density of states:

$$\nu_2(\epsilon) = \sum_{\mathbf{p}} \delta(\epsilon - \xi_- - \xi_+)(1 - n_F(\xi_+))(1 - n_F(\xi_-)) \tag{5.17}$$

and

$$\nu_2'(\epsilon) = \sum_{\mathbf{p}} \delta(\epsilon - \xi_- - \xi_+) \, n_F(\xi_+) n_F(\xi_-) \tag{5.18}$$

with $n_F(\epsilon) = 1/\left(e^{\beta\epsilon} + 1\right)$ the Fermi function.

The structure of the excitation rates in Eqs.(5.16) is rather transparent. The molecule dissociation part $S_{m\to 2a}$ is present only at negative detuning $w_0 < 0$ where stable molecules exist. The molecular distribution factor n_P together with the spectral weight Z counts the number of molecules at a given energy $\epsilon_0(k)$, while the density of states ν_2 gives the number of available energy states for atoms at absorbed energy $\epsilon_0(k) + \omega$ released during the dissociation of molecules. The atomic contribution

$S_{2a\to 2a}$ to the excitation rate has a similar structure where two-particle and two-hole densities of states count available energy states in the process of absorption of energy quanta $\hbar\omega$.

The next step is to evaluate the above expressions in the experimentally interesting limit of a dilute nondegenerate system. In this case, one can ignore the degeneracy effects, treating the occupation numbers in the Boltzmann limit. We obtain:

$$\nu_2(\epsilon) = \frac{\alpha_m}{\pi}\sqrt{\tilde{\epsilon}}, \quad \nu_2'(\epsilon) = \frac{\alpha_m}{\pi}\sqrt{\tilde{\epsilon}}\, e^{-\beta\epsilon}. \tag{5.19}$$

with $\tilde{\epsilon} = \epsilon - k^2/4m + 2\mu$.

At this stage it is convenient to relate $e^{2\beta\mu}$ with the number of molecules:

$$N_m = Z\sum_k e^{-\beta\left(\epsilon_0 + k^2/4m - 2\mu\right)} = Ze^{-\beta(\epsilon_0 - 2\mu)}\left(mT/\pi\hbar^2\right)^{3/2}. \tag{5.20}$$

This expression is obtained in a single pole approximation: $D(\epsilon, k) = Z/\left(\tilde{\epsilon} - \epsilon_0\right)$.

The number of atoms is given by

$$N_a = 2\sum_k e^{-\beta\left(k^2/2m - \mu\right)} = \frac{1}{4}\left(2mT/\pi\hbar^2\right)^{3/2} e^{\beta\mu} \tag{5.21}$$

These expressions for N_m and N_a can be used to relate μ with the total number of particles:

$$N = 2Ze^{-\beta(\epsilon_0 - 2\mu)}\left(mT/\pi\hbar^2\right)^{3/2} + \frac{1}{4}\left(2mT/\pi\hbar^2\right)^{3/2} e^{\beta\mu}. \tag{5.22}$$

Substituting the densities of states ν_2 and ν_2', as well as the expression for the molecular Green's function D^R, we come to the following rates of energy absorption:

$$\begin{aligned} S_{m\to 2a} &= (\delta w)^2 \frac{\theta(-w_0)\theta(\epsilon_0+\omega)\alpha_m g^2\sqrt{\epsilon_0+\omega}\, N_m}{\left(\epsilon_0+\omega-w_0\right)^2 + \alpha_m^2 g^4\left(\epsilon_0+\omega\right)}, \\ S_{2a\to 2a} &= (\delta w)^2 \sum_\varepsilon \frac{\alpha_m^2 g^4\sqrt{2}N_a\sqrt{\varepsilon+\omega}\sqrt{\varepsilon}\, e^{-\beta(\varepsilon-\mu)}}{\left[\left(\varepsilon+\omega-w_0\right)^2 + \alpha_m^2 g^4\left(\varepsilon+\omega\right)\right]\left[\left(\varepsilon-w_0\right)^2 + \alpha_m^2 g^4\varepsilon\right]} \end{aligned} \tag{5.23}$$

Here we note that in current experiments both the magnetic filed detuning from the

Feshbach resonance and the excitation frequency are larger than the atomic energy scales set by the Fermi energy. This means that degeneracy effects associated with the Pauli blocking of fermionic states can be safely ignored. The role of the densities of states in Eq. (5.16), therefore, is only to provide the energy distribution of molecules and atoms in the initial state. The temperature controls the width of such a distribution, and in the following we assume that it is smaller than the excitation frequency and the magnetic detuning. This allows further simplification:

$$S_{m\to 2a} = (\delta w)^2 \frac{\theta(-w_0)\theta(\epsilon_0+\omega)\alpha_m g^2 \sqrt{\epsilon_0+\omega}\, N_m}{(\epsilon_0+\omega-w_0)^2 + \alpha_m^2 g^4 (\epsilon_0+\omega)}, \tag{5.24}$$

$$S_{2a\to 2a} = \frac{(\delta w)^2}{8} \frac{\alpha_m g^4 \sqrt{\omega}\, N_a^2}{(w_0^2 + \alpha_m^2 g^4 O(T))\left((\omega-w_0)^2 + \alpha_m^2 g^4 \omega\right)}. \tag{5.25}$$

The temperature dependence in these expressions enters through the total numbers of molecules and atoms and also as a characteristic energy parameter $O(T)$ in the denominator of the atomic rate (5.25). To compare our results to the experiment [15] we set this scale at the Fermi energy of atomic gas defined by its density.

The behavior of the excitation rates in Eqs.(5.24) and (5.25) reproduces the main features observed in the experiment. On the molecular side of the Feshbach resonance $w_0 < 0$ the main contribution to the excitation spectrum comes from the molecule dissociation given by Eq.(5.24) with threshold corresponding to the binding energy. On the atomic side, the excitation rate is given by the atomic part (5.25) without a threshold. High frequency asymptotic behavior of the probabilities, $S \propto \omega^{-3/2}$ demonstrates the functional dependence observed in the experiment [15]. Such a dependence is a combination of density of states, $\omega^{1/2}$, and the energy denominator given in the second order of the perturbation, ω^{-2}.

5.5 Excitation spectrum of a paired state

To study the effect of fermionic pairing, we evaluate Green's functions of molecules paired with fermions and use it to compute the excitation spectrum. Here it will be

convenient to use Matsubara Green's functions. For noninteracting molecules and atoms, Matsubara Green's functions are

$$\mathcal{D}_0(i\omega,k)=\frac{1}{i\omega-\omega_k},\quad \mathcal{G}_0(i\epsilon,p)=\frac{1}{i\epsilon-\xi(p)}. \tag{5.26}$$

where now $\xi(p)=p^2/2m-\mu$, $\omega_k=w_0+k^2/4m-2\mu$, and μ is a chemical potential.

Developing theory along the lines of Beliaev's and Gorkov's approaches [79] to non-ideal Bose gas and BCS problems, one has to consider a pair of molecular Green's functions $\mathcal{D}(i\omega,k)$, $\breve{\mathcal{D}}(i\omega,k)$ as well as two Green's functions of paired fermions $\mathcal{G}(i\omega,p)$ and $\mathcal{F}(i\omega,p)$:

$$\mathcal{D}(i\omega,k)=\frac{-i\omega-\omega_k-\Sigma_1^*}{|i\omega-\omega_k-\Sigma_1|^2-|\Sigma_2|^2},\quad \breve{\mathcal{D}}(i\omega,k)=\frac{\Sigma_2}{|i\omega-\omega_k-\Sigma_1|^2-|\Sigma_2|^2}, \tag{5.27}$$

$$\mathcal{G}(i\omega,p)=-\frac{i\omega+\xi}{\omega^2+\xi^2+\Delta^2},\quad \mathcal{F}(i\omega,p)=\frac{\Delta}{\omega^2+\xi^2+\Delta^2}. \tag{5.28}$$

The molecular self-energy parts at zero temperature are given by

$$\Sigma_1(i\omega,k)=-g^2\sum_p\int\frac{d\epsilon}{2\pi}\frac{(i\epsilon_++\xi_+)(-i\epsilon_-+\xi_-)}{(\epsilon_+^2+\xi_+^2+\Delta^2)(\epsilon_-^2+\xi_-^2+\Delta^2)} \tag{5.29}$$

$$\Sigma_2(i\omega,k)=-g^2\sum_p\int\frac{d\epsilon}{2\pi}\frac{\Delta^2}{(\epsilon_+^2+\xi_+^2+\Delta^2)(\epsilon_-^2+\xi_-^2+\Delta^2)} \tag{5.30}$$

with $\epsilon_\pm=\epsilon\pm\omega/2$, $\xi_\pm=\xi(\mathbf{p}\pm\mathbf{k}/2)$. Here we introduced the order parameter $\Delta=g\sqrt{N_0}$, where N_0 is the density of molecules in the zero-momentum state.

There is a Goldstone mode associated with the broken symmetry of the paired state. In Beliaev's theory, the condition that this mode has vanishing frequency in long-wavelength limit leads to a self-consistency equation for Δ in the form $w_0-2\mu=-(\Sigma_1+\Sigma_2)_{\omega,k=0}$ or using expressions for self-energies Σ_1, Σ_2:

$$w_0-2\mu=g^2\sum_p\left(\frac{1}{2\tilde{\xi}}-\frac{m}{p^2}\right), \tag{5.31}$$

where $\tilde{\xi}=\sqrt{\xi^2+\Delta^2}$. The chemical potential μ is to be determined from particle

number constraint $2N_m + N_a = N$, where number of molecules and atoms has to be determined from the corresponding Green's functions,

$$N_m = \Delta^2/g^2 + \lim_{\delta\to 0} \mathcal{D}(\tau = -\delta, \mathbf{r} = 0),$$
$$N_a = 2\lim_{\delta\to 0} \mathcal{G}(\tau = -\delta, \mathbf{r} = 0). \tag{5.32}$$

Second term in the expression for N_m corresponds to condensate depletion and can be viewed as a measure of interaction strength between molecules. The necessary condition for our approach to hold would be a small fraction of the non-condensed molecules, and in the following we neglect the effects of condensate depletion. Then conservation of total number of particles gives the following condition:

$$\frac{2}{g^2}\Delta^2 + \sum_p \left(1 - \frac{\xi}{\tilde{\xi}}\right) = N. \tag{5.33}$$

In the presence of small oscillation of molecular energy offset, $\delta w_0(t) = \delta w \cos\omega t$, the excitation rate is given by

$$S(\omega) = \frac{2\pi}{\hbar}\left(\delta w/2\right)^2 N_m \mathrm{Im}\, D(\omega)_{k=0} \tag{5.34}$$

with $N_m = \Delta^2/g^2$ the density of condensed molecules. Here, $D(\omega)$ is a real-frequency molecular Green's function obtained by analytic continuation of $\mathcal{D}(i\omega)$.

Let us evaluate the self-energy parts. Setting $k = 0$, $\xi_\pm = \xi$, integrate over ϵ to obtain

$$\Sigma_1(i\omega) = -g^2 \sum_p \left(-\frac{\Delta^2}{\tilde{\xi}(4\tilde{\xi}^2 + \omega^2)} + \frac{2\tilde{\xi}}{4\tilde{\xi}^2 + \omega^2} + \frac{i\omega\xi}{\tilde{\xi}(4\tilde{\xi}^2 + \omega^2)}\right) \tag{5.35}$$

$$\Sigma_2(i\omega) = -g^2 \sum_p \frac{\Delta^2}{\tilde{\xi}(4\tilde{\xi}^2 + \omega^2)} \tag{5.36}$$

with $\tilde{\xi} = \sqrt{\xi^2 + \Delta^2}$.

Regularization $\Sigma_1 \to \Sigma_1 + g^2 \sum_p \frac{m}{p^2}$, brings the resonance at low density to $w_0 = 0$.

Regularized Σ_1 has the form

$$\Sigma_1(i\omega) = -g^2 \sum_p \left(-\frac{\Delta^2 + \omega^2/2}{\tilde{\xi}(4\tilde{\xi}^2 + \omega^2)} + \frac{i\omega\xi}{\tilde{\xi}(4\tilde{\xi}^2 + \omega^2)} \right) + g^2 \sum_p \left(\frac{m}{p^2} - \frac{1}{2\tilde{\xi}} \right) \tag{5.37}$$

Expressions (5.37),(5.36) form the basis of the forthcoming calculation.

It is convenient to rewrite Σ_1 as a sum of the parts even and odd in ω:

$$\Sigma_1(i\omega) = -w_0 + 2\mu + \Sigma_1'(i\omega) + i\Sigma_1''(i\omega) \tag{5.38}$$

with

$$\Sigma_1'(i\omega) = g^2 \sum_p \frac{\Delta^2 + \omega^2/2}{\tilde{\xi}(4\tilde{\xi}^2 + \omega^2)}, \quad \Sigma_1''(i\omega) = -g^2 \sum_p \frac{\omega\xi}{\tilde{\xi}(4\tilde{\xi}^2 + \omega^2)} \tag{5.39}$$

where we used the self-consistency relation (5.31) to express the last term of Eq.(5.37) in terms of w_0. With the help of Σ_1', Σ_1'' one can write the molecule Green's function as

$$\mathcal{D}(i\omega) = \frac{-i\omega - \Sigma_1' + i\Sigma_1''}{(\omega - \Sigma_1'')^2 + \Sigma_1'^2 - \Sigma_2^2} \tag{5.40}$$

To study this expression, we simplify

$$\Sigma_1'^2 - \Sigma_2^2 = \omega^2(\Delta^2 + \omega^2/4)\lambda^{-2} F_1^2(\omega), \quad \lambda = \frac{4}{\alpha g^2} \tag{5.41}$$

$$F_1(\omega) = \int_0^\infty \frac{x^{1/2} dx}{((x-\mu)^2 + \Delta^2)^{1/2}((x-\mu)^2 + \Delta^2 + \omega^2/4)}$$

where the variable x is atom kinetic energy, $x \equiv \epsilon = p^2/2m$. (The sum $\sum_p ...$ is evaluated as $\int_0^\infty ...N(\epsilon)d\epsilon$ with the $d = 3$ density of states is $N(\epsilon) = \alpha\epsilon^{1/2}$, $\alpha = (2m)^{3/2}/4\pi^2\hbar^3$.)

Similarly, we rewrite Σ_1'' as

$$\Sigma_1''(i\omega) = -\omega\lambda^{-1} F_2(\omega) \tag{5.42}$$

$$F_2(\omega) = \int_0^\infty \frac{(x-\mu)x^{1/2} dx}{((x-\mu)^2 + \Delta^2)^{1/2}((x-\mu)^2 + \Delta^2 + \omega^2/4)} \tag{5.43}$$

Using representation (5.41),(5.42), one can write the expression for the Green's function $\mathcal{D}$ as

$$\mathcal{D}(i\omega) = -\lambda \frac{(\Delta^2 + \omega^2/2)F_1(\omega) + i\omega(\lambda + F_2(\omega))}{\omega^2\left((\lambda + F_2(\omega))^2 + (\Delta^2 + \omega^2/4)F_1^2(\omega)\right)}. \tag{5.44}$$

The resulting expression (5.44) has a pole $\omega = 0$ (Goldstone mode). Also, from the structure of the functions $F_{1,2}$ one can deduce that, after continuation $i\omega \to \omega$, the imaginary part of $D(\omega)$ will have a BCS-like inverse square root singularity at $\omega = 2\Delta$ if μ is positive, and somewhat weaker singularity at a higher energy $\omega = 2(\Delta^2 + \mu^2)^{1/2}$ if μ is negative.

5.6 Summary

In summary, we studied the excitation spectrum of atomic gas at a Feshbach resonance, where strong coupling of the molecular and atomic states has been employed to excite the system using the modulation of the external magnetic field. To explore the role of statistics on the excitation spectrum we consider the non-degenerate limit as well as the degenerate paired state. There are two contributions, coherent and incoherent, to the excitation rate which are important on different sides of the Feshbach resonance. In the nondegenerate case the coherent contribution plays the dominant role on the molecular side of the resonance, disappearing on the atomic side where the incoherent contribution comes into play. The coherent contribution has the excitation threshold corresponding to the molecular binding energy as opposed by the incoherent part starting from zero excitation energy. The high frequency behavior of coherent and incoherent parts of the excitation rate follows the power-law $S(\omega) \propto \omega^{-3/2}$ confirmed by the experiment [15].

In the case of the paired state we calculate only coherent contribution and demonstrate that it has a BCS-like threshold singularity in the excitation spectrum at frequency corresponding to twice the pairing gap with the characteristic dependence on the detuning from the Feshbach resonance.

To compare the contributions to the excitation spectrum for the nondegenerate and paired state we plot the calculated excitation rates on Fig.5-1. At negative

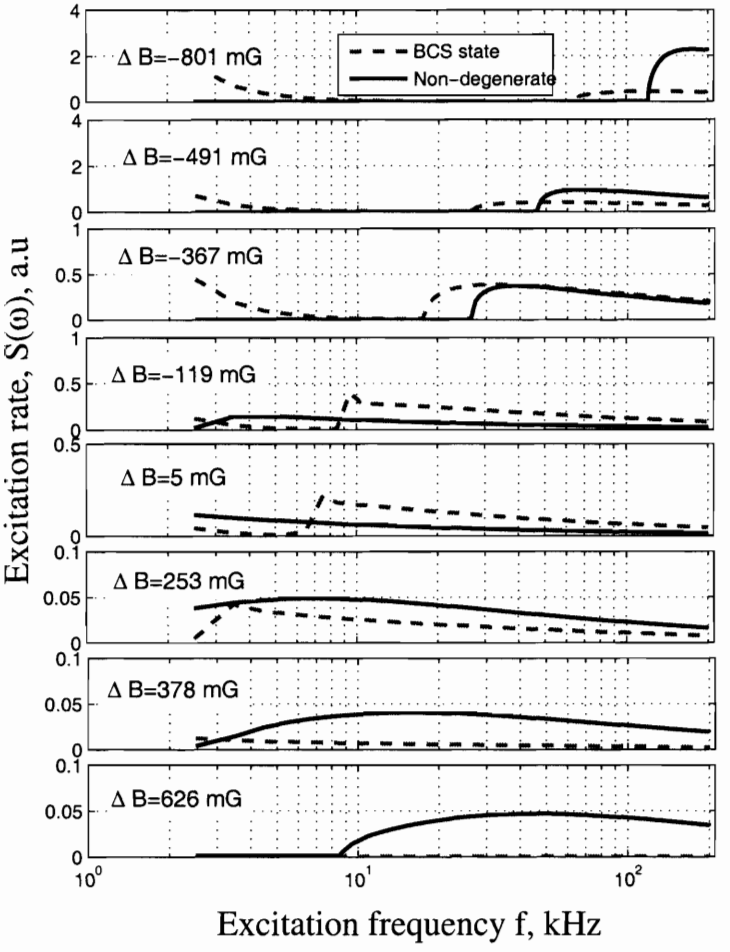

Figure 5-1: The excitation rate $S(\omega)$ *vs.* the perturbation frequency f. The solid line represents both coherent and incoherent contributions to the excitation rate in the nondegenerate case, while the dashed line corresponds to the paired state of the gas.

detuning, $\Delta B < 0$, there is a threshold corresponding to the molecular binding energy. At positive detuning, $\Delta B > 0$, the noticeable BCS-like singularity appears at the frequency equal twice the pairing gap. As one goes further to positive detunings from the Feshbach resonance the singularity shifts to lower frequencies and becomes less pronounced.

Bibliography

[1] M. H. Anderson, J. R. Ensher, M. R. Matthews, C. E. Wieman, and E. A. Cornell, Science **269**, 198 (1995)

[2] E. Timmermans, P. Tommasini, M. Hussein, and A. Kerman, Physics Reports **315**, 199 (1999).

[3] S. Inouye, M. R. Andrews, J. Stenger, Nature, **392**, 151 (1998)

[4] Ph. Courteille, R. S. Freeland, D. J. Heinzen, F. A. van Abeelen, and B. J. Verhaar Phys. Rev. Lett. **81**, 69 (1998)

[5] S. L. Cornish, N. R. Claussen, J. L. Roberts, E. A. Cornell, and C. E. Wieman, Phys. Rev. Lett. **85**, 1795 (2000).

[6] T. Loftus, C. A. Regal, C. Ticknor, J. L. Bohn, and D. S. Jin, Phys. Rev. Lett. **88**, 173201 (2002)

[7] K. M. O'Hara, S. L. Hemmer, M. E. Gehm, S. R. Granade, and J. E. Thomas, Science **298**, 2179 (2002);

[8] Z. Hadzibabic, S. Gupta, C. A. Stan, C. H. Schunck, M. W. Zwierlein, K. Dieckmann, and W. Ketterle Phys. Rev. Lett. **91**, 160401 (2003)

[9] J. L. Bohn, Phys. Rev. A **61**, 053409 (2000)

[10] M. Holland, S. J. J. M. F. Kokkelmans, M. L. Chiofalo, and R. Walser, Phys. Rev. Lett. **87**, 120406 (2001)

[11] E. Timmermans, K. Furuya, P. W. Milonni, and A. K. Kerman, Phys. Lett. A **285**, 228 (2001)

[12] Y. Ohashi and A. Griffin, Phys. Rev. Lett. **89**, 130402 (2002)

[13] J. N. Milstein, S. J. J. M. F. Kokkelmans, and M. J. Holland, Phys. Rev. A **66**, 043604 (2002)

[14] C. Chin, M. Bartenstein, A. Altmeyer, S. Riedl, S. Jochim, J. Hecker Denschlag, R. Grimm, Science, **305**, 1128 (2004)

[15] M. Greiner, C. A. Regal, and D. S. Jin, Phys. Rev. Lett. **94**, 070403 (2005)

[16] C. A. Regal, M. Greiner, and D. S. Jin, Phys. Rev. Lett. **92**, 040403 (2004)

[17] M. W. Zwierlein, C. A. Stan, C. H. Schunck, S. M. F. Raupach, A. J. Kerman, and W. Ketterle, Phys. Rev. Lett. **92**, 120403 (2004)

[18] J. Kinast, S. L. Hemmer, M. E. Gehm, A. Turlapov, and J. E. Thomas, Phys. Rev. Lett. **92**, 150402 (2004)

[19] M. Bartenstein, A. Altmeyer, S. Riedl, S. Jochim, C. Chin, J. Hecker Denschlag, and R. Grimm, Phys. Rev. Lett. **92**, 203201 (2004)

[20] M. W. Zwierlein, J. R. Abo-Shaeer, A. Schirotzek, C. H. Schunck and W. Ketterle, Nature **435**, 1047 (2005)

[21] J. Kinast, A. Turlapov, J. E. Thomas, Q. Chen, J. Stajic, K. Levin, Science **307**, 1296 (2005)

[22] J. Kinnunen, M. Rodríguez, P. Törma, Science **305**, 1131 (2004)

[23] M. Tinkham, *Introduction to Superconductivity*, (McGraw-Hill, 1996)

[24] P. W. Anderson, Phys. Rev. **112**, 1900 (1958)

[25] N. N. Bogoliubov, V. V. Tolmachev, and D. V. Shirkov, *A new method in the theory of superconductivity*, (New York, Consultants Bureau, 1959)

[26] J. Bardeen, L. N. Cooper, and J. R. Schrieffer, Phys. Rev. **108**, 1175 (1957)

[27] L. D. Landau and E. M. Lifshitz, *Quantum Mechanics*, (Pergamon, New York, 1987)

[28] L. P. Gor'kov and T. K. Melik-Barkhudarov, Zh. Eksp. Teor. Fiz. **40**, 1452, (1961) [Sov. Phys. JETP, **13**, 1018 (1961)]

[29] A. J. Leggett, in *Modern trends in the theory of condensed matter*, (Springer-Verlag, 1980)

[30] P. Nozières and S. Schmitt-Rink, J. Low Temp. Phys. **59**, 195 (1985)

[31] M. Randeria, in *Bose-Einstein Condensation*, edited by A. Griffin, D. Snoke, and S. Stringari (Cambridge University Press, Cambridge, England, 1994).

[32] A. Garg, H. R. Krishnamurthy, and M. Randeria, Phys. Rev. B **72**, 024517 (2005)

[33] A. Schmid, Phys. Kond. Mat. **5**, 302 (1966)

[34] E. Abrahams and T. Tsuneto, Phys. Rev. **152**, 416 (1966)

[35] L. P. Gor'kov, G. M. Eliashberg, Zh. Eksp. Teor. Fiz. **54**, 612 (1968) [Sov. Phys. JETP **27**, 328 (1968)]

[36] V. L. Ginzburg and L. D. Landau, Zh. Eksp. Teor. Fiz. **20**, 1064 (1950); translation: L. D. Landau, *Collected papers*, (Pergamon Press, 1965)

[37] L. P. Gor'kov, Zh. Eksp. Teor. Fiz. **36**, 1918 (1959) [Sov. Phys. JETP **9**, 1364 (1959)]

[38] G. M. Eliashberg, Zh. Eksp. Teor. Fiz. **61**, 1254 (1971) [Sov. Phys. JETP **34**, 668 (1971)]

[39] Yu. M. Gal'perin, V. I. Kozub, and B. Z. Spivak, Zh. Eksp. Teor. Fiz. **81**, 2118, (1981) [Sov. Phys. JETP, **54**, 1126 (1981)]

[40] A. F. Volkov and Sh. M. Kogan, Zh. Eksp. Teor. Fiz. **65**, 2038, (1973) [Sov. Phys. JETP, **38**, 1018 (1974)]

[41] L. P. Gor'kov, Zh. Exp. Teor. Fiz. **34**, 735 (1958) [Sov. Phys. JETP **7**, 505 (1958)]

[42] R. A. Barankov, L. S. Levitov and B. Z. Spivak, Phys. Rev. Lett. 93, 160401 (2004)

[43] C. Porter and R. Thomas, Phys. Rev. **104**, 483 (1956)

[44] G. L. Warner and A. J. Leggett, Phys. Rev. B **71**, 134514 (2005)

[45] E. A. Yuzbashyan, B. L. Altshuler, V. B. Kuznetsov, and V. Z. Enolskii, J. Phys. A **38**, 7831, (2005), cond-mat/0407501; cond-mat/0505493

[46] M. H. S. Amin, E. V. Bezuglyi, A. S. Kijko, and A. N. Omelyanchouk, Low Temp. Phys. 30, 661 (2004), cond-mat/0404401

[47] G. M. Falco and H. T. C. Stoof, Phys. Rev. Lett. **92**, 130401 (2004)

[48] G. M. Bruun and C. J. Pethick, Phys. Rev. Lett. **92**, 140404 (2004)

[49] R. H. Dicke, Phys. Rev. **93**, 99 (1954)

[50] K. Hepp and E. H. Lieb, Ann. Phys. (N.Y.) **76**, 360 (1973)

[51] M. O. Scully and M. S. Zubairy, *Quantum Optics* (Cambridge University Press, Cambridge, U.K., 1997).

[52] M. C. Cambiaggio, A. M. F. Rivas, M. Saraceno, Nucl. Phys. A **624**, 157 (1997)

[53] Y. Ohashi and A. Griffin, Phys. Rev. A **67**, 063612 (2003)

[54] S. L. McCall and E. L. Hahn, Phys. Rev. Lett. **18**, 908 (1967); Phys. Rev. **183**, 457 (1968)

[55] I. S. Gradshteyn and I. M. Ryzhik, *Table of integrals, series, and products*, (New York, Academic Press, 1965)

[56] F.H. Mies, E. Tiesinga, and P. S. Julienne, Phys. Rev. A **61**, 022721 (2000).

[57] K. Góral, T. Köhler, S. A. Gardiner, E. Tiesinga, and P. S. Julienne, J. Phys. B **37**, 3457 (2004).

[58] E. Hodby, S. T. Thompson, C. A. Regal, M. Greiner, A. C. Wilson, D. S. Jin, E. A. Cornell, and C. E. Wieman, Phys. Rev. Lett. **94**, 120402 (2005).

[59] S. J. J. M. F. Kokkelmans and M. J. Holland, Phys. Rev. Lett. **89**, 180401 (2002).

[60] T. Köhler, T. Gasenzer, and K. Burnett, Phys. Rev. A **67**, 013601 (2003).

[61] V. A. Yurovsky and A. Ben-Reuven, Phys. Rev. A **70**, 013613 (2004).

[62] R. A. Duine and H. T. C. Stoof, Phys. Rep. **396**, 115 (2004).

[63] M. Haque and H.T.C. Stoof, Phys. Rev. A **71**, 063603 (2005)

[64] J. Javanainen, M. Kostrun, Yi Zheng, A. Carmichael, U. Shrestha, P. J. Meinel, M. Mackie, O. Dannenberg, and K.-A. Suominen, Phys. Rev. Lett. **92**, 200402 (2004).

[65] R. A. Barankov and L. S. Levitov, Phys. Rev. Lett. **93**, 130403 (2004).

[66] K. Góral, T. Köhler, and K. Burnett, Phys. Rev. A **71**, 023603 (2005).

[67] R. B. Diener and Tin-Lun Ho, cond-mat/0404517

[68] A. V. Avdeenkov and J. L. Bohn, Phys. Rev. A **71**, 023609 (2005)

[69] A. Perali, P. Pieri, and G.C. Strinati, Phys. Rev. Lett. **95**, 010407 (2005)

[70] E. Altman and A. Vishwanath, Phys. Rev. Lett. **95**, 110404 (2005)

[71] C. Ticknor, C. A. Regal, D. S. Jin, and J. L. Bohn, Phys. Rev. A **69**, 042712 (2004).

[72] J. Zhang, E. G. M. van Kempen, T. Bourdel, L. Khaykovich, J. Cubizolles, F. Chevy, M. Teichmann, L. Tarruell, S. J. J. M. F. Kokkelmans, and C. Salomon, Phys. Rev A **70**, 030702(R) (2004).

[73] V. Gurarie, L. Radzihovsky, and A. V. Andreev, Phys. Rev. Lett. **94**, 230403 (2005)

[74] F. Chevy, E. G. M. van Kempen, T. Bourdel, J. Zhang, L. Khaykovich, M. Teichmann, L. Tarruell, S. J. J. M. F. Kokkelmans, and C. Salomon, Phys. Rev. A **71**, 062710 (2005)

[75] C. H. Schunck, M. W. Zwierlein, C. A. Stan, S. M. F. Raupach, and W. Ketterle, Phys. Rev. A **71**, 045601 (2005).

[76] L. D. Landau and E. M. Lifshitz, *Quantum Mechanics*, §133 (Pergamon, New York, 1987).

[77] R. W. Morse and H. V. Bohm, Phys. Rev. **108**, 10941096 (1957)

[78] L. H. Palmer and M. Tinkham, Phys. Rev. **165**, 588595 (1968)

[79] A.A. Abrikosov, L.P. Gor'kov, and I. Ye. Dzyaloshinskii, *Methods of quantum field theory in statistical physics*, (New York Dover Publications, 1975)